



LEIBNIZ-INSTITUT FÜR  
TROPOSPHÄRENFORSCHUNG

# *Annual Report*

## *Jahresbericht*

# 2003



Institute for Tropospheric Research



***Annual Report***  
***Jahresbericht***

**2003**



LEIBNIZ-INSTITUT FÜR  
TROPOSPHÄRENFORSCHUNG

## Impressum

### **Published by**

Institute for Tropospheric Research (IfT)  
Leibniz-Institut für Troposphärenforschung e.V. Leipzig (IfT)

Member of the Leibniz Association (WGL)

*Postal address:* Permoserstr. 15  
04318 Leipzig  
Germany

*Phone:* ++49 - 341-235-2321  
*Fax:* ++49 - 341-235-2361  
*E-mail:* monika@tropos.de  
*Internet:* <http://www.tropos.de>

### **Editors**

Konstanze Kunze, Claudia Peter, Heike Scherf, Katja Schmieder, Monika Schulze

### **Editorial Board**

Jost Heintzenberg, Hartmut Herrmann, Eberhard Renner

### **Technical management / DTP / Layout**

Katja Schmieder

### **Printed by**

MERKUR Druck- und Kopierzentrum GmbH  
Hauptmannstraße 4  
04109 Leipzig  
Internet: <http://www.merkurdruck.de>

### **Photo and illustration credits**

© IfT; all pages, except for pages:

**1 top right:** *Original photography from NASA*

**15, 49, 81 top right:** *NASA*

**105 down left:** *Leipziger Volszeitung*

**105 down right:** *Schulz & Schulz Architekten GmbH*

<b>Introduction and Synopsis of the contributions to the report</b>	3
<b>Einleitung und Übersicht der Einzelbeiträge</b>	8
<hr/>	
<b>Articles</b>	
◆ Multi-year aerosol observations with dual-wavelength Raman lidar at a central European EARLINET site	17
◆ A coupled field and modelling study on aerosol cloud interaction (AFO 2000 projects FEBUKO (FKZ 07ATF01 - 395) and MODMEP (FKZ 07ATF40))	24
◆ Chemical and Physical characterization of biomass burning aerosol: Results from the research project EFEU	35
◆ Atmospheric particle formation from H <sub>2</sub> SO <sub>4</sub> /H <sub>2</sub> O: An experimental study	42
<hr/>	
<b>Short contributions</b>	
◆ First observations of high ultrafine particle numbers near the inversion of a continental planetary boundary layer	51
◆ Airborne Measurements of Spectral Surface Albedo over Different Sea and Land Surfaces	54
◆ Siberian forest fire smoke travels around the world	57
◆ LACIS: Instrumental development and measurements	60
◆ Modeling the synoptic situation during SATURN: First results from mesoscale and large-eddy simulations	63
◆ Coupled treatment of microphysics and chemistry in a parcel model	65
◆ Determination of emission rates of diffuse sources by DOAS measurements and inverse dispersion modeling	68
◆ Flow measurements of main carbonyl compounds by the relaxed eddy accumulation (REA) technique	70
◆ Uptake of acetone, 2-butanone, 2,3-butanedione, and 2-oxo-propanal on a water surface	73
◆ NH <sub>3</sub> -concentrations in Melpitz and the Eastern Erzgebirge Mountains – test of a new measuring device	76
◆ Aqueous phase reactions of free radicals with selected organic compounds	78
<hr/>	
<b>Appendices</b>	
◆ Publications	83
◆ University courses	92
◆ Master theses	94
◆ Doctoral theses and habilitation	95
◆ Guest scientists and visits	96
◆ Scientific events	97
◆ Memberships	98
◆ Cooperation	99
◆ Boards	103
◆ Local map	104

## IfT-Intern

### ***Haushalt***

- ◆ Betriebs- und Investitionshaushalt 107
- ◆ Laufende Drittmittelprojekte 108
- ◆ Eingeworbene Drittmittel - Auftragsforschung 110
- ◆ Zusätzlich eingeworbene Drittmittel und Gesamteinwerbung 111

### ***Personal***

- ◆ Stellenplan - Haushaltmittel 112
- ◆ Übersicht aller Beschäftigten 112

### ***Öffentlichkeitsarbeit***

- ◆ IfT in den Medien 113
- ◆ IfT in der Presse 113
- ◆ Allgemeine Aktivitäten 114

### ***Organigramm***

115



*Introduction and synopsis*  
*Einleitung und Übersicht*



## Introduction

In the outskirts of Leipzig, on the campus of the former Academy of Sciences, in close neighborhood of the Environmental Research Center, other research establishments and businesses you find the Institute for Tropospheric Research. It was founded in 1991 for the investigation of physical and chemical processes in the polluted troposphere (roughly the first 10 km of our atmosphere).

analytical difficulties with the very small samples and with the complex behavior of tropospheric multiphase systems, in which individual processes seldom can be distinguished. In climate research this limitation is reflected in much larger uncertainties in predicted anthropogenic aerosol and cloud effects in comparison to numbers published by the Intergovernmental Panel on



*Fig. 1: IfT main building.*

Meanwhile a well-defined and globally unique research profile emerged with a focus on aerosols, i.e. small airborne particles, and clouds. Despite their minute absolute amount, aerosols and clouds are essential parts of the atmosphere because they control the budgets of energy, water and trace substances of the Earth System. The research interest in these highly disperse systems is stimulated foremost by their potential change through human activities. These system changes feed back into the anthroposphere not only through regional and global climate change but also directly through health effects of inhaled haze and fog particles.

Despite strong connections between humans, aerosols, and clouds important physico-chemical processes of aerosol and cloud formation and the relationships with climate and health are poorly understood. This limitation is mainly due to

Climate Change for additional greenhouse gases.

Rapid advances in our understanding of tropospheric multiphase processes and an application of this process understanding to the prediction of the consequences of human impacts can only be expected from concerted approaches from several directions. Consequently, the Institute for Tropospheric Research conducts field studies in several polluted regions parallel to the development of analytical methods for aerosol and cloud research.

These tools are not only applied in field experiments but also in extensive laboratory investigations, which form a second major activity. A third and equally important approach consists of the formulation and application of numerical models that reach from process models to regional simulations of the formation, transformation and effects of tropospheric multiphase systems.



*Fig. 2: Particle sampling systems during the INTERCOMP 2000 campaign at the research station Melpitz.*

### Field experiments

The atmosphere is an aerosol, i.e. a carrier gas mixture with suspended solid and liquid particles. Field experiments elucidate the atmospheric life cycle and related processes of aerosol and cloud particles. This task is vastly more difficult than comparable trace gas studies, in which only one number has to be known for each substance at each point in time and space. Particle sizes over more than six orders of magnitude occur in atmospheric aerosols and clouds, all of which play an important role in certain processes. All condensable substances of the Earth System can be found in the aerosol and a large number of them contribute to climate and biospheric effects. As a consequence of this multidimensional system essential aerosol and cloud properties are not well established on a global scale yet.

The uncertainty and thus the studies of the Institute for Tropospheric Research start with particle sources. The combustion of fossil and contemporary fuels is one of the most prominent aerosol sources. However, these sources are still poorly characterized in terms of climate-relevant aerosol parameters. In collaboration with car manufacturers the institute establishes size dependent particle emission data of cars at test stands, in particular in the nanometer size range that was not covered by conventional emission studies. According to long-term measurements of the institute in a street canyon the car related emissions of particles and their precursor gases are subject to strong physical and chemical transformations even before they reach the sidewalk. These transformations will be investigated by a new mobile aerosol laboratory on a trailer behind a moving car in traffic.

Emission studies at cars are complemented by measurements at stationary combustion sources. Here the research focuses on particle properties that determine the absorption of solar radiation.

Dedicated methods have been developed for the analysis of soot components, a major absorber of sunlight. With aerosol measurements at welding stands finally the Institute for Tropospheric research characterizes toxic industrial particle emissions. Health related aerosol studies will be expanded in the future in collaboration with the Environmental Research Center with coupled indoor and outdoor aerosol experiments and concurrent clinical investigations in the urban region of Leipzig.



*Fig. 3: Impression from the SATURN experiment.*

Even the largest highly polluted regions in the plumes of North America, Europe, the Indian subcontinent and Eastern Asia are insufficiently characterized in terms of aerosol burdens and ensuing climate effects. Thus, the institute focused the most recent field campaigns on the European and Indian plumes. These experiments were conducted within a large framework of international collaboration.

As baseline reference an austral area near Tasmania has been studied. By means of an intercontinental commercial aircraft, the results of the regional experiments are connected through regular CARIBIC flights between Germany, the Indian Ocean and Southern Africa.

Process studies are conducted at suitable locations such as mountain observatories, tethered balloons and over cooling towers of large power plants.

These experiments are dedicated to particle nucleation, particle processing through clouds and

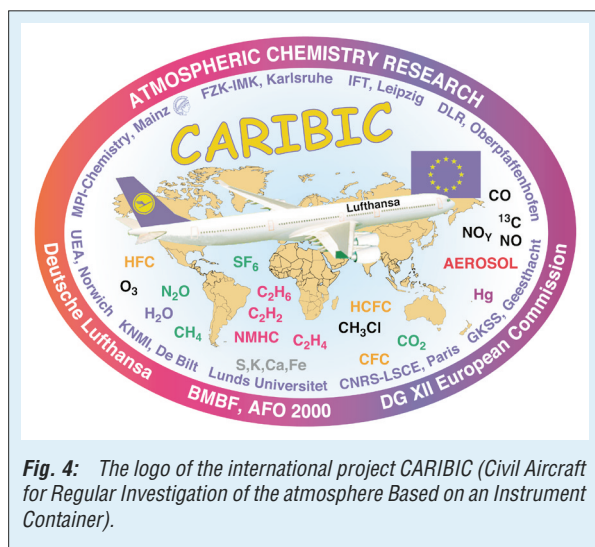


**Fig. 4:** The logo of the international project CARIBIC (Civil Aircraft for Regular Investigation of the atmosphere Based on an Instrument Container).

the influence of anthropogenic aerosols on the optical properties of clouds.

The vertical aerosol distribution over Europe is observed with the worldwide first coordinated lidar network EARLINET (European Aerosol Research Lidar Network).

### Laboratory experiments

In atmospheric research, there is a continuous development of physico-chemical models for the description of the most relevant process. These models are based on process parameters, which need to be determined in physical and chemical laboratory experiments.

In the physics section of the institute laboratory experiments cover the development of a large number of methods to characterize atmospheric particles and drops, in particular their size distribution and thermodynamic properties. Complex measuring and sampling systems are being designed for the characterization of cloud drops and interstitial particles.

Spectroscopic techniques such as the Differential Optical Absorption Spectroscopy have been developed for the analysis of trace gases and aerosol particles. The ongoing development of the multi-wavelength aerosol LIDAR (Light Detection and Ranging) technique includes the measurement of atmospheric state parameters such as temperature and relative humidity. A new Doppler LIDAR for vertical wind profiling will perform first test measurements in the autumn of 2003. Graphitic carbon is specified and quantified with a dedicated Raman spectrometer combined with multi-wavelength absorption measurements on aerosol samples.

The physics and chemistry sections in two main areas are carrying out process-oriented laboratory studies jointly. The first of these activities concerns a laminar flow tube reactor in which particle formation



**Fig. 5:** Multiwavelength Raman lidar measurement after sunset performed in the framework of the European Aerosol Research Lidar Network (EARLINET).

from ( $\text{SO}_2$ ) and organic precursors (e.g., terpenes) is being investigated. In the second activity, the transition from a moist aerosol to a cloud will be simulated in a large laminar flow channel for which presently is a dedicated laboratory building is being erected.

The chemistry section conducts several process-oriented laboratory studies. Gas phase reactions of the radicals OH and  $\text{NO}_3$  are being investigated in flow reactors. These reactions are important for ozone and particle formation caused by biogenic and anthropogenic emissions of volatile hydrocarbons. The chemical identity of atmospheric particles will be characterized in reaction chambers. In a single drop experiment, phase transfer parameters of trace gases and radicals are being determined for different chemical species and surfaces. Mechanisms of non-radical oxidations in the liquid phase are being studied with the stopped-flow technique and optical detectors. Experiments with radical reactions in the liquid phase form a core activity of the laboratory experiments because of their importance for processes in haze particles, fogs and clouds. For the understanding of the oxidation of organic trace gases in the tropospheric multi-phase system a large number of reactions with the OH and  $\text{NO}_3$  radicals are being studied as well as reactions of halogenated oxidants. The latter species are of interest for the emission of reactive halogen compounds from sea salt particles.

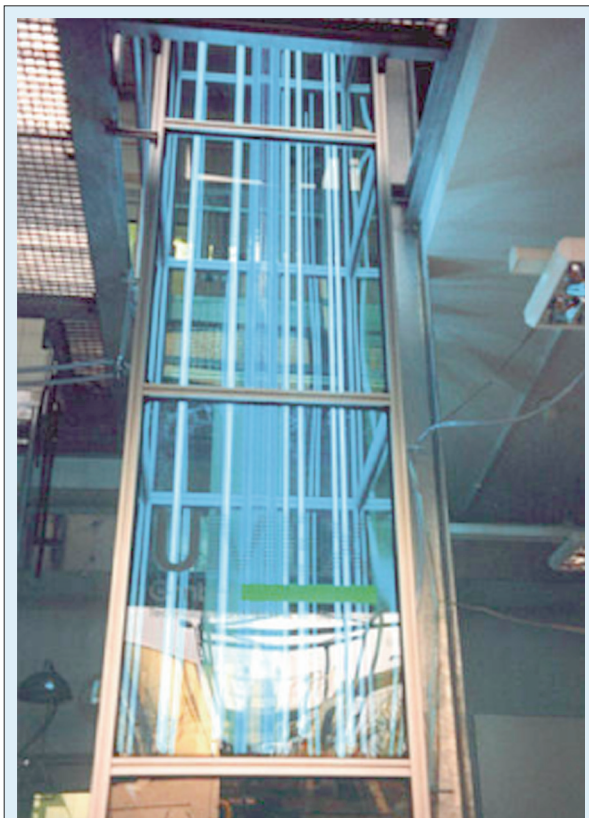


**Fig. 6:** The IFT laminar flow tube reactor (IFT-LFT).

Several laboratory experiments are dedicated to the chemical characterization of atmospheric organic aerosol components. Besides the conventional combustion techniques, mass spectroscopic and chromatographic techniques coupled directly to analysis by mass spectrometry or capillary electrophoresis with different sampling and segregation techniques are being developed. The close cooperation of the physics and chemistry section has led to the development of a patented and commercially exploited sampling method for narrow well-defined particle size ranges that is coupled directly to the mass spectroscopic analyses.



**Fig. 7:** A laser photolysis-long path laser absorption experiment for the study of nitrate radical kinetics in aqueous solution.

## Modeling

For the description of complex atmospheric processes, model systems of varying dimensions and complexity are developed, tested and applied to micro and mesoscale problems. The ultimate goal is to simulate the many interactions between aerosol particles, gases and clouds in a coupled three-dimensional meteorology-chemistry-transport model. With this model system as a toolbox scientific as well as legal tasks are addressed.

Models are indispensable tools in the search for efficient and cost-effective possibilities of compliance of relevant limit values for protection of human health for gaseous and particulate air pollutions defined or suggested in directives by the European Commission. As done in the past for the Saxonian government, the Institute for Tropospheric Research will work on this field in the context of national and international projects in the future too.

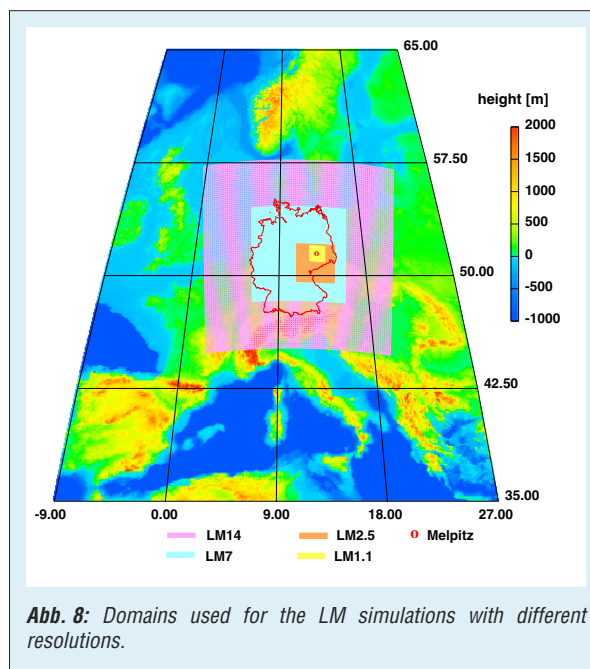


**Abb. 8:** Domains used for the LM simulations with different resolutions.

One example is the cooperation in the CITY-DELTA project, an EU-activity in the framework of CAFE – Clean Air for Europe Program. The modeling system LM-MUSCAT was used for investigation of long-term model responses to urban-scale emission-reduction scenarios with regard to ozone and PM.

Mixing processes and particle formation in the troposphere are being investigated with process studies. For that purpose the third-order planetary boundary layer chemistry aerosol model TOPCAM has been developed.

To understand better the interaction, effects and evolution of the different physico-chemical processes in the atmosphere their modeling requires a detailed description of all transformations

with equal rigor. To this end, the air parcel model SPACCIM was developed for the description of cloud processes by coupling complex multiphase chemistry and detailed microphysics. The model allows a detailed description of the transformation of gases and particles shortly before cloud formation,

during the cloud lifetime and shortly after cloud evaporation.

New and effective numerical methods will be developed and applied for a permanent improvement of the performance of the used models.

## Synopsis of the contributions to the report

The medium-term scientific concept of the institute defines the three major research themes:

1. Evolution, transport and spatio-temporal distribution of the tropospheric aerosol
2. Influence of the tropospheric aerosol on clouds and on the radiation budget
3. Chemical processes in tropospheric multiphase systems.

The improvement of the predictability of the evolution and effects of tropospheric multiphase systems is the long-term goal of the research along the lines of the major themes.

In the present report eight articles contribute to theme one. Ammonia is a key component in particle nucleation and tropospheric multiphase processes. Thus, in two of these papers new methods for measuring ammonia emissions are presented. Because of an increasing scientific interest in the participation of organic components in particle formation and cloud processes a new fast flux method for carbonyl compounds has been developed within the BMBF project BEWA. A technical description and first results with this new technique are given in a short contribution.

In 2002 a first particle nucleation experiment (SATURN), supported by all IfT departments, took place at the IfT research station Melpitz. With the balloon-borne payload ACTOS new information on the evolution of particle nucleation in the continental boundary layer was derived and is reported in a short contribution. Another short article covers the modeling of the synoptic conditions of SATURN. Not just meteorological control but also mechanisms and species participating in atmospheric particle nucleation are highly uncertain. The necessary systematic process studies cannot be done in the complex tropospheric multiphase system. Instead, laboratory simulations are conducted in a large laminar flow reactor at IfT. An extended contribution covers new results concerning the potential influence of ammonia on the ternary system sulfuric acid, water, and ammonia.

A shorter and an extended contribution dedicated to aerosols from biomass burning exemplify the wide range of aerosol research at IfT. The long contribution comprises detailed physico-chemical results of laboratory studies of biomass combustion

whereas the short paper covers the global transport and optical properties of aerosols from large fires in Siberia that have been observed by IfTs stationary lidar.

Research theme two is addressed in one extended and three shorter contributions in the present report. As an essential part of the new Leipzig Aerosol Cloud Interaction Simulator LACIS, a new optical technique for online measurements of drop sizes is reported together with new laboratory results on pressure-dependent drop growth. For the use with LACIS and cloud experiments a coupled microphysics-chemistry cloud parcel model is developed, which is presented in a short contribution.

One extended and a shorter paper cover radiative effects of the atmospheric aerosol. With IfTs unique stabilized airborne spectrometer and a new retrieval method surface albedo spectra have been derived from flights over the North Sea and adjacent coastal areas. These albedo values are key boundary conditions in any radiative transfer calculations in the atmosphere.

Within the European research project EARLINET regular lidar profiling was conducted with the stationary IfT lidar. In an extended contribution aerosol optical properties are evaluated from these lidar data and compared with older optical measurements over Leipzig yielding the evolution of the radiative properties of the urban aerosol over the past 15 years.

Finally, new findings concerning research theme three are reported in one extended and two shorter contributions. Two large BMBF projects cover aerosol cloud interaction experimentally and with model studies, FEBUKO and MODMEP, respectively. First results of related field campaigns in central Germany are compared with multiphase numerical simulations. In part, the model predictions still deviate substantially from the experimental results. On the other hand, significantly improved understanding of the role of organic aerosol and cloud water components has been reached. Laboratory simulations are one way to fill the gaps between model simulations and experimental findings. A shorter contribution along this line is dedicated to the uptake of organic compounds by cloud drops while a second paper covers liquid phase reactions of radicals with organic aerosol components.

### Einleitung

Auf dem ehemaligen Akademiegelände in der Permoserstraße, in guter Nachbarschaft zum Umweltforschungszentrum, anderen Forschungseinrichtungen und verwandten Firmen, befindet sich seit 1992 das Leibniz-Institut für Troposphärenforschung e.V. (Mitglied der Wissenschaftsgemeinschaft Gottfried Wilhelm Leibniz). Gegründet wurde es zur Erforschung

physikochemischen Prozesse von Aerosol- und Wolkenbildung und die Wechselwirkungen mit Gesundheit und Klima noch wenig verstanden. Dies liegt vor allem an Schwierigkeiten bei der Analyse der beteiligten kleinsten Stoffmengen und an dem komplexen Verhalten troposphärischer Mehrphasensysteme, deren Einzelprozesse in der Atmosphäre nicht klar getrennt beobachtet werden



Abb. 1: IFT Hauptgebäude.

physikalischer und chemischer Prozesse der belasteten Troposphäre, also etwa der ersten zehn Höhenkilometer über dem Meeresspiegel.

Inzwischen hat sich ein klares und weltweit einzigartiges Forschungsprofil herausgebildet, in dessen Mittelpunkt Aerosole, also kleinste luftgetragene Partikel und Wolken, stehen. Trotz kleinster absoluter Mengen sind diese wesentliche Bestandteile der Atmosphäre, weil sie den Energie-, Wasser- und Spurenstoffhaushalt des Erdsystems mitbestimmen. Das Forschungsinteresse an diesen hochdispersen Systemen geht auf deren mögliche Beeinflussung durch menschliche Aktivitäten zurück. Diese Systemveränderungen wirken nicht nur über regionale und globale Klimaänderungen auf den Menschen zurück, sondern auch direkt über gesundheitliche Wirkungen eingeatmeter Dunstpartikel und Nebeltröpfchen.

Trotz dieser wichtigen Beziehungen zwischen Mensch, Aerosolen und Wolken sind die

können. In der gegenwärtigen Klimadiskussion zum globalen Wandel spiegelt sich diese Kenntnislage in den sehr viel größeren Unsicherheiten in allen zu Aerosol- und Wolkenwirkung veröffentlichten Zahlen im Verhältnis zu Treibhauseffekten der Gase wider.

Rasche Zuwächse beim Verständnis troposphärischer Mehrphasenprozesse und eine Anwendung dieses Prozessverständnisses auf die Vorhersage der Folgen menschlicher Eingriffe lassen sich nur durch ein konzertiertes Vorgehen in mehreren Richtungen erwarten. Das Leibniz-Institut für Troposphärenforschung betreibt daher neben Feldstudien in mehreren belasteten Regionen auch die Entwicklung eigener analytischer Verfahren zur Untersuchung von Aerosolen und Wolken. Diese Verfahren werden auch in ausgedehnten Laboruntersuchungen eingesetzt, der zweiten Hauptarbeitsrichtung des Instituts. Ein dritter, gleichermaßen wichtiger Arbeitsansatz ist die



**Abb. 2:** Partikelsammler während des Feldexperiments INTERCOMP 2000 auf der Forschungsstation Melpitz.

Formulierung und Anwendung numerischer Modelle von der Prozessbeschreibung bis zur Beschreibung der regionalen Bildung, Umwandlung und Wirkung troposphärischer Mehrphasensysteme.

Nach Begutachtung durch den Wissenschaftsrat im Herbst 1999 wurde das Institut aufgrund insgesamt guter Forschungsleistungen auf dem Gebiet der Troposphärenforschung positiv evaluiert. Die Forschungsleistungen sind von überregionaler Bedeutung und gesamtstaatlichem Interesse. Das Institut wurde zur Weiterförderung als Forschungseinrichtung der Blauen Liste empfohlen.

### Feldexperimente

Die Feldexperimente des Instituts dienen der Aufklärung des atmosphärischen Kreislaufs und der damit verbundenen Prozesse dieser Aerosol- und Wolkenpartikel. Diese Aufgabe ist unvergleichlich schwerer als entsprechende Spurengasuntersuchungen, bei denen für jeden Stoff an jedem Ort nur eine Zahl bestimmt werden muss. In Aerosolen und Wolken treten mehr als sechs Zehnerpotenzen von Partikelgrößen auf, die alle bei bestimmten Prozessen eine Rolle spielen. Alle kondensationsfähigen Stoffe des Erdsystems sind im Aerosol zu finden, und eine große Zahl davon ist bei Klima- und Biosphärenwirkungen beteiligt. Als Folge dieser Vielfalt und der mengenbedingten analytischen Schwierigkeiten sind wesentliche globale Aerosol- und Wolkeneigenschaften noch wenig festgelegt.

Diese Unsicherheit beginnt bei den Partikelquellen, und deshalb setzen schon hier die Forschungsarbeiten des Leibniz-Instituts für Troposphärenforschung ein. Die Verbrennung fossiler und erneuerbarer Brennstoffe bei der Energieerzeugung und im Verkehr gehören zu den wichtigsten Aerosolquellen, sind aber in Bezug auf klimarelevante Aerosolparameter noch wenig charakterisiert. In Zusammenarbeit mit Automobilherstellern erstellt das Institut daher

am Prüfstand größenabhängige Partikelemissionsdaten von Kraftfahrzeugen, insbesondere in dem von konventionellen Verfahren nicht erfassten Nanometerbereich. Wie sich aus Langzeitmessungen des Instituts in einer Straßenschlucht ergab, unterliegen diese Emissionen von Partikeln und deren Vorläufern enormen physikalischen und chemischen Umwandlungen, noch bevor sie den Straßenrand erreichen. Diese werden in Zukunft mit einem speziellen mobilen Aerosollabor direkt hinter einem fahrenden Kraftfahrzeug bestimmt.

Die Kraftfahrzeugemissionsstudien werden ergänzt durch Untersuchungen an stationären Verbrennungsquellen an einem Kraftwerk und bei Testverbrennungen von Biomasse. Hier sind es vor allem die Partikeleigenschaften, die die Absorption von Sonnenstrahlung bestimmen, auf die sich das Leibniz-Institut für Troposphärenforschung konzentriert. Eigene Analyseverfahren zur



**Abb. 3:** Impression vom SATURN Experiment.

Bestimmung von Rußkomponenten wurden entwickelt und sowohl bei Quell- als auch Immissionstudien eingesetzt. Mit Aerosolmessungen an Schweißarbeitsplätzen widmet sich das Institut schließlich wichtigen gesundheitsschädlichen Partikelemissionen der verarbeitenden Industrie. Gesundheitsbezogene Aerosolstudien werden in Zusammenarbeit mit dem Umweltforschungszentrum Leipzig/Halle verstärkt, speziell durch gekoppelte Innenraum- und Außenluftmessungen mit gleichzeitiger Bestimmung von Gesundheitseinwirkungen im urbanen Raum Leipzigs.

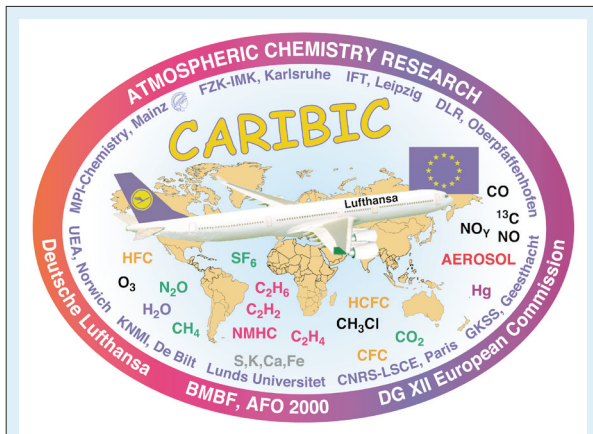


Abb. 4: Das Logo des internationalen Projekts CARIBIC (Civil Aircraft for Regular Investigation of the atmosphere Based on a In-strument Container).

Selbst die größten hoch verunreinigten Regionen, wie die Rauchfahnen von Nordamerika, Europa, dem indischen Subkontinent und Ostasien sind noch bei weitem nicht hinreichend bezüglich ihrer Aerosolbelastungen und den daraus resultierenden Klimawirkungen charakterisiert. Auf diese Regionen konzentrieren sich daher in internationaler Zusammenarbeit die Feldexperimente des Instituts mit guten Erfolgen in der jüngsten Vergangenheit in Europa, über dem Indischen Ozean und in einem südhemisphärischen Reinluftreferenzgebiet bei Tasmanien. Durch Nutzung eines interkontinental arbeitenden kommerziellen Verkehrsflugzeuges werden dabei die örtlich und zeitlich begrenzten Einzelexperimente auf regelmäßig beflogenen Routen zwischen Deutschland, dem Indischen Ozean und Südafrika in der oberen Troposphäre verbunden.

Neben Aerosol- und Wolkencharakterisierungsexperimenten werden an geeigneten Orten, wie Bergstationen, an Fesselballonen und über Kraftwerkskühltürmen Prozessstudien durchgeführt, die sich dem Verständnis von Einzelprozessen, wie der Partikelneubildung, der physikochemischen Veränderung des Aerosols beim Wolkendurchgang und dem Einfluss von Aerosolen auf die Reflektionseigenschaften von Wolken widmen.

### Laborexperimente

In der Atmosphärenforschung werden kontinuierlich physikochemische Modelle zur Beschreibung der wesentlichen Prozesse entwickelt. Grundlage derartiger Modelle sind stets Prozessparameter, die in physikalischen und chemischen Laborexperimenten ermittelt werden.

In der Abteilung Physik des IfT werden im Bereich der Laborexperimente eine Vielzahl von Messmethoden entwickelt, die zur Partikelcharakterisierung in boden- und luftgestützten Feldmesskampagnen eingesetzt werden. Im

Einzelnen betreffen diese Arbeiten die Weiterentwicklung von sog. „Differential Mobility Analysen (DMA)“ zur Messung von Partikelgrößenverteilungen sowie komplexe Messsysteme zur physikalischen und chemischen Charakterisierung von Wolkentröpfchen und dem interstitiellen Aerosol, also denjenigen Aerosolpartikeln, die innerhalb von Wolken neben den Wolkentröpfchen selbst in der Gasphase suspendiert sind.

Optische Messmethoden werden zur Bestimmung der Extinktion von Partikeln und der Absorption von Spurengasen und Radikalen mittels der differentiellen Absorptionsspektroskopie (DOAS) angewendet. Ein Mehrwellenlängen-LIDAR wird zur Untersuchung der Rückstreuung von Laserstrahlung verschiedener Wellenlängen eingesetzt und im Labor weiterentwickelt. Weitere spektroskopische Methoden werden im Bereich der Ramanspektroskopie zur Spezifizierung graphitischen Kohlenstoffs in Aerosolproben entwickelt. Die Bestimmung schwarzen Kohlenstoffs in Aerosolproben durch spektrale Absorptionsmessungen wird untersucht.

In zwei Bereichen werden direkt prozessorientierte Laboruntersuchungen gemeinsam von den Abteilungen Physik und Chemie durchgeführt. Diese abteilungsübergreifenden Aktivitäten betreffen zunächst einen als Laminarströmungsrohr ausgeführten Reaktor, an dem die Bildung von Partikeln aus anorganischen ( $\text{SO}_2$ ) und organischen Vorläufersubstanzen (z.B. Terpene) untersucht

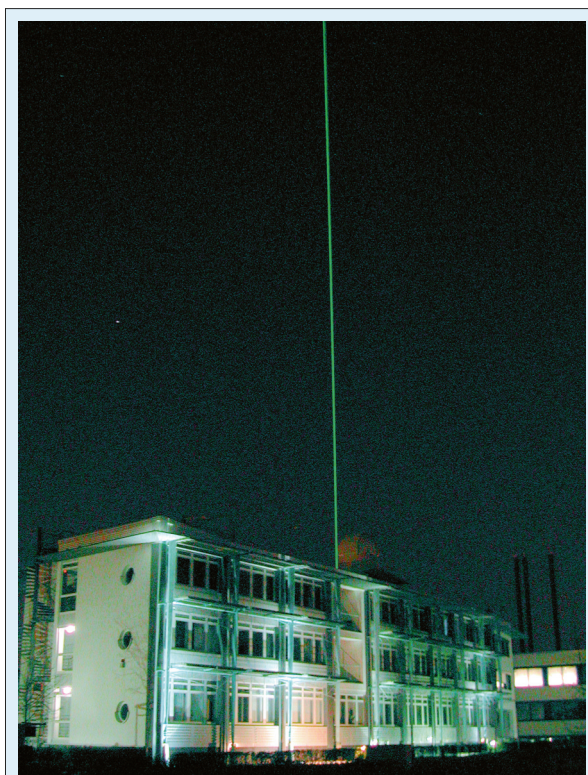


Abb. 5: Mehrwellenlängen-Raman-Lidarmessung im Rahmen des Europäischen Lidarnetzwerkprojekts EARLINET.

wird. Zum anderen befindet sich ein Strömungsreaktor im Aufbau, in dem das Wachstum von Aerosolpartikeln zu Wolkentröpfchen sowie die chemische Wirkung von Wolken in einem dezidierten Labor untersucht werden.



**Abb. 6:** Der laminare Rohrreaktor des IFT.

Die in der Abteilung Chemie durchgeführten Laboruntersuchungen sind stark prozessorientiert. Es werden Gasphasenreaktionen der Radikale OH und  $\text{NO}_3$  in Strömungsreaktoren untersucht. Diese Reaktionen sind von Interesse für die Ozon- und Partikelbildung aufgrund anthropogen oder biogen emittierter flüchtiger Kohlenwasserstoffe. Die chemische Identität von Partikelinhaltsstoffen wird auch in Reaktionskammern studiert, die gegenwärtig aufgerüstet werden. In einem Einzeltropfenexperiment werden Phasentransferparameter für Spurengase und Radikale untersucht. Die Bestimmung von Phasentransferparametern und reaktiven Aufnahmekoeffizienten wird dabei auf bisher nicht betrachtete chemische Spezies und Oberflächen ausgeweitet. Im Bereich von Flüssigphasenmechanismen werden Reaktionen von nichtradikalischen Oxidantien mittels der sog. Stopped-Flow-Technik mit optischem Nachweis untersucht. Einen besonderen Schwerpunkt bilden schließlich die Experimente mit Radikalreaktionen in wässriger Lösung, die in der Umwelt in den Tröpfchen von Wolken, Regen und Nebel sowie in wässrigen Partikeln ablaufen. Hier werden zum Verständnis der Oxidation organischer Spurengase

im troposphärischen Mehrphasensystem eine Vielzahl von Reaktionen der Radikale OH und  $\text{NO}_3$  sowie Reaktionen von halogenhaltigen Oxidantien untersucht. Letztere Spezies sind von Interesse bei der Freisetzung von Halogenverbindungen aus maritimen Seesalzpartikeln, der sog. Halogenaktivierung.

In der analytischen Messtechnik werden in Laborexperimenten Verfahren zur besseren chemischen Charakterisierung der organischen Bestandteile des troposphärischen Aerosols entwickelt und getestet. Diese Techniken beruhen zumeist auf massenspektrometrischen Verfahren, die in verschiedenen Kopplungstechniken eingesetzt werden. Im Bereich der Probenahmetechniken gibt es auch hier eine enge Kooperation mit der Abteilung Physik zur Entwicklung einer gezielten Abscheidung von Partikeln bestimmter Größe und deren kontinuierlicher chemischer Analyse.



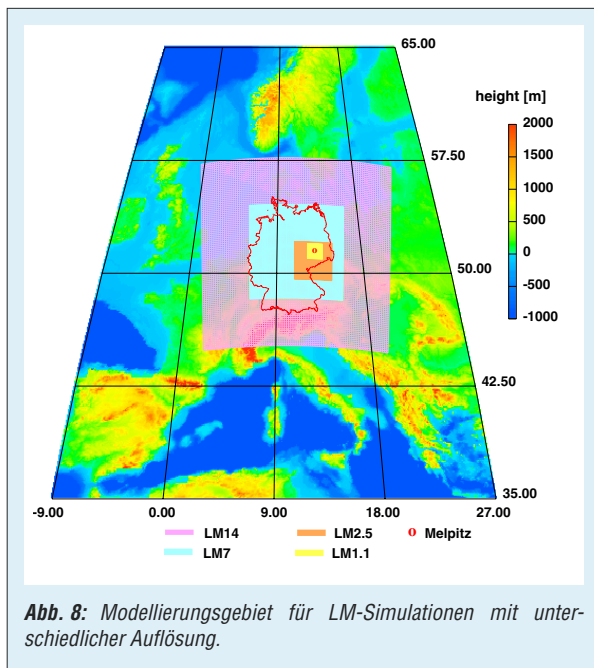
**Abb. 7:** Eine Laserphotolyse-Laserlangwegabsorptionsanordnung zur Untersuchung der Kinetik des Nitrat-Radikals in wässriger Lösung.

### Modellierung

Zur Beschreibung der komplexen atmosphärischen Vorgänge werden Modellsysteme verschiedener Dimension und Komplexität für die Mikro- bis Mesoskala entwickelt, überprüft und angewendet. Zur Modellierung von troposphärischen Multiphasenprozessen erfolgen vor allem Arbeiten zur Entwicklung von Wolkenmodulen, die eine komplexe Multiphasenchemie mit einer detaillierten Mikrophysik verbinden. Mit deren Integration in komplexe dreidimensionale Modelle kann man die vielfältigen Wechselwirkungen zwischen Aerosolpartikeln, Gasen und Wolken in einem gekoppelten dreidimensionalen Meteorologie-Chemie-Transport-Modell beschreiben, und so zu einer Verbesserung des Systemverständnisses der Troposphäre gelangen. Mit einem solchen Modellsystem hat man ein Instrument zur Bearbeitung wissenschaftlicher Aufgaben und

gleichermaßen zur Beantwortung von Fragen zur Luftqualität im legislativen Bereich.

Bei der Suche nach effektiven und kostensparenden Möglichkeiten zur Einhaltung bestehender und zukünftiger nationaler und europäischer Grenzwerte für gasförmige Luftbeimengungen und Partikeln unterschiedlicher Größe ist der Einsatz von Modellen unverzichtbar. Nach bisheriger guter Zusammenarbeit mit dem Sächsischen Staatsministerium für Umwelt und Landwirtschaft beabsichtigt das Institut, auch weiterhin auf diesem



Gebiet national und international tätig zu sein. Jüngstes Beispiel dafür ist die Mitarbeit am „**CITY-DELTA project**“, einer EU-Aktivität im Rahmen von „CAFE – Clean Air for Europe Programme“, koordiniert vom JRC in Ispra. Mit dem Modellsystem **LM-MUSCAT** konnten innerhalb des Modellvergleichs hinsichtlich „long-term model responses to urban-scale emission-reduction scenarios with regard to ozone and PM 2.5“ bisher gute Ergebnisse erzielt werden.

Im Bereich Prozessstudien zur Aerosol- und Wolkendynamik erfolgen Arbeiten zu turbulenten Mischungsprozessen und deren Auswirkungen u.a. auf die Partikelneubildung. Hierfür wurde in der Abteilung Modellierung das eindimensionale Grenzschichtmodell TOPCAM (Third-Order PBL Chemistry Aerosol Model) entwickelt.

Gleichermaßen erfolgen Simulationen im Zusammenhang mit den geplanten Experimenten am Wolkenkanal LACIS. Insbesondere ist ein von der chemischen Zusammensetzung abhängiges Diffusionswachstum in Abhängigkeit von der umgebenden Gasphase (einschließlich Wasserdampf) Ziel der Modellierung.

Die modelltechnische Behandlung eines so umfassenden atmosphärischen Systems ist numerisch sehr aufwendig. Die zu entwickelnden Modelle müssen hinreichend genau sein und numerisch sehr effizient auf den jeweils zur Verfügung stehenden Rechnerarchitekturen laufen. Zur Entwicklung auf diesem Gebiet liefert die Abteilung Modellierung wesentliche Beiträge.

## Übersicht der Einzelbeiträge

In dem mittelfristigen Arbeitskonzept des Instituts wurden 2003 folgende übergeordneten Forschungsthemen festgelegt:

1. Evolution, Transport und raumzeitliche Verteilung des troposphärischen Aerosols
2. Einfluss des troposphärischen Aerosols auf Wolken und Strahlungshaushalt
3. Chemische Prozesse in troposphärischen Mehrphasensystemen.

Langfristiges Ziel der damit verbundenen Arbeiten ist die Verbesserung der Vorhersagefähigkeit für die Entwicklung und die Effekte von troposphärischen Mehrphasensystemen.

In dem vorliegenden Jahresbericht tragen acht Beiträge zu Thema 1 bei. In zwei dieser Artikel werden neue Methoden zur Bestimmung von Ammoniakemissionen vorgestellt, die eine Schlüsselkomponente für die Neubildung von Partikeln und für troposphärische Mehrphasenprozesse betreffen. Die Beteiligung organischer Komponenten an der Partikelbildung und in Wolken-

prozessen hat in den letzten Jahren bei den Arbeiten des Instituts an Gewicht gewonnen. Aus diesem Grunde wurde eine schnelle Methode zur Bestimmung der Flüsse von Carbonylkomponenten entwickelt und im Rahmen des BEWA-Projektes des BMBF eingesetzt. Die Methode und erste Ergebnisse werden hier vorgestellt.

2002 fand das erste institutsinterne Feldexperiment zur Partikelneubildung (SATURN) in Melpitz statt, das von allen Abteilungen getragen wurde. Neue Erkenntnisse zum Verlauf der Neubildungsprozesse in der kontinentalen Grenzschicht ergaben sich daraus und werden in einem Kurzbeitrag vorgetragen. Ein weiterer Kurzbeitrag ist der Modellierung der synoptischen Situation während SATURN gewidmet. Nicht nur die meteorologischen Einflüsse auf die Partikelneubildung, sondern auch die Nukleationsmechanismen selbst und die daran beteiligten Spurenstoffe sind noch weitgehend unklar. Die dafür nötigen systematischen Prozessuntersuchungen können nicht im Felde durchgeführt werden,

sondern bedürfen Laborsimulationen, die im IfT an einem großen Laminarströmungsrohr durchgeführt werden. Für das in der Atmosphäre wichtige System Schwefelsäure-Wasser-Ammoniak werden neue Erkenntnisse zum möglichen Ammoniak einfluss in einem Langbeitrag dargelegt.

Ein Kurz- und ein Langbeitrag ist Aerosolen aus Biomassenverbrennung gewidmet und zeigt beispielhaft die Breite der Aerosoluntersuchungen des IfT. Während in dem Langbeitrag detaillierte physikochemische Laboruntersuchungen zur Aerosolemission aus Biomassenbränden beschrieben werden zeigt der Kurzbeitrag die weltweite Verfrachtung und die optischen Effekte von Waldbrandaerosolen aus Sibirien auf, so wie sie von dem stationären Mehrwellenlängenlidar des Instituts gemessen wurden.

Hauptforschungsthema 2 wird von einem Lang- und drei Kurzbeiträgen des vorliegenden Berichts aufgegriffen. Ein wesentlicher Teil der optischen Messmethodik für den neuen Leipziger Wolken-simulator LACIS wurde bis zur Ergebnisreife entwickelt und liefert nun genaue Partikelgrößen im kritischen Übergangsbereich zwischen feuchtem Dunst und Wolkentropfen. An der kleinskaligen Version von LACIS wurden erste Ergebnisse zur Druckabhängigkeit des Tropfenwachstums erarbeitet. Zur Nutzung des mit LACIS verbesserten Prozessverständnisses wird ein gekoppeltes Mikrophysik-Chemie Model entwickelt, das in einem Kurzbeitrag vorgestellt wird.

Strahlungswirkungen des atmosphärischen Aerosol werden in einem Kurz- und einem Langbeitrag behandelt. Mit dem weltweit einzigartigen stabilisierten, flugzeuggetragenen Albedospektrometer des IfT wurden im Jahre 2000 Messflüge über der Nordsee und dem angrenzenden Küstengebiet durchgeführt. Der

Kurzbeitrag beschreibt die Ergebnisse, die zur Entwicklung einer neuen Methode zur Bestimmung der Oberflächenalbedo führten, die für Strahlungstransportberechnungen in der Atmosphäre eine entscheidende Randbedingung darstellt.

In dem europäischen Projekt EARLINET wurden über mehrere Jahre hinweg regelmäßige Lidarprofilierungen mit dem stationären IfT-Lidar durchgeführt. Diese werden nun in einem Langbeitrag bezüglich aerosoptischer Eigenschaften ausgewertet. Durch den Vergleich mit älteren optischen Messungen über Leipzig konnte die Entwicklung der Strahlungseigenschaften des urbanen Aerosols im Laufe der letzten 15 Jahre abgeleitet werden.

Schließlich werden neue Erkenntnisse zum Hauptforschungsthema 3 in einem Lang- und zwei Kurzbeiträgen vorgelegt. Erste Ergebnisse zweier Großprojekte zur Wechselwirkung von Aerosolen und Wolken des BMBF (FEBUKO und MODMEP) im Zusammenhang mit einem physikochemischen Feldexperiment im Thüringer Wald werden mit Mehrphasenmodellrechnungen verglichen. Es zeigt sich, dass die Modellvorhersagen teilweise noch stark von den experimentellen Ergebnissen abweichen. Andererseits zeichnet sich ein deutlich verbessertes Prozessverständnis bezüglich der Rolle organischer Partikel- und Wolkenwasserinhaltsstoffe bereits ab. Laborsimulationen zum besseren Mehrphasenprozessverständnis sind ein Weg, der im IfT beschränkt wird, um Modelle und Experimente zukünftig in noch bessere Übereinstimmung zu bringen. Ein Kurzbeitrag hierzu ist der Aufnahme von organischen Komponenten in Wolkentropfen gewidmet, während ein zweiter Kurzaufsatz Flüssigphasenreaktionen von Radikalen mit organischen Aerosolkomponenten behandelt.





*Articles*



## Multi-year aerosol observations with dual-wavelength Raman lidar at a central European EARLINET site

Ina Mattis, Dietrich Althausen, Albert Ansmann, Detlef Müller, Ulla Wandinger

*Nach Abschluss des EARLINET-Projekts Anfang 2003 sind nun auch die Auswertearbeiten abgeschlossen. Der Beitrag liefert einen Überblick über die wesentlichen Ergebnisse. Hervorzuheben ist, dass weltweit erstmals spektral und vertikal aufgelöste optische Partikeleigenschaften über einen Zeitraum von etwa 3 Jahren gemessen wurden. Während anthropogene Partikel die optischen Eigenschaften der Grenzschicht bestimmen, dominieren Saharastaub und gealterte Waldbrand-Aerosole die optischen Effekte in der freien Troposphäre. Im Mittel trägt die freie Troposphäre etwa 20% zur gesamt optischen Dicke bei. Der Vergleich mit optischen Messungen der Universität Leipzig (1990-1994) zeigt den drastischen Rückgang der Luftverschmutzung über Ostdeutschland. Die winterlichen Partikelbelastungen sind heute um gut einen Faktor 5 geringer als 1991.*

### Introduction

Coordinated, three-dimensional monitoring of the global aerosol distribution is a basic requirement of climate research. These observations are needed for a proper consideration of particles in atmospheric models that are used to simulate the regional and inter-continental aerosol transport and the influence of particles on short-term weather, the Earth's radiation budget (direct climate effect), and on cloud processes (indirect climate effect). However, such a monitoring system is not available. As a consequence, the uncertainty in the estimate of the aerosol impact on future climate is rather large (IPCC, 2001).

Vertically resolved lidar observations are needed to complement the two-dimensional, column-integrated satellite observations and ground-based Sun photometer measurements, on which the information about the global aerosol distribution mainly rests. A first attempt to improve this unsatisfactory situation was the implementation of the European Aerosol Research Lidar Network (EARLINET, Bösenberg et al., 2003). More than 20 lidar stations distributed from Sweden to Greece and from Wales to Belarus were involved in this effort and monitored the European aerosol distribution with high vertical resolution on a routine basis from May 2000 - November 2002. The observations presented here were performed in the framework of the EARLINET project.

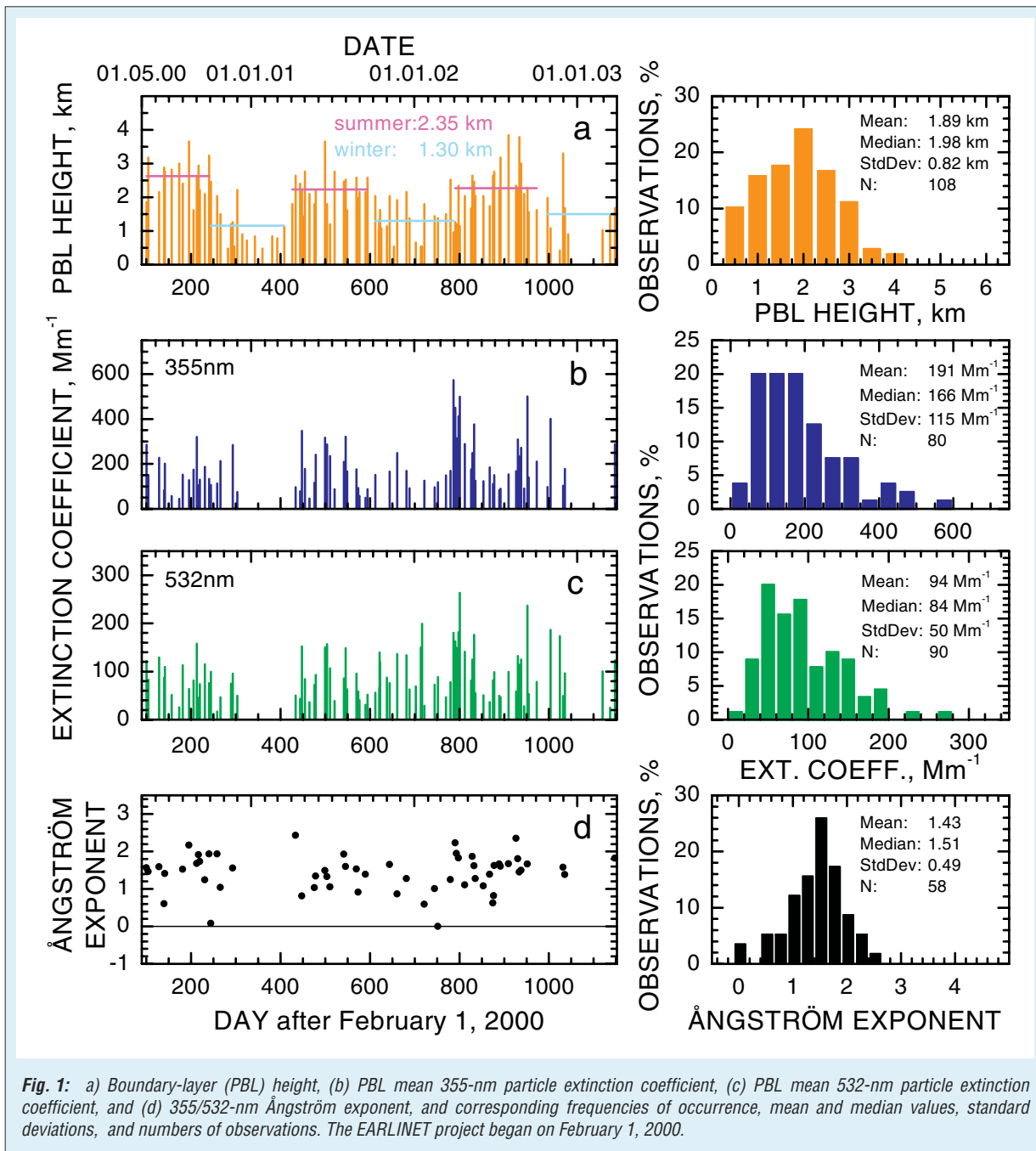
For quantitative studies of the optical properties of tropospheric aerosol particles with lidar, Raman lidars have proven to be most useful. Here, we present for the first time routine, long-term observations with a dual-wavelength aerosol Raman lidar. The advantage of this lidar is that vertical profiles of the volume extinction coefficient are simultaneously measured at 355 nm and 532 nm so that the spectral slope of the extinction coefficient (Ångström exponent) is obtained. This exponent is often used to characterize anthropogenic particles

because it is very sensitive to changes in the accumulation mode (particle diameters  $< 1 \mu\text{m}$ ) of the aerosol size distribution. The lidar measurements are compared with Sun photometer observations on the roof of the IFT building performed in the framework of the Aerosol Robotic Network (AERONET) (Holben et al., 2001). The EARLINET measurements are also compared with observations taken by the Leipzig University from 1990-1994, and thus shortly after the industrial breakdown in the former German Democratic Republic.

### Observations

Lidar is the only monitoring technique which allows a clear separation of optical properties of boundary-layer (PBL) aerosols which originate from local and regional emissions of particles and gases and of free tropospheric particles which are often advected over long distances from other continents and are usually very different from the PBL particles regarding their optical and microphysical properties. To obtain the PBL optical properties, we have to determine the PBL depth first. The top height of the PBL is indicated by a sharp decrease of the backscatter signal. The determined PBL heights presented in Figure 1a include the entrainment layer depth.

As can be seen in Figure 1a the PBL depth was largest during the summer half year because of strong convective processes in spring and summer. Three-year mean PBL top heights are 2350 m (summer half year, April to September) and 1300 m (winter half year). The seasonal mean PBL heights are 950 m (December to February), 1850 m (March to May), 2450 m (June to August), and 1300 m (September to November). The annual mean PBL height (based on the seasonal averages) is 1640 m. Note that these numbers do not include PBL heights of very cloudy and rainy days.



The PBL mean extinction coefficient, i.e., the vertically integrated extinction coefficient divided by the PBL depth, is plotted in Figures 1b and c. The values mostly range from 80-300  $\text{Mm}^{-1}$  at 355 nm and 40-150  $\text{Mm}^{-1}$  at 532 nm. Mean values are close to 200 and 100  $\text{Mm}^{-1}$  at 355 and 532 nm, respectively. Figure 1c shows the corresponding Ångström exponents. Most values are between one and two with a mean value of 1.43. These values are typical for an urban site (Holben et al., 2001).

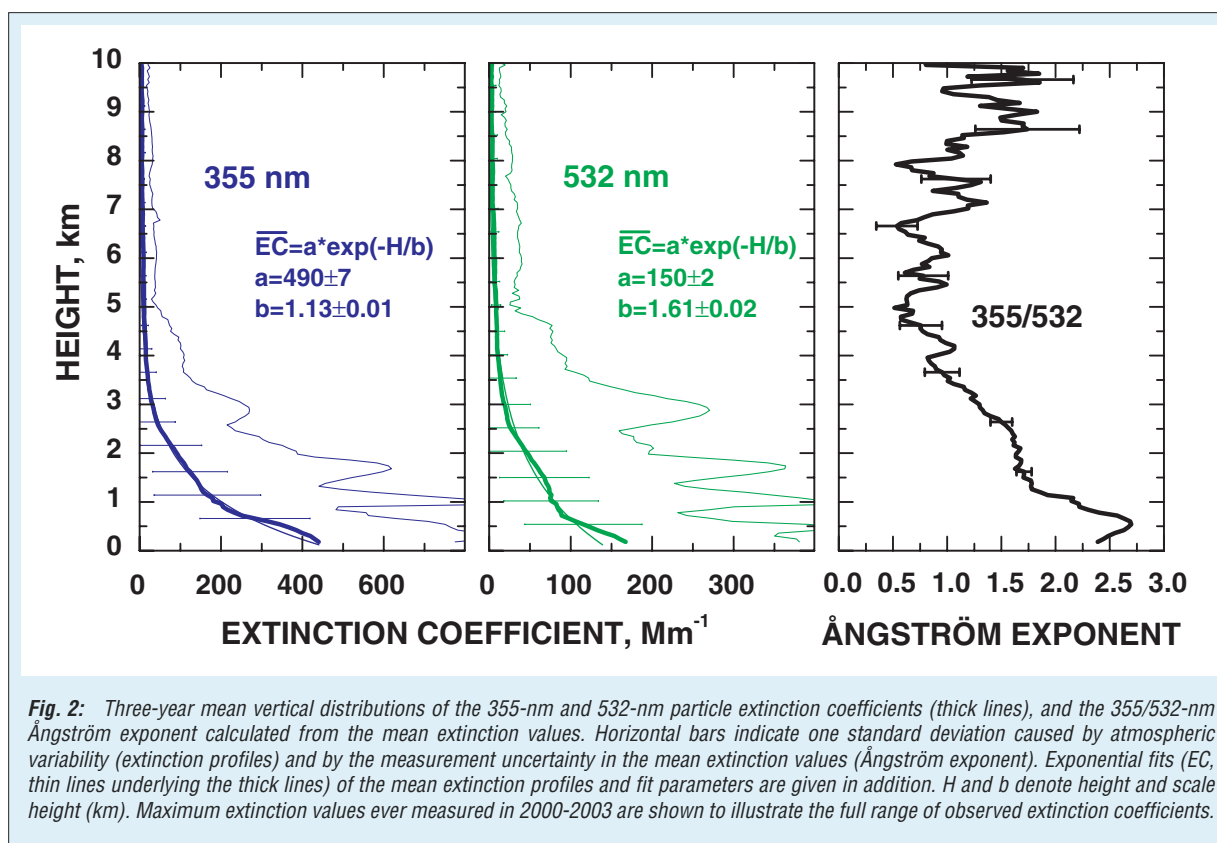
It is worth mentioning that similar extinction coefficients were found during the Indian Ocean Experiment (INDOEX, tropical Indian Ocean south of India, Franke et al., 2003) and the Asian Aerosol Characterization Experiment (ACE Asia, eastern

Asia off the Chinese coast, Redemann et al., 2003). Asian pollution plumes caused mean extinction coefficients of the order of 100 - 550  $\text{Mm}^{-1}$  at 500 - 550 nm several hundreds (ACE Asia) to several thousands of kilometers (INDOEX) away from the industrial source regions. Seasonally averaged PBL extinction coefficients are larger with values of 130 - 150  $\text{Mm}^{-1}$  over the eastern part of the United States during the summer months (Holben et al., 2001) and lower (50 - 60  $\text{Mm}^{-1}$ ) over the rural Oklahoma (Turner et al., 2001). Such low values were also observed during ACE 2 (southern Portugal, Ansmann et al., 2001).

Figure 2 shows the three-year mean height profiles of the particle extinction coefficients. Error bars indicate the standard deviation caused

by atmospheric variability. The mean extinction coefficients decrease approximately exponentially with height. The smaller scale height of 1100 m for the wavelength of 355 nm, compared to the scale height of 1600 m for 532 nm, results from the strong extinction of 355-nm radiation in the lowermost 700 m (close to the sources of new particles and precursor gases). Small particles scatter radiation at 355 nm much stronger than light at 532 nm.

dominate the wavelength dependence of light extinction in the PBL (Ångström values are around 1.6 in the 1.2-2.6-km height range) whereas Saharan dust and aged smoke determine the spectral slope of the extinction coefficient in the middle free troposphere. Both aerosol types, aged smoke and dust, cause a low Ångström exponent of 0.5-1 up to 7-8 km height. Ångström exponents above 7-8 km height increase again towards values for the free tropospheric background (sulfate)



In Figure 2, the maximum extinction coefficients ever measured during the EARLINET period are included to give an impression of the full range of observed extinction coefficients. The maximum values do not belong to one measured profile. Rather, they were determined from the data that are available for each height bin of 60 m. Urban particles (in combination with high humidities) were responsible for the maximum values at heights < 2 km, whereas Saharan dust caused the highest values in the free troposphere > 2-km height.

The Ångström exponent shown in Figure 2 is simply calculated from mean values of the extinction coefficients at 355 and 532 nm. As a result of this computation, the extinction-weighted mean Ångström exponent rather than the mean Ångström exponent which is calculated from the individual Ångström exponent profiles (as shown in Figure 1d) is obtained. The difference between these two mean values is however small (< 0.3 above 1200 m) in the present case. Urban particles

aerosol. The large, extinction-weighted Ångström values > 2.5 in Figure 2 must be handled with caution. A few very strong scattering events can dominate the result.

Figure 3 shows the 532-nm particle optical depth of the PBL calculated from the mean extinction coefficients in Figure 1c and the PBL depth in Figure 1a. Also shown is the contribution of the PBL particle optical depth to the total tropospheric particle optical depth at 532 nm. The troposphere is defined here as the height range from the surface to 12-km height. In addition, the daytime mean 532-nm particle optical depths determined from the AERONET Sun photometer are presented. To obtain values for 532 nm we applied the Ångström exponents computed from the AERONET measurements at 440, 500, 670, and 870-nm wavelength to the observed 500-nm optical depths. Quality assured, cloud screened AERONET data for the IFT Leipzig station are available for the period from May 2001 to December 2002.

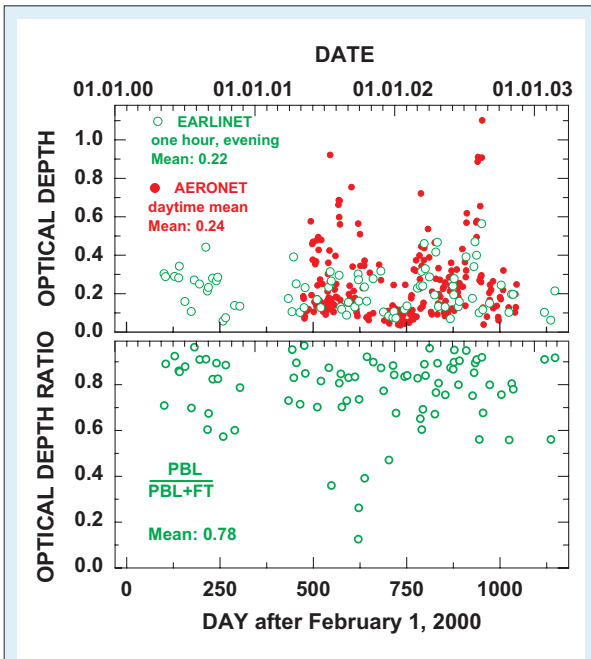


Fig. 3: 532-nm particle optical depth measured with EARLINET lidar (open green circles) and AERONET Sun photometer (solid red circles) and ratio of the PBL particle optical depth to the total particle optical depth derived from the lidar data.

Both, AERONET and EARLINET data show a strong variability of the optical depth during the summer half years of 2001 and 2002 and a comparably low variability and a lower mean optical depth in the winter of 2002. This behavior may reflect a significant influence of agricultural activities especially during the spring and fall seasons, strong washout events and larger humidity effects on particle growth during the summer half year as suggested by Weller et al. (1998) and recent investigations at our institute. Forest fires in southern Europe accumulating in late summer and arctic haze events in spring 2002 also have contributed to the large variability of the optical depth in the summer half year 2002.

Concerning the AERONET data it must be mentioned that about 40% of the 227 daytime mean values shown here are calculated from less than 10 observations usually taken within two hours. More than 30 and 60 observations per day are possible in late winter (February) and in summer (May to August), respectively. Days with a low frequency of observations indicate that clouds and thus humid conditions prevailed. The maximum value of the particle optical depth observed with Sun photometer decreases to 0.68 at 532 nm if we

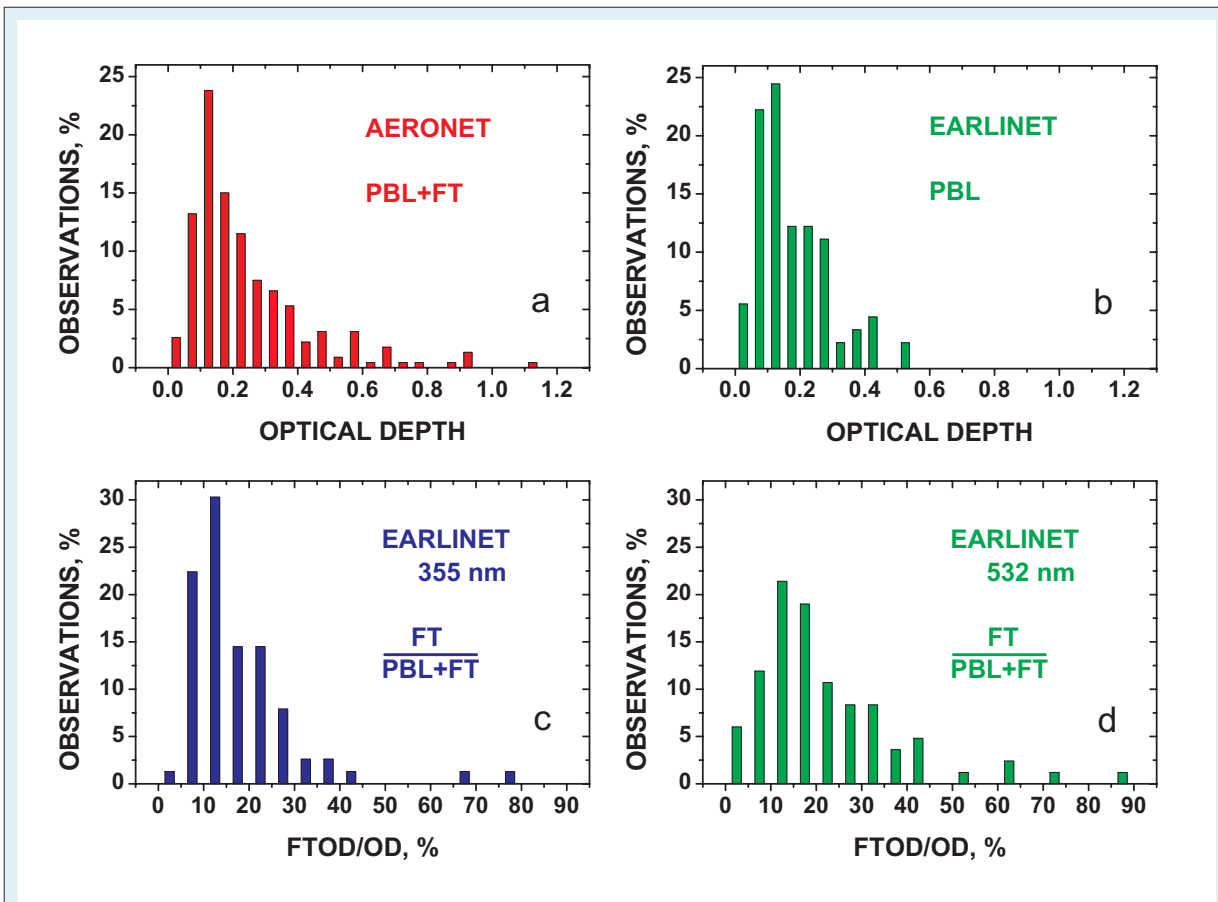


Fig. 4: Frequency of occurrence of (a) 532-nm particle optical depth observed with the AERONET photometer, (b) PBL particle optical depth, (c) ratio of the free tropospheric particle optical depth to the total particle optical depth at 355 nm, and (d) same as (c) except for 532-nm wavelength. (b)-(d) are derived from EARLINET lidar observations.

omit these days with observations  $< 10$ . However, even under clear-sky conditions as suggested by a high frequency of observations (more than 30-40 per day) often a clear anticorrelation between optical depth and Ångström exponent (440-870 nm, variations  $< 20\%$ ) is visible in the cloud-screened time series. Thin cirrus fields may have caused this effect.

The ratio of the PBL optical depth at 532 nm to the tropospheric particle optical depth ranged from 0.12 to 0.98 (cf. Figure 3). Values  $< 0.6$  indicate strong Saharan dust events. PBL particles contribute more than 80% to the total particle optical depth of the troposphere in almost 60% of all cases.

Figure 4 presents histograms of the total 532-nm optical depth (AERONET), the lidar-derived 532-nm PBL optical depth, and the ratio of the free tropospheric optical depth to the total tropospheric particle optical depth for the two measurement wavelengths. The free troposphere extends from the PBL top to 12-km height. The lidar-derived mean PBL particle optical depth and mean tropospheric particle optical depth for the EARLINET period (May 2000 to March 2003) are 0.18 (0.12 standard deviation) and 0.22 (0.11 standard deviation), respectively. The same mean values hold for the shorter AERONET period (May 2001 to December 2002). The mean value of the total particle optical depth calculated from the AERONET data in Figure 4 is 0.24 (0.18 standard deviation). Lidar observations indicate an almost negligible contribution ( $< 0.01$ ) of stratospheric particles to optical depth.

The contribution of light extinction by free tropospheric particles to the total tropospheric optical depth was, on average, 22% at 532 nm and 17% at 355 nm over Leipzig during the three-year period. The mean value of the optical depth ratio is higher at 532 nm because of the dominant influence of desert dust in the free troposphere (similar extinction coefficients at 355 and 532 nm) and the dominant influence of urban particles in the PBL (comparably large 355-nm extinction coefficients).

In agreement with our observations, the ratio of the free tropospheric optical depth to the total optical depth over Hamburg and other EARLINET stations at latitudes  $> 50^\circ$  N was found to be close to 0.2 at 351-355 nm (Bösenberg et al., 2003). In contrast, Mediterranean EARLINET stations in southern Italy and Greece observed respective optical depth ratios of, on average, 0.3-0.4 (Bösenberg et al., 2003) because of the strong influence of Saharan dust on the aerosol optical properties in these regions.

### Optical haze properties at Leipzig: 1990-1994 versus 2000-2003

We compare our findings with aerosol parameters measured shortly after the unification of Germany. During this time significant parts of polluting industries were closed down in the former East Block countries and especially in the former German Democratic Republic. According to von Hoyningen-Huene et al. (1996) the seasonal mean optical depth (at 532-nm wavelength, derived from spectrally resolved Sun photometer observations) decreased from values of 0.35-0.4 in the summer of 1991 (June-August), to 0.3-0.35 in the winter of 1991-1992 (December-February), and then to values around 0.2 in the winter of 1992-1993. According to this extraordinary downward trend, the seasonal mean optical depth must have been 0.4-0.5 in the winter of 1990-1991 and thus more than a factor of two higher than the 2000-2003 average. The maximum three-month mean tropospheric particle optical depth was 0.41 at 550 nm at the Lindenberg Meteorological Observatory (Weller et al., 1998) during the 1986-1995 period. This maximum occurred in January-March of 1991.

By means of transmission measurements with a Helium Neon laser (wavelength of 632.8 nm) the particle extinction coefficient in the height range from 20-120 m was monitored along a slant path of 810 m in the downtown area of Leipzig from March 1990 to December 1992 (Uhlig and von Hoyningen-Huene, 1993, Stettler and von Hoyningen-Huene, 1994). Values of up to  $2700 \text{ Mm}^{-1}$  (at relative humidities below 90%) were measured in March 1991 (Uhlig and von Hoyningen-Huene, 1993). This corresponds to 532-nm extinction coefficients of  $> 3000 \text{ Mm}^{-1}$  at ambient conditions. We found maximum values of  $400 \text{ Mm}^{-1}$  at 532 nm according to Figure 2 during the EARLINET period. Ångström exponents of 1.0-1.2 (400 to 900 nm) measured with photometer in 1991 (before the Pinatubo eruption) were significantly lower than the respective Ångström exponents of 1.5 for the AERONET period (2002-2003). Large coarse mode particles (diameters  $> 1 \mu\text{m}$ ) still had a considerable influence on light scattering and extinction in 1991-1993.

The rapid decrease of the PBL mean extinction coefficient at 532 nm from 1991 to 1994 is illustrated in Figure 5. Several calculations were necessary for this figure. We first computed seasonal mean 532-nm particle extinction coefficients at the surface for ambient conditions. Stettler and von Hoyningen-Huene (1994) present monthly mean extinction values at 632.8 nm at dry conditions (0% relative humidity). We used the measured Ångström exponent of 1.15 to convert the extinction coefficients to values at 532 nm, and we

recalculated particle extinction at ambient conditions. For that we applied the same equation as used by Stettler and von Hoyningen-Huene (1994) to correct for the hygroscopic growth of particles. We assumed a relative humidity of 50% what leads to ambient extinction values a factor of 1.33 larger than the values for dry particles. In the next step, we calculated seasonal mean PBL extinction coefficients at 532 nm from the spectrally resolved optical depths measured with Sun photometer from summer 1991 to winter 1994/1995 (von Hoyningen-Huene, 1996). Here, we assumed the seasonal mean PBL heights of 950 m (winter), 1850 m (spring), 2450 m (summer), and 1300 m (fall) as determined from the EARLINET data set. By comparing the surface extinction values (for 532 nm and ambient conditions) with the photometer-derived PBL mean values for the overlapping time period from the summer of 1991 to the autumn of 1992 (six seasons) we estimated the ratio of the PBL mean to the surface extinction coefficient as a function of the season. Based on this analysis we divided the surface values by 2.4 (summer), 1.7 (spring and autumn), and 1.3 (winter) to estimate the PBL mean extinction coefficients from the surface extinction values (from the spring of 1990 to the autumn of 1992). The factors are in good agreement with Figure 2. The 2000-2003 mean extinction coefficient at the surface of  $170 \text{ Mm}^{-1}$  at 532 nm is a factor of 1.8 larger than the PBL mean value of  $94 \text{ Mm}^{-1}$ .

The resulting uncertainty in the PBL mean values for the time period from 1990-1994 caused by the estimates of the PBL heights, the fixed

humidity correction factor of 1.33 (50% relative humidity), and of the ratio of the surface extinction value to the PBL mean extinction value is estimated to be of the order of 50%. However, the obtained results are consistent with the optical depth measurements discussed above. We concluded that the mean optical depth over Leipzig in the winter of 1990/1991 must have been about 0.4-0.5. This value is in agreement with the respective PBL mean extinction coefficient of  $475 \text{ Mm}^{-1}$ . Multiplied with the assumed PBL height of 950 m we obtain a PBL optical depth of 0.45.

As can be seen in Figure 5, a drastic aerosol reduction occurred within a few years from 1991 to 1994. The winter mean value of the PBL extinction coefficient decreased exponentially with time and was a factor of almost five lower in 2002-2003 compared to the maximum in 1991. The winter value decreased by roughly a factor of three within four years. The summer values were a factor of 2-5 lower than the winter values in 1990-1994. Significant differences between summer and winter values are no longer observable in the EARLINET data (since 2000). The summer-1992 extinction values were already in the range of the 2000-2003 summer values.

## Summary

For the first time, a dual-wavelength aerosol Raman lidar was used for long-term monitoring of climate relevant aerosol optical properties. The lidar at the urban central European site Leipzig, Germany, is part of EARLINET, the first continental-scale aerosol lidar network. The three-year mean, planetary boundary-layer (PBL) extinction coefficients were  $191 \text{ Mm}^{-1}$  at 355 nm and  $94 \text{ Mm}^{-1}$  at 532 nm. The respective mean Ångström exponent (355-532-nm wavelength range) was 1.4. The PBL stretched, on average, to heights of 1300 m (winter half year) and 2350 m (summer half year). PBL mean particle optical depths were 0.38 (355 nm, 0.23 standard deviation) and 0.18 (532 nm, 0.11 standard deviation). Free tropospheric particles contributed 2%-88% to the tropospheric optical depth. The average was 17% (355 nm) and 22% (532 nm) in 2000-2003. Ångström exponents in the free troposphere of about one reflect the dominant influence of Saharan dust and aged smoke on the optical properties in this height range. The comparison of AERONET Sun photometer with EARLINET Raman lidar observations showed that the lidar observations are representative for the field site. Comparisons with observations of particle optical properties in 1990-1994 clearly indicate a remarkable reduction of haze pollution over urban areas in eastern Germany since the unification of Germany.

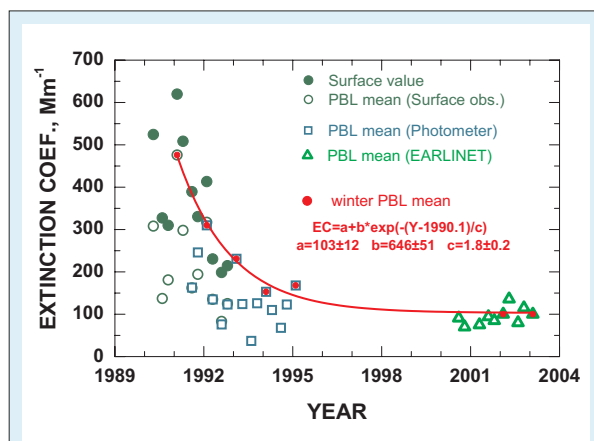


**Fig. 5:** Temporal development of the seasonal mean PBL particle extinction coefficient at 532 nm. The PBL mean extinction coefficient is estimated from combined photometer/surface observations (open circles, 1990-1992), from photometer observations (open squares, 1991-1994), and from lidar observations (open triangles, 2000-2003). Extinction values observed close to the surface are shown for comparison (closed circles). The exponential fit (EC) of the winter values (indicated by red dots) illustrates the rapid decrease of the haze. Fit parameters are included in the plot.  $Y$  denotes the year.

## References

- Ansmann, A., Wagner, F., Althausen, D., Müller, D., Herber, A. and Wandinger, U. 2001.** European pollution outbreaks during ACE 2: Lofted aerosol plumes observed with Raman lidar at the Portuguese coast. *J. Geophys. Res.*, **106**, 20725-20734.
- Bösenberg, J., et al. 2003.** *EARLINET: A European Aerosol Research Lidar Network to establish an aerosol climatology*. Report 348, Max-Planck-Institut für Meteorologie.
- Franke, K., Ansmann, A., Müller, D., Althausen, D., Venkataraman, C., Reddy, M. S., Wagner, F. and Scheele, R. 2003.** Optical properties of the Indo-Asian haze layer over the tropical Indian Ocean. *J. Geophys. Res.*, **108**, doi: 10.1029/2002JD002473.
- Holben, B., et al. 2001.** An emerging ground-based aerosol climatology: Aerosol optical depth from AERONET. *J. Geophys. Res.*, **106**, 12067-12098.
- Intergovernmental Panel on Climate Change (IPCC), 2001.** *Climate Change 2001: The Scientific Basis*, J. T. Houghton, Cambridge University Press, New York, 1, 896 pp.
- Hoyningen-Huene von, W., Stettler, M. and Weller, M. 1996.** Determination of climate-relevant aerosol parameters in the vicinity of an industrial region in eastern Germany. *Meteor. Z.*, **5**, 269-278.
- Redemann, J., Masonis, S. J., Schmid, B., Anderson, T. L., Russell, P. B., Livingston, J. M., Dubovik, O. and Clarke, A. D. 2003.** Clear-column closure studies of aerosols and water vapor aboard the NCAR C-130 during ACE-Asia, 2001. *J. Geophys. Res.*, **108**, 27485-27495, doi: 10.1029/2003JD003442.
- Stettler, M. and von Hoyningen-Huene, W. 1994.** Three years of aerosol extinction measurements with a He-Ne-Laser in the urban boundary layer of Leipzig, Germany. *Contr. Atmos. Phys.*, **67**, 169-180.
- Turner, D. D., Ferrare, R. A. and Brasseur, L. A. 2001.** Average Aerosol Extinction and Water Vapor Profiles Over the Southern Great Plains. *Geophys. Res. Lett.*, **28**, 4441-4444.
- Uhlig, E.-M. and Hoyningen-Huene, W. v. 1993.** Correlation of the atmospheric extinction coefficient with the concentration of particulate matter for measurements in a polluted urban area. *Atmos. Res.*, **30**, 181-195.
- Weller, M., Schülz, E., Leiterer, U., Naebert, T., Herber, A. and Thomason, L. W. 1998.** Ten years of aerosol optical depth observation at the Lindenberg Meteorological Observatory. *Contr. Atmos. Phys.*, **71**, 387-400.

### Funding

- EU (EARLINET)

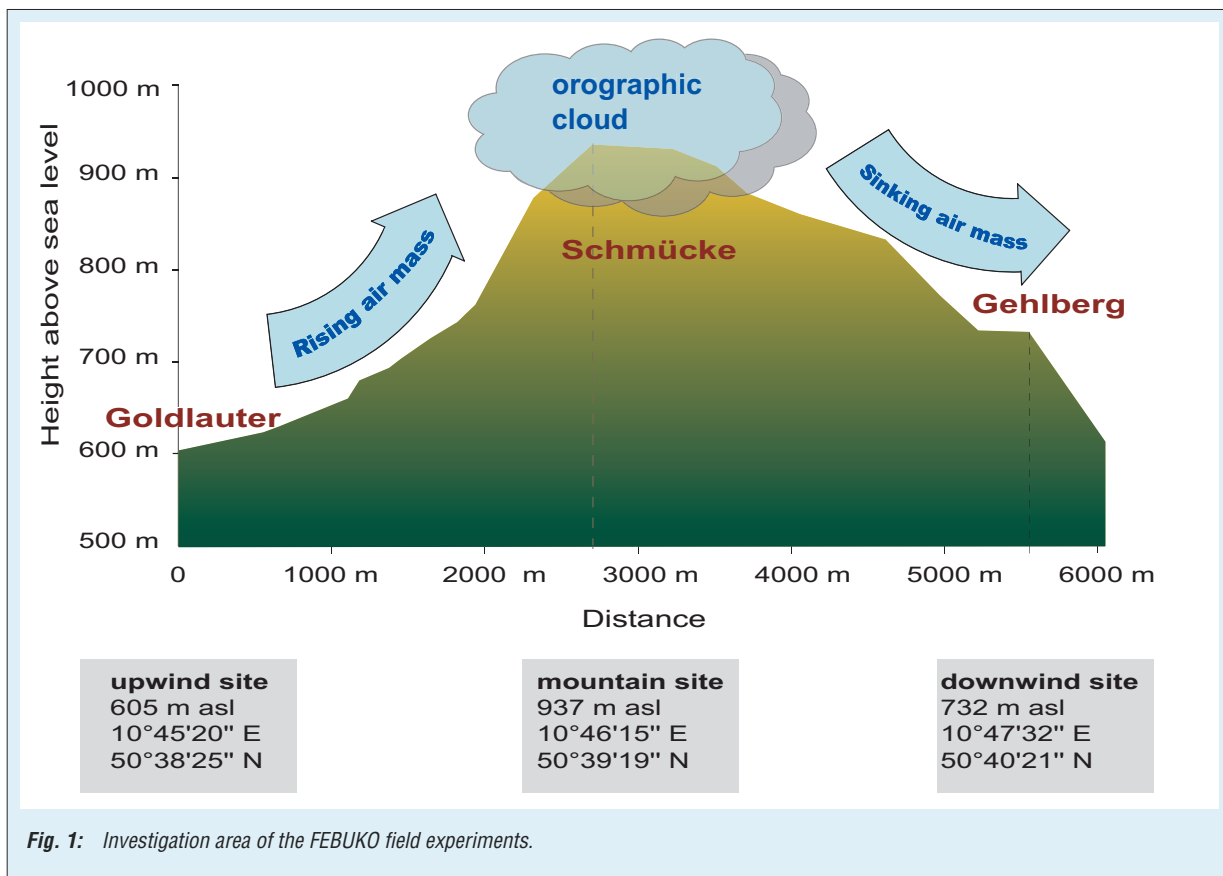
### Cooperation

- EARLINET-Consortium

## A coupled field and modelling study on aerosol cloud interaction (AFO 2000 projects FEBUKO (FKZ 07ATF01 - 395) and MODMEP (FKZ 07ATF40))

Erika Brüggemann, Renè Chemnitzer, Karoline Diehl, Diane Galgon, Thomas Gnauk, Bernd Heinold, Hartmut Herrmann, Diana Hofmann, Oswald Knoth, Katrin Lehmann, Zoltan Majdik, Andreas Maßling, Stephan Mertes, Konrad Müller, Andreas Nowak, Dominik van Pinxteren, Antje Plewka, Carsten Rüd, Kathrin Schwirn, Aissa-Mounir Seheli, Martin Simmel, Andreas Tilgner, Alfred Wiedensohler, Ralf Wolke, Sabine Wurzler

Das FEBUKO/MODMEP-Projekt innerhalb des AFO-2000-Programmes soll das Verständnis der troposphärischen Multiphasenprozesse und im Besonderen die Wechselwirkungen des Aerosols mit Wolken mit besonderem Augenmerk auf organische Partikelbestandteile verbessern. Innerhalb zweier Feldkampagnen (2001 und 2002) wurde ein experimenteller Datensatz von meteorologischen Parametern, Spurengaskomponenten, Wolkenparametern, physikalischer und chemischer Partikelcharakteristika, Wolkenwasser- sowie interstitielle Aerosol- und Tropfenresiduen-Chakterisierungen zur Verfügung gestellt. Mittels des SPACCIM-Modells werden Wolkendurchgänge eines Luftpaketes, welches einer Trajektorie von der Luv-Station zur Bergstation (Wolke) folgt, simuliert. Ein Vergleich zwischen gemessenen und modellierten Konzentrationen an der Bergstation ist für einige Spezies gut, für andere ergeben sich größere Differenzen. Das SPACCIM-Model wird weiterentwickelt und Simulationen von Luftpaketen von der Luv-Station, passierend die Bergstation, bis zur Lee-Station sind geplant.



### Introduction

The FEBUKO/MODMEP research cluster within the AFO 2000 programme will improve the understanding of tropospheric multiphase processes and especially the interaction of aerosols and clouds with an emphasis on organic particle constituents. Field experiments on aerosol and cloud chemistry and physics, model development

and model application are combined to investigate chemical and physical transformation of particles within a cloud passage.

The main focus of the FEBUKO field studies is to lay the groundwork for the further development of tropospheric cloud chemistry models, which may also serve as the basis for mechanism development for the tropospheric aqueous aerosol. A complex experimental data set was provided by

two field campaigns. In MODMEP the development is directed towards a cloud module which combines a complex multiphase chemistry with detailed microphysics. The description of both is given by means of a high resolution size-resolved drop spectrum.

The FEBUKO experiments at the three research sites in the Thüringer Wald (Goldlauter, Schmücke and Gehlberg) were carried out in the autumn of 2001 and 2002, respectively, to characterize the aerosol and cloud water with respect to their chemical composition and their physical properties (Figure 1). The speciation of organic components was one of the most important tasks for the different size classes of the particle phase and in cloud water. The air masses of the experimental region are of anthropogenically influenced origin which have been exposed to biogenic emissions on their way from the Rhein-Main area to the Thüringer Wald.

## Experimental

At the two valley measurement sites (Goldlauter (GL) – upwind site, 605 m asl., and Gehlberg (GB) – downwind site, 732 m asl) and at the mountain site (Schmücke (SM), 937 m asl) a set of meteorological parameters, trace gas components, cloud parameters and particle characteristics was determined. The sampling of particles using filter samplers and impactors for the chemical constitution measurements was carried out at the valley stations together with measurements of particle number concentrations, size distributions and hygroscopic properties. On top of a 20 m research tower a variety of different cloud water samplers were operated on the Schmücke. The interstitial aerosol and the cloud droplet residues were collected and physically characterized by means of a counterflow virtual impactor (CVI) and an inlet to interstitial particles (INT) as well.

The flow connection between the three stations is an important prerequisite for the whole experiment. Hence, special tracer experiments, measurements of number and size distribution of particles as well as trace gas concentrations were performed. In addition, the synoptic experimental conditions were carefully investigated and flow simulations for the complex terrain area are ongoing.

## Results and discussion

In both campaigns in 2001 and 2002 a total set of 14 cloud events was identified for intensive measurements. The most important conditions (i) connected flow, (ii) an orographic cloud, and (iii) good data coverage were best fulfilled during three events. The results within the present contribution

refer to a 15 hours measurement period on 26/27-October 2001 (22:00 to 13:00 UTC).

On the modeling side, at the time of writing of this contribution simulations were made with an air parcel travelling from Goldlauter to the top of the mountain into the orographic cloud. The goal of the simulations was to investigate the multiphase chemistry occurring in orographic clouds and to understand the interaction of particle phase and gas phase of atmospheric trace constituents due to phase transfer and chemical transformation. Simulation results have been compared with cloud water measurements in order to interpret the experimental data and for validation of the multiphase chemistry model.

## Physical aerosol characterization

**Particle number concentration.** Particle number size distributions were measured in GL and GB using a Differential Mobility Particle Sizer (DMPS) system. These measurements are complementary to the interstitial (INT) and Counter Flow Virtual Impactor (CVI) number size distribution measurements on the mountain station Schmücke (SM). In Figure 2, mean number size distributions at all sites are plotted for 27<sup>th</sup> of October 2001, 0:00 to 13:00 UTC. The black and green curves show the number size distribution measured in GL and GB while the red one represents the interstitial aerosol at the top of Schmücke in cloud. The peak number concentrations of the Aitken modes at GB and Schmücke are adjusted by a factor of 1.13 to the peak concentration at GL to recognize also small deviations. By this adjustment, the rising edge in the small particle size range between 25 and 60 nm of both curves are becoming identical

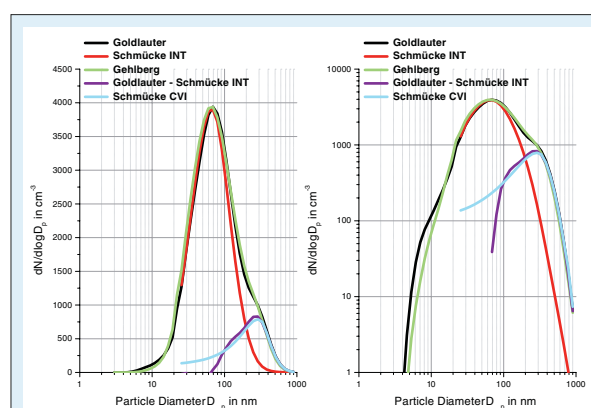


**Fig. 2:** Particle number size distributions at Goldlauter, Gehlberg and Schmücke on October 27, 2001. The black and green curves show the mean size distribution at Goldlauter and Gehlberg, respectively, whereas the red and light blue curves represent the interstitial and CVI size distributions. The size distributions of Schmücke INT and Gehlberg have been normalized to the level of Goldlauter by a factor of 1.13. Finally the dark blue curve shows the deviation between the Goldlauter and Schmücke INT size distribution.

not only qualitatively but also quantitatively. The mean number size distributions between GL and GB do not show a significant difference.

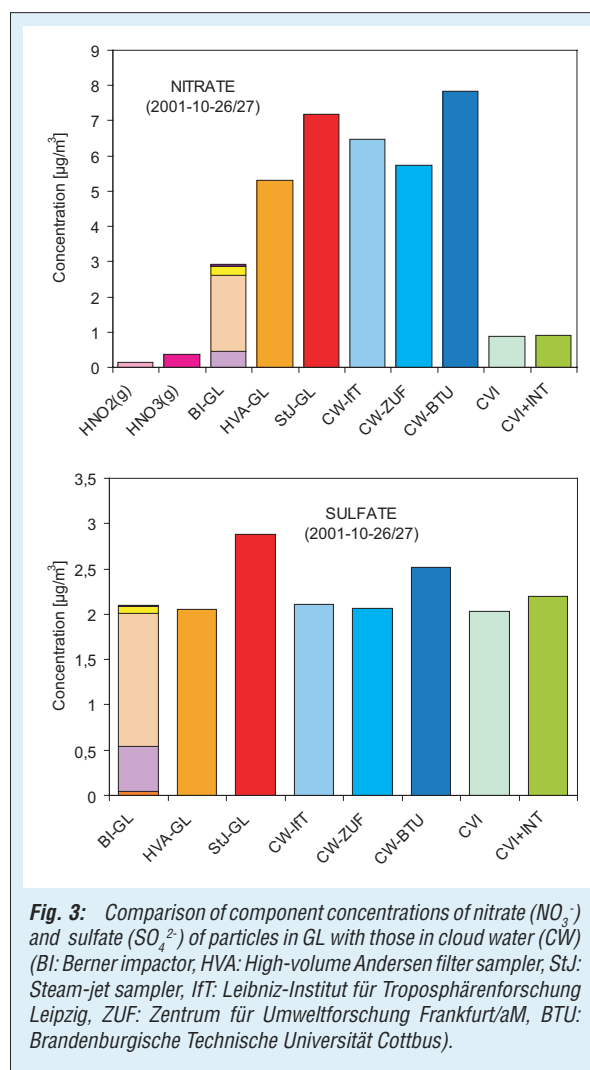
Mean number size distributions of the droplet residues (light blue) and interstitial particles (red) are shown. They have been measured in-cloud at SM during the cloud event in the size range between 25 and 900 nm by two DMPS systems attached to the CVI and INT inlet system. Particles larger than a certain size are expected to become activated, which is demonstrated by the deviation of both distributions above 70 nm. Figure 2 shows this difference (dark blue) and represents the indirect determination of the CCN number size distribution. This curve agrees well with the direct CVI measurement, which confirms that the phase partitioning due to the droplet activation is successfully observed during the connected flow between GL and SM.

**Hygroscopicity.** Hygroscopic growth of 50, 150 and 250 nm particles was measured using a HTDMA (Hygroscopic Tandem Differential Mobility Analyzer) at the GL site. The particles were humidified to 90% r.h. and grew toward larger diameters depending on their dry size and chemical composition. The spectra for 150 and 250 nm particles reveal a bimodal behaviour with an average growth factor (gf) around 1.1 for the more hydrophobic particles and a gf around 1.7 for the more hygroscopic particles. The hydrophobic particles are probably of a more regional origin whereas the more hygroscopic particles may have been aged corresponding to a longer range transport. Contrary to this the growth of larger particles 50 nm particles showed only one peak in the gf curve during this cloud event. The peak of the growth factor curve for 50 nm particles was found around 1.3. A possible reason for this single mode with a relatively small growth factor might be a stronger regional influence of anthropogenic emissions on particles in the mentioned size range.

### Chemical aerosol characterization

**Major ion concentrations.** About 90% of the particle ionic mass concentration consist of sulfate, nitrate, and ammonium. A comparison of nitrate and sulfate concentrations in size-segregating samples and in the sum  $PM_{10}$  in GL with those obtained by the averaging over different cloud water samples is presented in Figure 3 for all sampling techniques applied. In cloud water the sulfate concentration agrees reasonably well with the concentration in particles. A possible  $SO_4^{2-}$  production from GL to SM could be verified by comparing the  $SO_4^{2-}$  concentration of the GL aerosol (BI) with the concentration of cloud droplets and interstitial

aerosol particles (CVI+INT) at SM. A slight increase in sulfate concentration of about 5% was observed, within the error margin of the measurement but very well inline with the model findings (see below). Nitrate is clearly higher concentrated in the cloud droplets than in the particles sampled by Berner impactor, HVA filter sampler, droplet CVI, and INT. Only the nitrate concentration in particles sampling by the Steam-Jet collector agrees with that in cloud water. The sampling by Berner impactor shows also a difference in the ammonium concentration of particles to the one in cloud water. The difference of these samplers might be due to uptake and evaporation processes of gaseous and semivolatile compounds during collection.



**OC/EC concentration.** The total TC concentration summarized over all stages found at the GL station was  $2.1 \mu\text{g m}^{-3}$  consisting of  $1.1 \mu\text{g m}^{-3}$  OC and  $1.0 \mu\text{g m}^{-3}$  EC. The OC/EC ratio ranges from 0.7 on stage 2 (corresponding to 60% OC and 40% EC) to 2.6 on stage 5 (corresponding to 70% OC and 30% EC). The higher EC contribution on stage 2 is due to aged traffic emissions in the narrow valley and also partly due to direct domestic heating

emissions beginning at the end of October. The high OC proportion on stage 5 indicates biogenic coarse particles by abrasion of plant surfaces. Size-segregated OC/EC values from GL were used for initialization of the model describing the processes before entering cloud, during cloud passage on the top of the Schmücke and after evaporation of cloud droplets.

OC/EC concentrations in the cloud were estimated by CVI and INT, the sum of both should correspond to the GL particulate carbon. CVI + INT for EC ( $1.1 \mu\text{g m}^{-3}$ ) are in good agreement with the GL value, whereas CVI + INT for OC ( $2.8 \mu\text{g m}^{-3}$ ) exceed the GL value one and a half times. This may be a hint to phase transfer of organic compounds into the growing particles on their upwind way from GL to the Schmücke summit.

**Organic species incl. carboxylic acids.** In order to gain a deeper insight into budgets and conversions of specific organic compounds in tropospheric clouds and to have a realistic data set for the model initialisation, one of the aims of FEBUKO is a comprehensive organic speciation at all three measuring sites. Organics are usually trace compounds in different atmospheric phases which make their determination a challenging task. A variety of sampling devices was applied, some of them exclusively for organic speciation. With impactors, filters and spray collectors aerosol particles were sampled. Sorbent-filled cartridges were used for gas-phase measurements and four different types of cloud water samplers collected the liquid phase on the mountain. Most of the instruments give time-resolved information about organic concentration levels with a sampling time interval of 2 hours. Complementary to this the impactors allow insights into the size distribution of condensed organic material before and after cloud processing. After the campaign the samples were analysed using analytical equipment like gas chromatography/mass spectrometry (GC/MS), high performance liquid chromatography/mass spectrometry (HPLC/MS) or capillary electrophoresis (CE).

With this described field measurement equipment it was possible to create an extensive pool of data for dozens of organic substances in their respective most relevant atmospheric phases. Aliphatic and aromatic aldehydes and ketones as well as other volatile organic compounds (VOCs) like short-chain alkanes, alkenes, and volatile aromatics could be identified and quantified in the gas phase on a time-resolved basis. Depending on their polarity some of them can be scavenged by the cloud and therefore they were measured also in the liquid phase. The possible photooxidation products of carbonyls and VOCs such as higher oxygenated species like monocarboxylic acids

in the gas phase and in cloud water and dicarboxylic acids in the particle phase and in cloud water were analysed in a time-resolved manner. Size distributions before and after the cloud passage as well as the corresponding liquid-phase concentrations are as well available for lower vapour pressure compounds such as long-chain alkanes, alcohols, sugars, fatty acids, dicarboxylic acids, and several biogenic compounds such as pinonaldehyde, squalene, and others. Bulk concentrations from filters for interstitial particles allow us to calculate directly the in-cloud scavenging for some of these compounds.

This complex data set is of great importance for the MODMEP model initialisation and validation. Besides, we can interpret it by comparing, correlating and balancing concentrations of selected species for different atmospheric phases, different times and different particle sizes. In combination with the model results we may now be able to achieve a better understanding of phase partitioning and chemical multiphase processes of tropospheric organic material.

In Figure 4 comparison for the example of oxalic acid concentration measured by Berner impactor (BI) and spray collector with the respective cloud water content is presented. The oxalic acid concentration of particles from BI show lower values than measured by spray collector and in the cloud water much higher concentrations. This might be due to uptake and evaporation processes of gaseous oxalic acid during impactor sampling. Oxalic acid present in the gas phase is on the one hand unlikely because of the low vapour pressure of dicarboxylic acids on the other hand it cannot be fully ruled out as an explanation for the observed phenomena. This issue is controversially discussed in literature, see Saxena and Hildemann, (1996) and Limbeck et al., (2001).

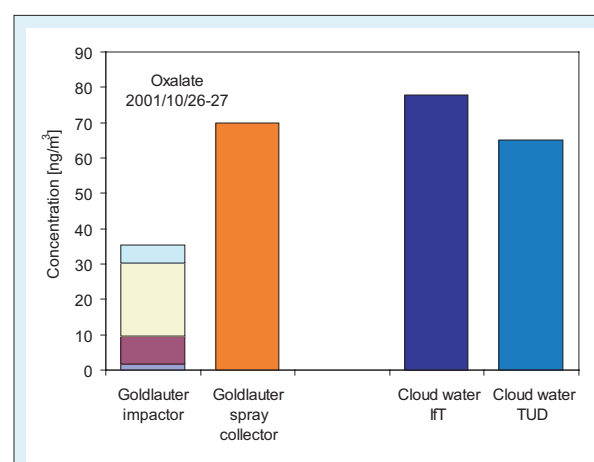


**Fig. 4:** Comparison of different oxalate measurements (impactor: size-segregated) for 2001/10/26-27 (TUD: Technische Universität Darmstadt).

## Model initialization

The model developed within the course of the MODMEP project is initialized by means of the particle composition based on measurements with a five stage Berner impactor at the upwind site GL as described before. In the case of the cloud event on the 27<sup>th</sup> of October 2001, most of the mass was found on the third impactor stage, which collects aerosol particles with a diameter between 0.42  $\mu\text{m}$  and 1.2  $\mu\text{m}$ . Nitrate, sulfate, ammonium, organic and elementary carbon are the main components of the aerosol. In order to correct for losses encountered by the Berner impactor in the case of chloride and nitrate, data obtained with the Steam Jet sampler were used and distributed over the impactor stages according to the relative size distribution of each of these species derived with the Berner impactor. The alkaline and earth alkaline metal initial concentrations, i.e. sodium, magnesium, calcium and potassium, are taken from the Berner impactor. Other metal ion concentrations, i.e. manganese, iron, copper, aluminium and zinc, are initialized according to measurements made with a High-Volume-Sierra-Anderson ( $\text{PM}_{10}$ ) sampler. These measure total contents are distributed over the impactor stages as the mass determined by the impactors. The initialization of the dicarboxylic acids is based on impactor and spray collector measurements. To calculate the water mass of the Goldlauter, aerosol growth factors were used. The used growth factors were measured during the ACE2 campaign, and are in a good agreement with the measured growth factors by a HTDMA analyzer within the FEBUKO field campaign.

In the gas phase  $\text{NO}$ ,  $\text{NO}_2$ ,  $\text{O}_3$ , and  $\text{SO}_2$  were measured every 5 seconds with commercial instruments. For the measurement of  $\text{HNO}_2$  and  $\text{HNO}_3$  the wet effluent diffusion denuder technique was used. The measured organic species were implemented as stand-alone species or were lumped together into groups as used in the regional atmospheric chemistry mechanism RACM. Implemented stand-alone species are: formaldehyde, ethane, ethene, formic acid, glyoxal, methylglyoxal, and isoprene. Measured lumped gas phase species considered are aldehydes, ketones, unsaturated monoaldehydes, acetic acid and higher acids. For example 19 measured aldehydes were summed up to the lumped species "ALD". For some unmeasured species initial concentrations were adapted from the CAPRAM standard scenario "urban" due to a reasonable agreement between measurements and the above-mentioned scenario.

Tracer experiments were carried out within the FEBUKO field campaign in order to verify the existence of a connected flow and to determine the

transport time between the three sampling stations. Based on the experiments a realistic transport time between Goldlauter and Schmücke of 10-20 minutes resulted, depending on meteorological conditions. For the initial wind speed data from the measurement site of the German weather service station located in Meiningen was used. For the cloud event on the 27<sup>th</sup> of October 2001 at 9.00 UTC an initial wind speed of 4  $\text{m}\cdot\text{s}^{-1}$  was applied, which led to a simulation time of about 11 minutes from the downwind site to the summit. For the simulations described here, a constant size-independent deposition velocity of  $1\cdot 10^{-3} \text{ s}^{-1}$  was considered.

## Coupled time-integration of detailed microphysics and complex multiphase chemistry in a size resolved cloud box model

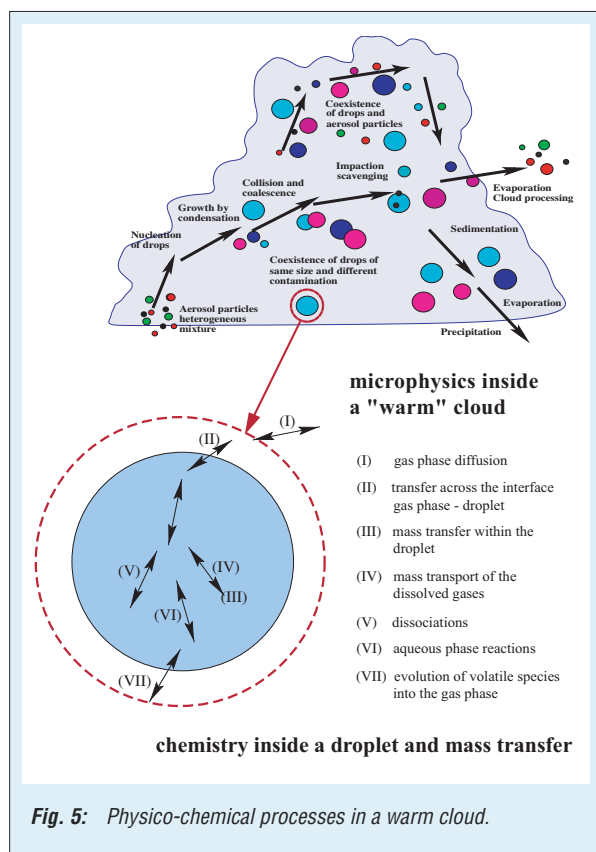
To better understand the interaction, effects and evolution of the different physico-chemical processes taking place in the atmosphere their modeling requires a detailed description of all transformations with equal rigor. The most recently available models focus either on detailed microphysics or complex multiphase chemistry. In the framework of the joint AFO2000-project MODMEP the air parcel model SPACCIM ("SPectral Aerosol Cloud Chemistry Interaction Model") was developed for the description of cloud processes by coupling complex multiphase chemistry and detailed microphysics. The description of both process groups is given for a size-resolved particle/drop spectrum. Either the movement of the air parcel can follow a predefined trajectory (e.g., simulated by a 3D atmospheric model) or the vertical velocity is calculated based on the parcel updraft compared to prescribed environmental conditions such as vertical profiles of temperature and humidity from the regional model system LM-MUSCAT. Entrainment and detrainment processes are included in a parameterized form. The model allows a detailed description of the transformation of gases and particles shortly before cloud formation, during the cloud life time and shortly after cloud evaporation. The consideration of convective, stratiform and orographic clouds is possible depending on the dynamic forcing of the parcel.

## The physical and chemical processes

Figure 5 illustrates several pathways of the physico-chemical interactions inside a warm cloud. In a box model the mass balance equations for a size-resolved droplet spectrum are the governing ones. The particle/drop spectrum is described using a sectional approach. The prognostic microphysical variables for each bin are water mass, total

and soluble particulate mass as well as particle number. The model considers growth/shrinking and impaction of aerosol particles as well as nucleation, condensation/evaporation and collision-coalescence of drops as most important physical processes. One important feature of the model is the description of the water phase transfer feedback on water vapor and air temperature (latent heat release) which is done in an iterative way to avoid overestimation of super-saturation (and, therefore, nucleation) especially at cloud base. The model accounts for the fact that larger aerosol particles do not have enough time to reach their equilibrium size at high relative humidities near 100% due to the faster changing environment.

A moving section version of the microphysical model was also implemented, motivated by the predominance of condensation/evaporation processes in some case studies.



The spectral multiphase chemistry model considers two types of chemical reactions:

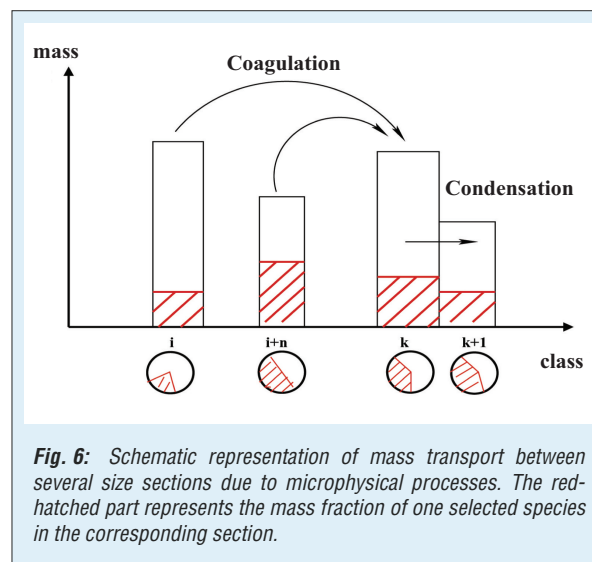
- Forward reaction types in gas and aqueous phase including photolysis and temperature dependent reactions,
- Equilibrium reaction types, considered as forward and backward reaction.

The phase transfer is parameterized by the Schwartz approach with the hypothesis of well mixed droplets.

The used mechanism (including phase transfer and kinetic constants) is given as an input file.

Therefore, a high flexibility concerning changes in the chemical mechanism or the replacement of the entire reaction system is allowed (Wolke et al., 2001). The performance of the model was shown for simple chemical test mechanisms (with only inorganic chemistry) as well as for very complex mechanisms of the CAPRAM family which contain descriptions of particle phase organic chemistry in a varying degree of complexity dependent of the CAPRAM version.

**Coupling scheme.** The model variables can be grouped into microphysical variables, chemical variables and mass fluxes between different particle/droplet classes caused by microphysical exchange processes (e.g., by aggregation, break up, condensation). These mass fluxes are schematically shown in Figure 6. When two particles coagulate, for instance, their masses are added to the resulting particle class assuming internally mixed aerosol in each class. The implemented processes have been described earlier.



The feedback of changes in the chemical composition by gas scavenging and chemical reactions on microphysical processes (e.g., water condensation growth rates via changes in surface tension and the Raoult term) is also implemented, see Figure 7. The activation of droplets is explicitly described in the microphysical model.

The time integration scheme for solving the multiphase problem is based on the multistep implicit method (Backward Differentiation Formula) widely used for the integration of stiff differential equations. In our approach, the resulting linear sparse systems are solved exploiting the properties of the Jacobian (sparsity, block structure, different types of coupling). An approximate matrix factorization to decouple the microphysical transport terms and the other parts of the Jacobian is possible. This is seen as an operator splitting at

the linear algebra level and yields a computing gain (Wolke and Knoth, 2002). In addition to the higher order BDF scheme, the non-autonomous second order Rosenbrock method is implemented, presenting a low computing effort and showing a satisfactory accuracy. The model SPACCIM is evaluated with data from the FEBUKO field campaign and other case studies from literature. It offers several parameter setups allowing sensitivity studies to reach optimal runs for each studied case.

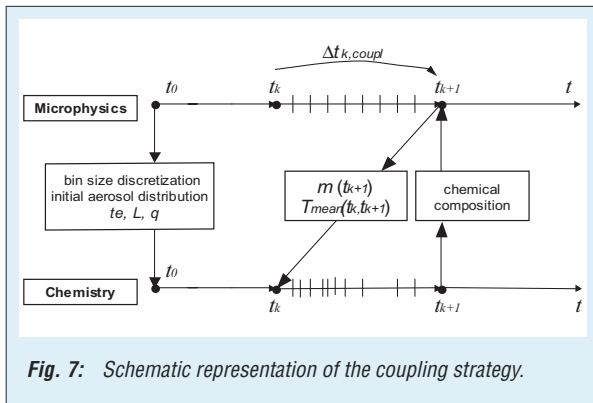


Fig. 7: Schematic representation of the coupling strategy.

**Microphysical model results.** Figure 8 shows the cloud liquid water content (LWC, left) and drop number concentration (right) on Schmücke for the event 26/27<sup>th</sup> of October 2001. The model calculates the LWC adiabatically which leads to an overestimation of about 25% compared to the findings of the three different measurements carried out. The time dependent structures are represented rather well.

In contrast to the LWC drop number depends on transport time from Goldlauter to Schmücke. Two model cases (red line: slow transport, green line: fast transport) are compared with measurement data. Drop number highly depends on the vertical velocity and, therefore, super-saturation especially at cloud base. The faster the transport and the

higher the vertical velocity, the higher is the super-saturation and the more drops are activated. High LWC corresponds to a low cloud base and a rather gentle terrain (compare Figure 1) connected with weak updrafts leading to the lowest drop numbers in the model (2-4 UTC, 7-9 UTC). The opposite is true for low LWC: steep orography with high velocities leads to (unrealistically) higher drop numbers in the model (4 UTC, 6 UTC, 11-13 UTC). These strong variations in the modeled drop numbers are not reflected by the experimental data where drop numbers are rather constant between 400 and 600  $\text{cm}^{-3}$ .

Generally, drop numbers fit very well with the experimental findings for LWCs above 0.4  $\text{g m}^{-3}$ , corresponding to a rather low cloud base. For lower LWCs the model seems to overestimate the vertical velocity and, therefore, super-saturation and activation.

**Simulations with the coupled chemistry microphysics model SPACCIM and CAPRAM**

By means of SPACCIM, simulations of the hill cap cloud passage experiment taken place on 27<sup>th</sup> of October 2001 were carried out. Calculations with an air parcel following a trajectory from the upwind site to the summit station Schmücke were performed. The simulation results have been compared to experimental data from the summit station.

The applied explicit aqueous phase radical mechanisms consist of CAPRAM 2.3 (Herrmann et al., 2000) and CAPRAM 2.4 (MODAC-mechanism, Ervens et al., 2003). The gas phase chemistry is described by the regional atmospheric mechanism RACM (Stockwell et al., 1997). Phase transfer processes are treated by means of the resistance model of Schwartz considering Henry's equilibrium, gas phase diffusion and mass accommodation. For the simulations a highly resolved particle spectrum is considered. A total number of 64 size bins

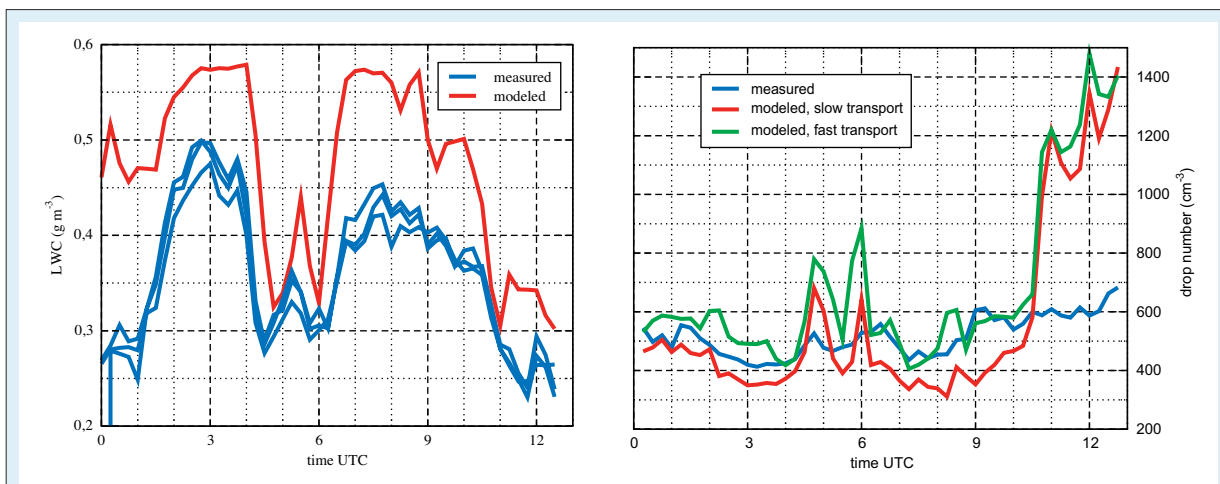
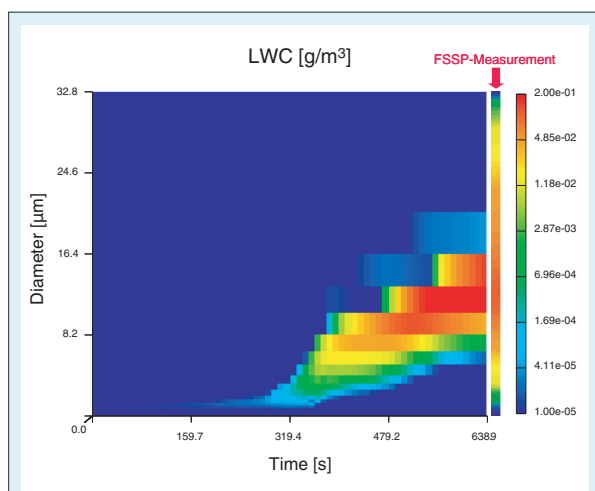


Fig. 8: Cloud liquid water content (LWC, left) and drop number concentration (right) on Schmücke for 2001-10-26/27.

( $2.3 \cdot 10^{-3} \mu\text{m} < d < 7.5 \cdot 10^3 \mu\text{m}$ ) is considered, where multiphase chemistry occurs in droplets where the LWC exceeds  $1 \cdot 10^{-9} \text{ g m}^{-3}$ . In the near future a feedback from the chemistry to the microphysics will also be implemented.

For the initial wind speed data from the measurement site of the German weather service station located in Meiningen was used. For the cloud event on 27<sup>th</sup> of October 2001 at 9:00 UTC an initial wind speed of  $4 \text{ m s}^{-1}$  was applied, which led to a simulation time of about 11 minutes from the upwind station to the summit. For the simulations a constant deposition velocity of  $1 \cdot 10^{-3} \text{ s}^{-1}$  was considered.

**Simulation results.** For the respective cloud event on 27<sup>th</sup> of October 2001 the exact time for the simulations was fixed at 9:00 UTC due to a good agreement between the microphysical model and the measurement with regards to the total LWC and number concentration. At the upwind station a LWC of about  $1 \cdot 10^{-4} \text{ g m}^{-3}$  exists. At the summit station the total LWC will reach a value of  $4.9 \cdot 10^{-1} \text{ g m}^{-3}$ . At the end of the simulation, at the top of the mountain most of the LWC will be in the droplets with a diameter between 8 and 16  $\mu\text{m}$ . The maximum of the LWC distribution, as can be seen from Figure 9, occurs at droplets with a diameter of circa 12  $\mu\text{m}$ . In Figure 9 also the LWC spectra measured by an FSSP (Forward Scattering Spectrometer Probe) is plotted. It can be seen that the measured spectrum of the orographic cloud is broader than the calculated spectra. This discrepancy could be caused by a too broad spectra produced by the FSSP a too narrow spectrum resulted from the microphysical model or a combination of both. Activation of the aerosol particles will occur after a simulation time of about 300 s.



**Fig. 9:** Size and time dependent evolution of the LWC between the upwind and summit station, comparison between measurement and simulation result at Schmücke.

In Figure 10 the size-resolved sulfate concentration is represented. The concentration profile represents the sum of sulfate concentration over the size bins with a diameter bigger than 3.5  $\mu\text{m}$ . At the summit the concentration was measured with a cloud water bulk collector. The collector had sampled cloud droplets with a diameter bigger than 3.5  $\mu\text{m}$ . At the summit the calculated  $\text{SO}_4^{2-}$  concentration reached a value of  $4.1 \cdot 10^{-5} \text{ mol l}^{-1}$ ,  $\text{HSO}_4^-$  a value of  $3.8 \cdot 10^{-7} \text{ mol l}^{-1}$  and  $\text{H}_2\text{SO}_4$  a value of  $1.6 \cdot 10^{-12} \text{ mol l}^{-1}$ . As can be seen from the plot there is a good agreement between the calculated and measured value. As expected, due to uptake of liquid water the concentration decreases in time. At the summit, in the small droplets with less water content there will be a high sulfate concentration. In the small interstitial aerosol particles the sulfate concentration reaches values of about  $2 \cdot 10^{-1} \text{ mol l}^{-1}$ . In the size range where most of the liquid water can be found a sulfate concentration of circa  $5 \cdot 10^{-5} \text{ mol l}^{-1}$  occurs. Analyzing the sources of sulfate, it can be said that sulfur oxidation proceeds mainly via the oxidation of bisulfite by hydrogen peroxide (R1). Before activation, in the small droplets sulfur oxidation via aqueous phase radical chemistry involving transitional metal ions as well plays a role. At the final stage of this radical pathway sulfate is formed by the reduction of  $\text{SO}_4^-$  by  $\text{Fe}^{2+}$  (R2).

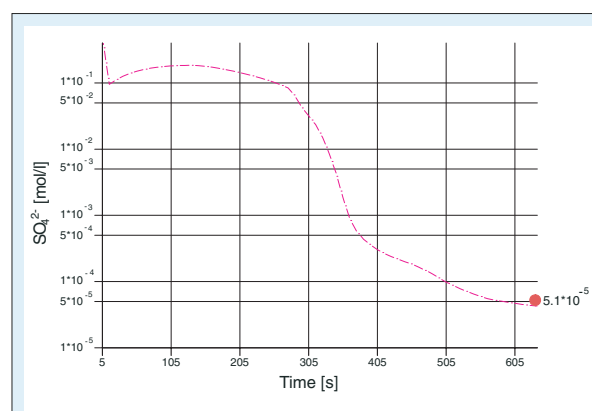
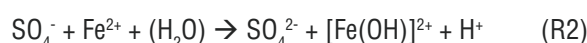
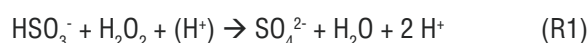


**Fig. 10:** Size-resolved  $\text{SO}_4^{2-}$  concentration profile, comparison between measurement and simulation result at the summit, the red point representing the experimentally determined value.



Sulfate production will be controlled by the  $\text{SO}_2$  uptake from the gas phase, process significantly influenced by the pH value. The model exactly reproduces the measured  $\text{H}^+$  concentration of  $6.3 \cdot 10^{-5} \text{ mol l}^{-1}$  at Schmücke. The calculated hydrogen peroxide concentration at the summit station is about a factor of four higher than the

measured concentration. The main source of  $\text{H}_2\text{O}_2$  in the aqueous phase is uptake from the gas phase. The main sinks will be the reactions of  $\text{H}_2\text{O}_2$  with transition metal ions and  $\text{S(IV)}$ .

In the case of  $\text{Cl}^-$  at the summit a factor of two between the measured and calculated concentration exists. The model confirms the observation that in the droplets the  $\text{Cl}^-$  concentration increases due to uptake of  $\text{HCl}$  from the gas phase. In the gas phase, from Goldlauter to Schmücke the  $\text{HCl}$  concentration decreases from about 0.2 ppb to about  $1.6 \cdot 10^{-6}$  ppb.

Ammonia is the only atmospheric gaseous species of alkaline character. In the pH regime encountered here ammonia exists as the ammonium cation in aqueous solution after its phase transfer. There is a good agreement between the simulated concentration and the bulk cloud water collector value (Figure 11). In the gas phase the  $\text{NH}_3$  concentration decreases from circa 1 ppb to 3 ppt on the way from the upwind site to the summit station.

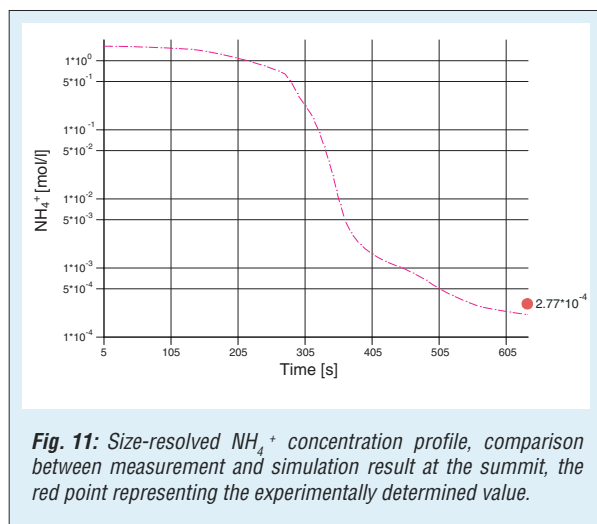


**Fig. 11:** Size-resolved  $\text{NH}_4^+$  concentration profile, comparison between measurement and simulation result at the summit, the red point representing the experimentally determined value.

Most of the  $\text{HNO}_3$  will dissociate to  $\text{H}^+$  and  $\text{NO}_3^-$ . The simulated  $\text{NO}_3^-$  and  $\text{HNO}_3$  concentration of  $1.6 \cdot 10^{-4}$  mol  $\text{l}^{-1}$  and  $1.5 \cdot 10^{-9}$  mol  $\text{l}^{-1}$ , respectively, is in relatively good agreement with the total measured  $\text{NO}_3^-$  and  $\text{HNO}_3$  concentration of  $2.1 \cdot 10^{-4}$  mol  $\text{l}^{-1}$ . Production of nitric acid and nitrate in the droplets occurs mostly by uptake of  $\text{HNO}_3$  from the gas phase. Another smaller source of  $\text{NO}_3^-$  is the aqueous phase decomposition of  $\text{N}_2\text{O}_5$ , where  $\text{N}_2\text{O}_5$  is an oxidation product of  $\text{NO}_2$  in the gas phase. In cloud droplets containing a mixture of oxidants and reductants the concentration of  $\text{Fe(II)}$  and  $\text{Fe(III)}$  is determined by the rates of the oxidation and reduction reactions taking place. During the day in the presence of sunlight, due to high  $\text{HO}_2$  concentrations,  $\text{Fe(II)}$  will be predominant. At the summit the calculated sum concentration of all iron species is  $1.1 \cdot 10^{-7}$  mol  $\text{l}^{-1}$ , with a factor of seven smaller than the measured concentration of

$7.5 \cdot 10^{-7}$  mol  $\text{l}^{-1}$ . The simulated  $\text{Fe(II)}$  concentration is  $7.4 \cdot 10^{-8}$  mol  $\text{l}^{-1}$ . About one third of the total iron is existing in form of iron-oxalate complexes. The main source of  $\text{Fe(II)}$  is the reduction of  $\text{Fe(III)}$  by copper. The main sink is the reaction with manganese and hydrogen peroxide. At the beginning of the simulation there is an  $\text{Fe(II)}$  production. After the activation the concentration decreases not just due to dilution, but also due to loss by chemical transformations. A possible explanation could be that at the beginning of the simulation there is a more efficient uptake of  $\text{HO}_2$  which reduces  $\text{Cu(II)}$  to  $\text{Cu(I)}$ .

Most of formaldehyde in the aqueous phase exists in its hydrated form. The total formaldehyde concentration at the summit is with about a factor of seven higher than the measured concentration (cf. Figure 12). At the beginning of the simulation the formaldehyde concentration is increasing. After approximately 200 s the concentration decreases from about  $2.5 \cdot 10^{-5}$  mol  $\text{l}^{-1}$  to  $5.0 \cdot 10^{-6}$  mol  $\text{l}^{-1}$ . After circa 350 seconds the concentration once again increases, at the end of the simulation reaching a value of  $2.5 \cdot 10^{-5}$  mol  $\text{l}^{-1}$ . It was modeled that when there is an increase in formaldehyde concentration, this increase is always accompanied by production of formaldehyde from methanol in the aqueous phase via the reactions R3-R5.

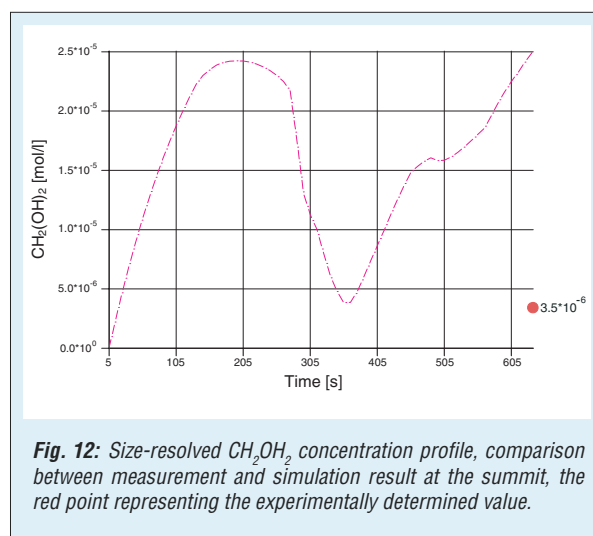
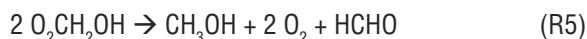


**Fig. 12:** Size-resolved  $\text{CH}_2\text{OH}_2$  concentration profile, comparison between measurement and simulation result at the summit, the red point representing the experimentally determined value.



It is also observed that formaldehyde is transported from the smaller into the bigger droplets. By reactions R3-R5 formaldehyde is produced in the small droplets followed by its phase transfer to the gas phase. At the same time formaldehyde released from the small droplets is taken up into the bigger droplets. The concentration

profile of acetaldehyde looks very similar to the formaldehyde concentration profile. In the case of oxalate and its possible precursor glyoxal, the measured concentration at the summit is higher with about a factor of 2 and 3, respectively. A further detailed analysis of the chemical conversions is ongoing at the time of writing of this article.

### Summary and outlook

The basic coupled version of detailed microphysics and a complex multiphase chemistry in a box model is realized, allowing a high flexibility concerning the use of chemical mechanisms and the simulation of case studies like the FEBUKO field experiment. The simulation of the latter experiments using SPACCIM and CAPRAM shows a reasonable agreement between the simulated and the measured results. There is still a sustainable effort of refinement and development of the model focusing essentially on issues such as the explicit description of deposition and emission. Currently a model with a two-component treatment of the microphysics (water and aerosol mass) is being included into SPACCIM. This allows drops of the same size to have different particulate contents and, therefore, different gas scavenging properties. In this way, the mixing state of the particles can be taken into account.

Table 1 contains a comparison between the measured and calculated concentrations at the summit station Schmücke. Whereas for some species there is a quite good agreement between the measurements and model results, with deviations below a factor of two, e.g.,  $\text{NO}_3^-$ ,  $\text{SO}_4^{2-}$ ,  $\text{K}^+$ ,  $\text{HCOOH}$ ,  $\text{CH}_3\text{COOH}$ , for other species, e.g.  $\text{Na}^+$ ,  $\text{Mg}^{2+}$ ,  $\text{Fe(II)-Fe(III)}$ ,  $\text{HCHO}$ , bigger differences, about one order of magnitude, were encountered. It has to be noted that some of the negative deviations are due to the fact that for the current model results the input aerosol size distribution is only considered for up to  $D_p = 900$  nm. A course mode treatment is under development and may lead to better agreement for species such as most of the cations.

For a better description of organic chemistry, simulations with the CAPRAM 2.5 mechanism will be conducted. The CAPRAM 2.5 mechanism consisting of the CAPRAM 2.4 (MODAC mechanism) reduced, coupled to the CAPRAM organic extension considers the oxidation of organic compounds with up to four carbon atoms. Also in the near future simulations with an air parcel traveling from the upwind site, passing through a hill cap cloud, and then transported to the downwind site will be carried out to better chemical modifications of the particle ensemble after a single cloud process under real field conditions.

Species	Measured concentration Date: 27.10.01 Time: 09.00 UTC	Calculated concentration CAPRAM 2.4 with depositions	relative difference [%]
$\text{NO}_3^-$	$2.1 \cdot 10^{-4}$	$1.6 \cdot 10^{-4}$	-23.8
$\text{HNO}_3$		$1.5 \cdot 10^{-9}$	
$\text{SO}_4^{2-}$	$5.1 \cdot 10^{-5}$	$4.1 \cdot 10^{-5}$	-18.9
$\text{HSO}_4^-$		$3.8 \cdot 10^{-7}$	
$\text{H}_2\text{SO}_4$		$1.6 \cdot 10^{-12}$	
$\text{Cl}^-$	$1.2 \cdot 10^{-5}$	$2.0 \cdot 10^{-5}$	+66.6
$\text{HCl}$		$4.5 \cdot 10^{-16}$	
$\text{H}^+$	$6.3 \cdot 10^{-5}$	$6.3 \cdot 10^{-5}$	0.0
$\text{OH}^-$		$3.4 \cdot 10^{-11}$	
$\text{NH}_4^+$	$2.8 \cdot 10^{-4}$	$2.0 \cdot 10^{-4}$	-28.6
$\text{NH}_3$		$4.3 \cdot 10^{-10}$	
$\text{Na}^+$	$1.7 \cdot 10^{-5}$	$9.6 \cdot 10^{-7}$	-94.4
$\text{Mg}^{2+}$	$2.5 \cdot 10^{-6}$	$1.6 \cdot 10^{-7}$	-93.6
$\text{K}^+$	$2.8 \cdot 10^{-6}$	$3.0 \cdot 10^{-6}$	+7.1
$\text{Ca}^{2+}$	$9.7 \cdot 10^{-6}$	$1.9 \cdot 10^{-7}$	-98.0
$\text{Zn}^{2+}$	$1.2 \cdot 10^{-6}$	$2.0 \cdot 10^{-7}$	-83.0
$\text{H}_2\text{O}_2$	$6.0 \cdot 10^{-7}$	$2.1 \cdot 10^{-6}$	+250
$\text{Mn}^{3+}$	$9.1 \cdot 10^{-8}$	$6.2 \cdot 10^{-16}$	-76.7
$\text{Mn}^{2+}$		$1.8 \cdot 10^{-8}$	
$\text{Mn}^{4+}$		$1.0 \cdot 10^{-20}$	
$\text{MnBr}^{2+}$		$0.10^0$	
$\text{MnCl}^{2+}$		$3.5 \cdot 10^{-20}$	
$\text{MnHSO}_3^+$		$4.0 \cdot 10^{-10}$	
$\text{Mn(OH)}^{2+}$		$2.5 \cdot 10^{-9}$	
$\text{MnOH}^{2+}$		$2.8 \cdot 10^{-10}$	
$\text{MnO}_2^+$		$2.2 \cdot 10^{-14}$	
$\text{MnO}^{2+}$		$1.7 \cdot 10^{-12}$	
$\text{Fe}^{3+}$	$7.5 \cdot 10^{-7}$	$1.9 \cdot 10^{-11}$	-86.0
$\text{Fe}^{2+}$		$7.4 \cdot 10^{-8}$	
$\text{Fe(OH)}_2^+$		$2.3 \cdot 10^{-10}$	
$\text{FeOH}^{2+}$		$1.8 \cdot 10^{-9}$	
$\text{FeSO}_4^+$		$8.6 \cdot 10^{-14}$	
$\text{Fe(C}_2\text{O}_4)_2^-$		$1.7 \cdot 10^{-8}$	
$\text{Fe(C}_2\text{O}_4)_3^{3-}$		$2.2 \cdot 10^{-9}$	
$\text{Fe(C}_2\text{O}_4)^+$		$1.0 \cdot 10^{-8}$	
$\text{FeCl}^{2+}$		$1.1 \cdot 10^{-15}$	
$[\text{FeCH}_3\text{OO}]^{2+}$		$1.8 \cdot 10^{-14}$	
$[\text{Fe(OH)}_2\text{Fe}]^{4+}$		$1.7 \cdot 10^{-13}$	
$\text{FeO}^{2+}$		$3.8 \cdot 10^{-12}$	
$\text{Cu}^{2+}$	$7.9 \cdot 10^{-8}$	$7.9 \cdot 10^{-8}$	+0.3
$\text{Cu}^+$	$2.0 \cdot 10^{-10}$		
$\text{HCHO}$	$3.5 \cdot 10^{-6}$	$1.1 \cdot 10^{-8}$	+614.6
$\text{CH}_2\text{OH}_2$	$2.5 \cdot 10^{-5}$		
$\text{CH}_3\text{CHO}$	$5.2 \cdot 10^{-7}$	$2.6 \cdot 10^{-8}$	-89.4
$\text{CH}_3\text{CHOH}_2$	$2.9 \cdot 10^{-8}$		
$\text{HCOOH}$	$4.9 \cdot 10^{-6}$	$1.8 \cdot 10^{-6}$	+40.8
$\text{HCOO}^-$	$5.1 \cdot 10^{-6}$		
$\text{CH}_3\text{COOH}$	$2.8 \cdot 10^{-6}$	$3.9 \cdot 10^{-6}$	+78.6
$\text{CH}_3\text{COO}^-$	$1.1 \cdot 10^{-6}$		
$\text{C}_2\text{H}_2\text{O}_2$	$2.7 \cdot 10^{-6}$	$5.3 \cdot 10^{-12}$	-67.0
$(\text{CH(OH)}_2)_2$	$8.9 \cdot 10^{-7}$		
$\text{C}_2\text{O}_4^{2-}$	$2.1 \cdot 10^{-6}$	$4.3 \cdot 10^{-7}$	-57.8
$\text{HC}_2\text{O}_4^-$		$4.5 \cdot 10^{-7}$	

**Tab. 1:** Comparison between the measured and calculated concentrations ( $\text{mol l}^{-1}$ ) in cloud water at the summit site Schmücke.

The SPACCIM model development initiated after MODMEP will continue to further refine the available model framework. The CAPRAM mechanism will be continuously updated and last, but not least, the Schmücke hill-capped cloud experimental site is ready for further focussed ground based aerosol-cloud-interaction experiments with emphasis on organics under real conditions and hence complementary to more specialized laboratory experiments.

### Acknowledgement

The work was supported by the Bundesministerium für Bildung und Forschung (BMBF). We thank the Umweltbundesamt (UBA) and the Deutscher Wetterdienst (DWD Offenbach) for good cooperation and support. We thank all the colleagues that participated in the FEBUKO experiments and for the realization of the numerous analytical measurements: H. Bachmann, B. Gerlach, S. Haferkorn, N. Heim, A. Kappe, A. Thomas.

### References

- Ervens, B., Buxton, G. V., Salmon, G. A., Williams, J., Bydder, M., Dentener, F., George, C., Mirabel, P., Wolke, R. and Herrmann, H. 2002.** CAPRAM2.4 (MODAC mechanism): An extended and condensed tropospheric aqueous phase mechanism and its application. *J. Geophys. Res.*, **108**, 4426.
- Herrmann, H., Ervens, B., Jacobi, H.-W., Wolke, R., Nowacki, P., and Zellner R. 2000.** Capram2.3: A chemical aqueous phase radical mechanism for tropospheric chemistry. *J. Atmos. Chem.*, **38**, 231-184.
- Herrmann, H., Buxton, G. V., Salmon, A., Mirabel, P., George, C., Jelieveld, J. and Dentener, F. 2000.** MODAC-Model Development for Tropospheric Aerosol and Cloud Chemistry. Final report to Project ENVA-CT97-0388. Report CEC Brussels.
- Limbeck, A., Puxbaum, H., Otter, L., and Scholes, M. C. 2001.** Semivolatile behavior of dicarboxylic acids and other polar organic species at a rural background site (Nylsvley, RSA). *Atmos. Environ.*, **35**, 1853-1862.
- Saxena, P. and Hildemann, L. M. 1996.** Water-soluble organics in atmospheric particles: A critical review of the literature and application of thermodynamics to identify candidate compounds. *J. Atmos. Chem.*, **24**, 57-109.
- Schwartz, S. 1986.** Mass transport consideration pertinent to aqueous phase reactions of gases in liquid water clouds. W. Jaeschke (Ed.), In *Chemistry of Multiphase Atmospheric System*. Springer, Berlin, **6**, p. 415-471.
- Stockwell, W., Kirchner, F., Kuhn, M. and Seefeld, S. 1997.** A new mechanism for regional atmospheric chemistry modeling. *J. Geophys. Res.*, **102**, 25847-25879.
- Wolke, R. and Knoth, O. 2002.** Time-integration of multiphase chemistry in size-resolved cloud models. *Appl. Num. Math.*, **42**, 473-487.

#### Funding

- Bundesministerium für Bildung und Forschung (BMBF)

#### Cooperation

- Brandenburgische Technische Universität, Cottbus (BTU)
- Zentrum für Umweltforschung (ZUF), Universität Frankfurt/M.
- Technische Universität Darmstadt (TUD)
- Deutscher Wetterdienst (DWD)
- Umweltbundesamt (UBA)
- Max-Planck-Institut Hamburg (MPI)

## Chemical and Physical characterization of biomass burning aerosol: Results from the AFO 2000 project EFEU

Yoshiteru Iinuma, Hartmut Herrmann, Alfred Wiedensohler and Kristina Zeromskiene

*Das Ziel dieses Projektes ist, die Chemie und Physik von Aerosolpartikeln aus der Biomasseverbrennung zu untersuchen. Im Jahr 2003 wurden am MPI Mainz zwei Kampagnen durchgeführt, um die physikalischen und chemischen Eigenschaften von Partikeln aus der Verbrennung verschiedener Holzarten zu charakterisieren. Die chemischen Informationen werden zusammen mit physikalischen Daten, wie z.B. optische Eigenschaften (Streuung und Absorption) und Hygroskopizität, für ein besseres Verständnis des Aerosols aus Biomasseverbrennung benötigt.*

### Introduction

Biomass burning contributes significantly to the global trace gas and aerosol burden. It is also an important source of elemental carbon as well as organic aerosols. Large scale wildfires occur naturally as well as the results of human activities in various parts of the world. Figure 1 shows a photo of wildfire in southern California in 2003 which illustrates the extensive effects of smoke not only on local environment but also on regional to global scale environment. Vegetation fire is among the most important biomass burning in terms of the climate effects and its particles primarily consist of decomposed lignin, cellulose, hemicellulose products as well as elemental carbon. Although considerable effort has been made by various studies to identify compounds in the biomass burning aerosol (Simoneit, 2002), only a limited number of data exist for the size segregated physical and chemical characterization of biomass burning particles under controlled condition. It is known that each plant species emits source-specific fingerprint chemicals during the combustion. These chemicals are emitted as a result of direct vaporization and by thermal alteration of plant structures.

These fingerprint molecules may also be used as a tracer for the specific fire event. Identification of tracer organic compounds in biomass burning particles is an essential in order to improve our understanding of the behavior of organic aerosols in the atmosphere (chemical reactions, optical properties and radiative effects). Thus, there is a need to characterize simultaneously biomass burning for physical and chemical properties in order to understand its effect on climate.

### Experimental

The EFEU (Impact of Vegetation Fires on the Composition and Circulation of the Atmosphere) subproject "Chemical and Physical characterization of biomass burning" was designed to provide the data required to improve our knowledge of



**Fig. 1:** Wildfire in southern California, 2003. Red spots indicate fires. A photo from MODIS/Terra satellite (NASA).

the role of particles from biomass burning in the atmosphere. In order to cover a wide spectrum of biomass fuels, two sets of laboratory experiments were carried out in summer and autumn 2003 at the Max Planck Institute for Chemistry (MPIC) in Mainz. The summer 2003 campaign focused on the characterization of boreal woods (oak, pine and spruce with and without green materials) and the autumn 2003 campaign focused on African materials (savannah grass and mussasa), peat from Indonesia and northern Germany as well as a repetition of some boreal woods to test the repeatability of the experimental conditions.

**Sampling.** A laboratory combustion facility designed to study gaseous species from biomass burning was used to produce aerosols under controlled conditions. Figure 2 shows the schematic

diagram and photo of a laboratory combustion facility. The emission from the combustion facility was diluted in a container equipped with internal fans as a buffer in order to minimize sample overloading and temporal variability of samples. A field laboratory container was directly located underneath to sample particles in the first stage buffer container. The sample transfer line from the buffer container to a dilution tunnel was approximately 1.5 m. This transfer line was insulated with Styrofoam to minimize condensation. The sample was diluted 20 times with a dilution tunnel in the field laboratory container using clean compressed air. The dilution tunnel was connected to particle sampling devices for chemical analysis together with various physical instruments for the measurements of size distribution, scattering, absorption and total particle concentration.

In order to simulate wildfire conditions rather

**Physical measurements.** Online physical instruments connected to the dilution tunnels include: a Scanning Mobility Particle Sizer (SMPS) together with an Aerodynamic Particle Sizer (APS, TSI 3321) for particle size distributions from 12 nm to 10  $\mu\text{m}$  diameter (2 min/scan), a Hygroscopicity-Tandem Differential Mobility Analyser (H-TDMA) for hygroscopicity of emitted particles at 85% RH for particle diameter of typically 50, 100, 250 and 325 nm, a Condensation Particle Counter (CPC, TSI 3022A) for total particle counting, a TSI 3563 three wavelengths integrating nephelometer for scattering coefficients at 450, 550 and 700 nm, and a Radiance Research Particle Soot Absorption Photometer (PSAP) for absorption coefficient at 565 nm. The data from the optical instruments and CPC are averaged over 2 minute intervals in order to have a comparable data sets to size distributions from SMPS/APS.



Fig. 2: Schematic diagram and photo of combustion facility.

than fireplace or domestic heater burning conditions various parts of tree were burned in different mixture depending on the availability of burning materials. All biomass fuels were weighed before their combustion and during the experiment online in order to estimate the emission factor later. The biomass fuels were ignited using a butane burner and left for a few minutes to stabilize the combustion. Then the chimney connecting the fireplace to the buffering container was switched from a bypass position to a sample line position in order to fill a container with emissions from combustion. Small pieces of biomass fuels were added to the fireplace regularly in order to keep fire from extinguishing. In order to have representative and comparable data for different kind of combusted biomass fuels, an average around 7% for the ratio of excess CO to CO<sub>2</sub> ( $d\text{CO}/d\text{CO}_2$ ) was set as a target for the combustion condition which is generally found in typical biomass burning in nature (Pham-Vam-Dinh et al., 1996).

**Chemical measurements.** Samples for chemical analysis were taken using two 5 stage Berner type impactors and four stack filters. The impactors and stack filters were directly connected after the dilution tunnel. Substrates used for the Berner impactor were aluminum rings for the measurements of mass and OC/EC ratio and Tedlar rings for the analysis individual organics, inorganic ions as well as WSOC (Water Soluble Organic Carbons). Both PTFE (47 mm diameter, 1  $\mu\text{m}$  pore size) and quartz fiber filters were used for stack filter sampling in order to meet the requirement of analytical techniques used. The sampling was carried out during the course of continuous fire experiments. The methods used for the chemical analysis were a thermographic method for OC/EC, ion chromatography for inorganic ions, Shimadzu TOC (total organic carbon) analyzer for WSOC, CE-ESI-MS (Capillary Electrophoresis Electrospray Ionization Mass Spectroscopy) for individual organic species.

Date	Exp. No.	Fuel	Average $dCO/dCO_2$ (%) <sup>b</sup>
01.07.03	9a	Pine with green needles	6
02.07.03	11a	Pine with dry needles	3
03.07.03	12a	Pine	4
25.07.03	25a	Indonesian peat <sup>a</sup>	47
26.07.03	26a	Northern German peat <sup>a</sup>	39

a: samples were dried prior to the combustion session  
b: courtesy of Dr. R. S. Parmar and Dr. G. Helas, Max Planck Institute for Chemistry, Mainz.

Tab. 1: General experimental information.

## Results and Discussion

Since data processing and analysis are still under way only selected experiments are discussed here. Table 1 shows general experimental information for the selected experiments. Pine wood, pine wood with dry underbrush and pine wood with green needles were chosen to show the influence of vegetation parts combusted on the emitted particles. Indonesian peat and Northern German peat were also selected in order to illustrate the differences between fresh biofuels and “fossil” biofuels.

Generally, excess emission ratios of CO to CO<sub>2</sub> ( $dCO/dCO_2$ ) for fresh wood materials are much lower (i.e. more flaming) than that of fossil fuels. It was impossible to keep stable emissions of particles for fresh biofuels over  $dCO/dCO_2$  ratio of 10% whereas fossil fuel combusted very stably even in high smoldering phase ( $dCO/dCO_2 > 35\%$ ). In fact a flaming phase was nearly non-existent for fossil fuels.

### Physical measurements

**Size distributions.** During experiments with pine and various needles, an increase in the mode diameter of the size distribution was observed when needles were added. Figure 3 and Table 2 show aerosol particle size distributions and mode diameters for pine, pine with dry and green needles. Size distributions were averaged for the whole experiment, which usually took about 1 hour. Number concentrations were normalized to their maximum. The average mean diameter during the experiment with pine trunk and branches was 118 nm. The mode diameter increased by 11% (131 nm) for the experiment with pine and dry underbrush. A maximum mode diameter was observed for the experiment with pine and green needles which was 170 nm compared to pine with only trunk and branches. Generally, higher  $dCO/dCO_2$  ratios (i.e. more smoldering) yielded larger

particles. One of the reasons for more smoldering behavior of pine with green needles may come from a different amount of moisture in the biomass material. If the moisture content is high, an appreciable amount of energy is necessary to vaporize water, reducing the heating value of wood as well as decreasing combustion efficiency, which in turn increases smoke formation (more smoldering).

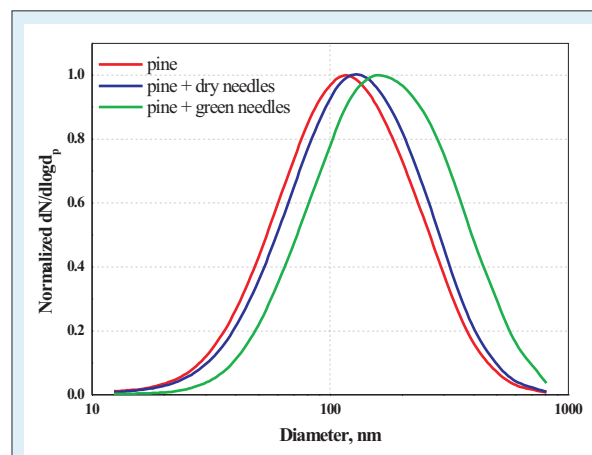


Fig. 3: Aerosol particle size distributions for pine, pine with dry and green needles averaged over the whole experiment (~1hour). Number concentrations are normalized to their maximum.

Material	$\bar{D}_p$	$\sigma$
Pine	118	1.95
Pine with dry needles	131	1.96
Pine with green needles	170	2.01
Indonesian peat	168	2.11
N. German peat	159	2.16

Tab. 2: Comparison of mode parameters for peat and pine experiments ( $\bar{D}_p$ -mode diameter,  $\sigma$ -standard).

During flaming combustible material is stripped off together with water vapor and undergoes partial to complete combustion, whereas during smoldering the temperature is not as high as during flaming and mostly wood decomposition products, which tend to be larger, are released. Another reason which might have influenced the difference between pine and pine with dry needles even with a similar  $dCO/dCO_2$  ratio is “needle blow-out” of dry underbrush and green needle which leads to primary emissions from needles themselves rather than secondary gas to particle conversion.

Size distributions and fitting parameters (mode diameter,  $\bar{D}_p$  and geometric standard deviation,  $\sigma$ ) of Indonesian and Northern German peat and pine are shown in Figure 4 and Table 2. Size distributions from both kinds of peat (Indonesian and Northern German) looked very different from boreal wood. The shape of the distribution is similar

for both kinds of peat, but it is quite different from the size distributions of pine (size distributions from other boreal wood were similar to pine). The distribution is much wider for peat and much larger particles were produced during the combustion of peat. The combustion of peat was very different from fresh wood materials. After the initial ignition, it moved quickly from flaming to smoldering phase and kept smoldering for the duration of experiments without extinction. On the other hand, boreal wood needed constant addition of fresh wood material otherwise temperatures became too low even for smoldering. Both kinds of peat had very high  $dCO/dCO_2$  ratios, ranging up to 50%, indicating the dominance of smoldering phase during the experiments. The tendency to produce larger particles during the smoldering phase than during flaming was noticed already during experiments with Boreal wood. It is interesting to note that the amount of combusted peat was much smaller than that of boreal wood, yet the emission ratios of both kinds of peat were much higher than that of boreal wood. Much more moderate burning condition of peat means chemical reactions which took place in peat combustion were less destructive and probably produced larger molecular weight compounds with lower vapor pressures leading to more intense particle formation.

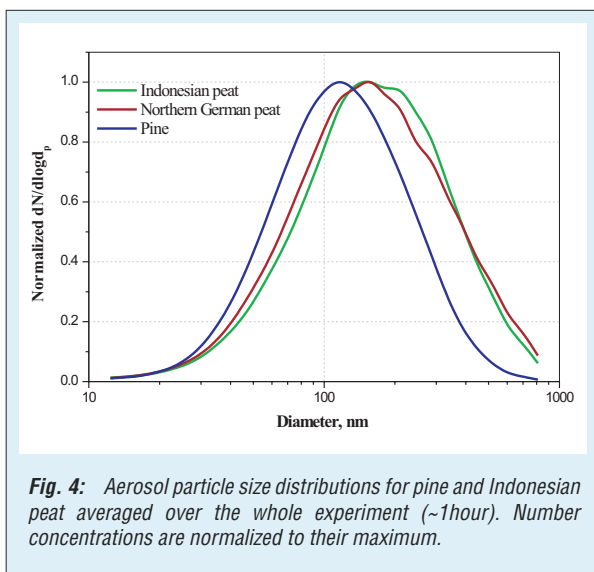


Fig. 4: Aerosol particle size distributions for pine and Indonesian peat averaged over the whole experiment (~1 hour). Number concentrations are normalized to their maximum.

**Optical properties.** Figure 5 shows the measured and simulated time series of scattering and absorption coefficients for experiment 12a (Pine). A Mie calculation is performed using a Mie code from (Bohren and Huffman, 1983) to derive scattering and absorption coefficients. The refractive indices for the simulation are selected as following: 1.4-0.02i (low scattering, low absorption), 1.4-0.1i (low scattering, high absorption), 1.8-0.02i (high scattering, low absorption) and 1.8-0.1i (high scattering, high absorption). Additionally, low

scattering and very high absorption particle (1.4-0.2i) are simulated as absorption values of initial flaming stage (Figure 5, 12:10-12:15) is much lower than the measured absorption value. During the intensive flaming stage (first 5-10 minutes), emitted particles showed lower scattering and higher absorption than that of more stable smoldering stage (12:20 till the end of experiment). This indicates that the flaming stage produced much higher concentrations of black carbon than the smoldering stage. Regardless of refractive indices used the time series of scattering coefficients derived from Mie-code follows the measured ones. This was not always the case for the absorption coefficient. There were some periods when modelled absorption coefficient values did not follow the measured ones, as well as the periods when they agreed pretty well (average 3% differences). This indicates that the real part of refractive index was more or less constant whereas the imaginary part was more significantly influenced by the burning condition throughout the experiment.

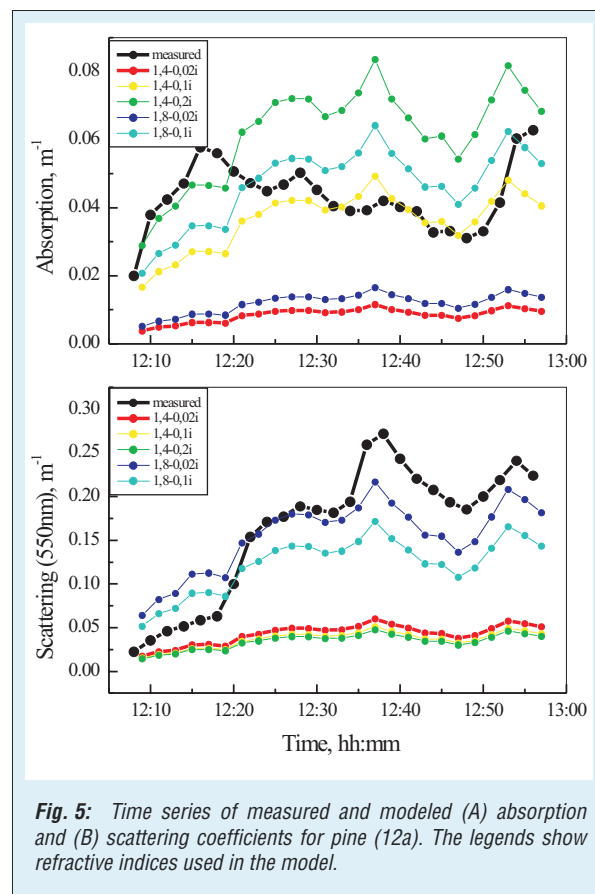
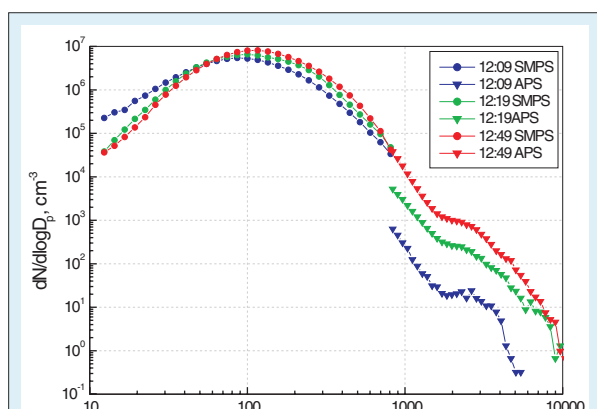


Fig. 5: Time series of measured and modeled (A) absorption and (B) scattering coefficients for pine (12a). The legends show refractive indices used in the model.

Particle size distribution and the shape of particle have a big influence on particle absorption and scattering. Size distributions of particular time periods were analyzed in order to see the influence on the optical measurements. Particle size distribution (Figure 6) was measured with

two instruments: Scanning Mobility Particle Sizer (SMPS) and Aerodynamic Particle Sizer (APS). SMPS measures geometric particle diameter and APS measures aerodynamic diameter. Geometric and aerodynamic diameters are related through particle density and the shape factor (Fuchs, 1964). The number concentrations measured with SMPS for the larger particles ( $\sim 800$  nm) did not change largely with time whereas APS measured number concentrations increased dramatically with time. Assuming density has been constant during the whole experiment, the difference in APS measured size distribution might be caused by shape factor. Particles seem to have become more spherical towards the end experiments because a smoldering phase produces lesser amount of EC (i.e. less fractal), and calculated absorption values start to follow the behavior of the measured ones.



**Fig. 6:** Aerosol particle size distributions during various fire stages. Circles stand for SMPS measurements and triangles stand for APS measurements. Particle density is assumed to be  $1 \text{ g cm}^{-3}$  for the APS measurements. Blue: the beginning of a flaming phase. Green: the end of a flaming phase. Red: the middle of a smoldering phase.

### Chemical measurements

**Comparison of OC/EC ratio.** Figure 7 shows the ratio of OC and EC to TOC (Total Organic Carbon) for the selected biofuel materials. Higher EC values can be explained by the lower  $d\text{CO}/d\text{CO}_2$  ratio as the flaming fire produces much higher concentration of EC (Patterson and McMahon, 1984). Smoldering fires of both kinds of peat materials produced much lower EC fractions than flaming fire from pine woods because the smoldering process produces more volatile/semi-volatile wood decomposition compounds by direct vaporization of wood structure (Simoneit, 2002).

The ratio of OC and EC to TOC is in reasonable agreement with the results of 98% OC and 2.4% OC to TOC for the fireplace combustion of pine (Schauer et al., 2001) considering the variation of combustion condition and differences

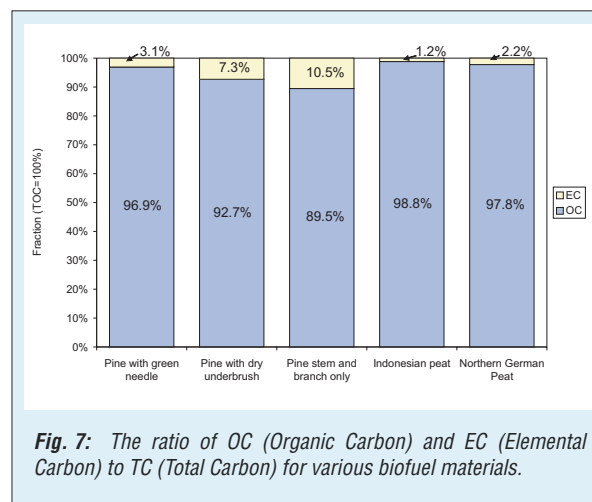


**Fig. 7:** The ratio of OC (Organic Carbon) and EC (Elemental Carbon) to TC (Total Carbon) for various biofuel materials.

in combusted amount. It is interesting to note that Northern German peat produced twice as much EC compared to Indonesian peat. This may be due the difference in the maturity and composition of peat samples considering the fact that both kinds of peat were well in the smoldering phase throughout the experiment.

**Tracer Analysis.** Biopolymers such as lignin, cellulose and hemicellulose are the major components of wood structure. All biopolymers produce volatile/semi-volatile organic compounds during the combustion process. The abundance and compound groups emitted in biomass burning are heavily influenced by the combustion condition (e.g. flaming or smoldering) and the type of biomass combusted. Methoxyphenols from lignin are an interesting class of compounds as a biomass finger print. Lignin is primarily derived from three aromatic alcohols: *p*-coumaryl, coniferyl and sinapyl alcohols. The enrichment of these biomonomers in plant tissues varies significantly and the combustion of lignin generates the breakdown products of these alcohols as phenols, aldehydes, ketons and acids with original substituent retained. These breakdown products and their relative ratio can be used as a specific tracer for the combustion source. Table 3 summarizes the list of detected softwood/hardwood traces for various biofuels. Emission ratios of tracers cannot be determined at this moment as some key parameters for the determination of emission ratio calculation are still in progress. No hardwood tracer was found from all pine wood combustions as the pine wood contains gymnosperm lignin enriched in coniferyl alcohol products. It is interesting to note that the addition of green or dry needle produced 4-hydroxycinnamic acid which is typically found in grass combustion. Contrary to softwood characteristics of pine wood combustion, peat smoke is enriched in all three groups of tracer compounds. This is not surprising as the peat is formed through a sequence of geo-

Tracer	Source wood type	9a	11a	12a	25a	26a
		01/07/03 Pine with green needles	02/07/03 Pine with dry underbrush	03/07/03 Pine branch and stems only	25/09/03 Indnesian peat	26/09/03 Northern German peat
4-hydroxycinnamic acid	Grass	○	○	×	○	○
3,5-dimethoxy-4-hydroxy acetophenone	Hard	×	×	×	○	○
Sinapic acid	Hard	×	×	×	○	○
Syringic acid	Hard	×	×	×	○	○
3-hydroxy-4-methoxy benzoic acid	Soft	○	○	○	○	○
Coniferyl aldehyde	Soft	○	○	○	○	×
Ferulic acid	Soft	○	×	×	×	○
Homovanillic acid	Soft	×	○	○	○	○
Vanillic acid	Soft	×	×	×	×	○
Vanillin	Soft	○	○	○	○	○
Levoglucofan	Soft/Hard	○	○	○	○	○

○: detected, ×: not detected

Tab. 3: List of detected soft/hard wood combustion tracers from various biofuel combustions.

bio-physical and chemical transformation of various plant remains. Therefore, tracers in peat smoke are expected to be maturity and origin (i.e. sampling location) specific. Indonesian peat and Northern German peat did not show significant differences in detected tracers and the difference is possibly due to the plant remain material which formed the peat. However, the mass fraction of impactor samples from Indonesian peat and German peat show significant differences for smaller particles which will be discussed in the next section.

**The comparison of Indonesian peat and Northern German peat: mass fraction.** Figures 8a and 8b show the mass fraction of OC, EC, WSOC, inorganic ions and unresolved mass found on Berner Impactor stage from the samples of Indonesian and Northern German peat combustions (exp. 25 and 26). Notable differences are relatively high WSO and inorganic ion fractions of Northern German peat on the stage 1 compared to Indonesian peat. This data seems to support the finding of the CCN (Cloud Condensation Nuclei) measurement from MPI which showed higher number of activated CCN for smaller particles from Northern German peat (data not shown). Inorganic ion analysis showed much higher nitrate concentration on the stage 1 of Northern German peat sample (nearly 3 times more compared to Indonesian peat in terms of mass fraction) suggesting the possibility of oxidation of hydrophobic organic compounds to

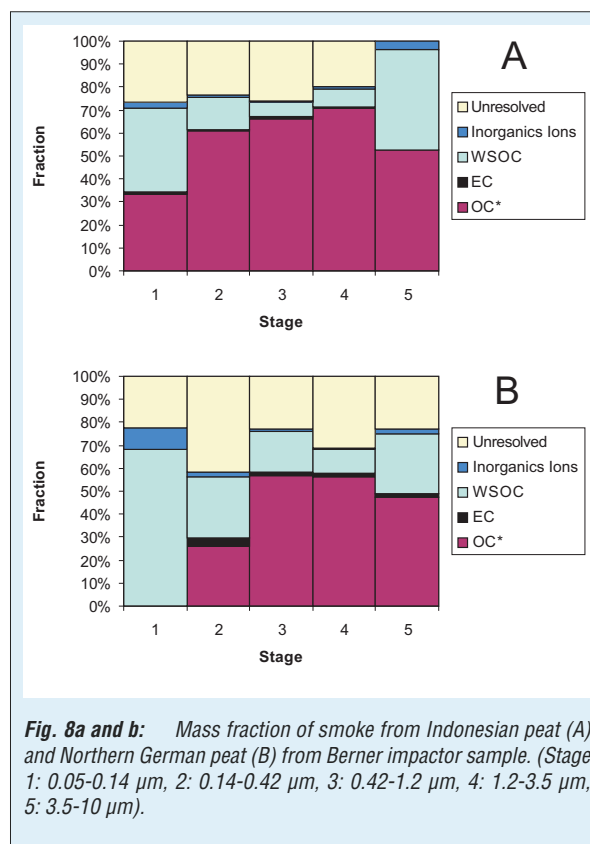


Fig. 8a and b: Mass fraction of smoke from Indonesian peat (A) and Northern German peat (B) from Berner impactor sample. (Stage 1: 0.05-0.14 μm, 2: 0.14-0.42 μm, 3: 0.42-1.2 μm, 4: 1.2-3.5 μm, 5: 3.5-10 μm).

form hydrophilic organics by nitrate. However, the exact reason for the difference in WSOC on stage 1 is not yet known at this moment.

### Summary and outlook

Two sets of laboratory experiments were carried out in summer and autumn 2003 at the MPI Mainz in order to characterize physical and chemical properties of biomass burning aerosols from different biofuels. Combusted biofuels include boreal woods (soft and hardwoods), African plants (savannah grass and mussasa), and peat from

Indonesia and northern Germany. Physical and chemical properties of emitted particles vary significantly by the materials and the phase of combustion.

The dataset obtained during the EFEU campaign will be used for the numerical models employed to investigate the impact of biomass burning on the micro to regional scale atmosphere.

### References

- Bohren, C. F. and Huffman, D. R. 1983.** *Absorption and scattering of light by small particles*. In John Wiley, New York, p. 477-482.
- Fuchs, N. A. 1964.** *The Mechanics of Aerosols*. Pergamon Press, Oxford, 39 pp.
- Patterson, E. M. and McMahon, C. K. 1984.** Absorption Characteristics of Forest Fire Particulate Matter. *Atmos. Environ.*, **18**, 2541-2551.
- Pham-Vam-Dinh, R., Serpolay, R. and Lacaux, J. P. 1996.** *Laboratory Investigations on Aerosols from the combustion of Savanna grass and Cereal straw* (Levine, J. S. The MIT Press ed.). Massachusetts, 473 pp.
- Schauer, J. J., Kleeman, M. J., Cass, G. R. and Simoneit, B. R. T. 2001.** Measurement of Emissions from Air Pollution Sources 3. C1-C29 Organic Compounds from Fireplace Combustion of Wood. *Environ. Sci. Technol.*, **35**, 1716-1728.
- Simoneit, B. R. T. 2002.** Biomass burning - A review of organic tracers for smoke from incomplete combustion. *Appl. Geochem.*, **17**, 129-162.

## Atmospheric particle formation from $H_2SO_4/H_2O$ : An experimental study

Torsten Berndt, Olaf Böge, Olaf Hellmuth, Frank Stratmann, Ralf Wolke

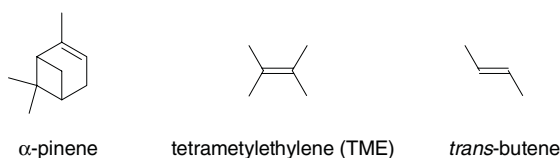
*Gegenstand der Untersuchungen war die Partikelneubildung im System  $H_2SO_4/H_2O$ . Die Experimente wurden unter Strömungsbedingungen im IFT-LFT (IFT-laminar flow tube) durchgeführt.  $H_2SO_4$  wurde ausgehend von der Ozonolyse von Alkenen oder photochemisch in situ gebildet. Dabei lagen die resultierenden  $H_2SO_4$  Konzentrationen im Strömungsrohr in der Größenordnung atmosphärischer Konzentrationen. Die experimentellen Befunde wurden mit Modellierungsergebnissen unter Verwendung des aktuellen ternären Nukleationsansatzes  $H_2SO_4/H_2O/NH_3$  von Kulmala et al. verglichen.*

### Motivation

Due to their radiative properties and the fact that they act as condensation nuclei for clouds, atmospheric particles have a strong impact on the Earth's radiation budget. In field measurements, newly formed particles were observed at different sites and under different experimental conditions (e.g. Birmili and Wiedensohler, 2000; Weber et al., 1999). The formation mechanisms leading to new particles are still subject of intensive research. Binary nucleation in the system  $H_2SO_4$ - $H_2O$  (Kulmala et al., 1998) or ternary nucleation,  $H_2SO_4$ - $H_2O$ - $NH_3$ , (Korhonen et al., 1999) are discussed for describing the events of particle formation. Other settings suggest homogeneous nucleation of iodine oxide in coastal environment (Hoffmann et al., 2001) or organic substances, e.g., clusters of diacids from atmospheric terpene degradation (Hoffmann et al., 1998). From chamber experiments investigating particle formation from the ozonolysis of  $\alpha$ -pinene, enhanced particle production was reported in the presence of  $SO_2$ , even for an  $SO_2$  mixing ratio of 0.5 ppb (Hoppel et al., 2001). The authors concluded that  $H_2SO_4$  (from  $OH + SO_2$ ;  $OH$  radicals from ozonolysis) represented the main nucleating species together with  $H_2O$  and probably  $NH_3$  whereas the organic compounds formed from the ozonolysis were more involved in the process of particle growth. In the case of  $\alpha$ -pinene, there was a possible contribution of ozonolysis products to the nucleation process. The aim of the present study was to investigate the particle formation in the system  $H_2SO_4/H_2O$  using in situ produced  $H_2SO_4$  from the reaction of  $SO_2$  with  $OH$  radicals.  $OH$  radicals were formed from alkene ozonolysis or photolytically. Furthermore, the possible contribution of organic ozonolysis products to particle growth was investigated. In contrast to earlier studies, the ozonolysis was conducted for reactant concentrations closer to realistic atmospheric conditions (mixing ratio for alkenes: mostly 2 ppb and for  $O_3$ : 25 - 30 ppb). The relatively short residence time in the reactor of 420 sec allowed an investigation of the particle formation in the "early stage".

### Experimental

The experiments have been performed in the IFT-LFT (Institute for Tropospheric Research – Laminar Flow Tube) at 295 K and a pressure of 1000 mbar. The IFT-LFT consists of a 505 cm quartz tube (i.d. 8 cm) surrounded with a thermo-jacket allowing a temperature stability of  $\pm 0.5$  K. For the photolytic generation of  $OH$  radicals, the flow-tube is equipped with eight low pressure UV-lamps for a quasi homogeneous and continuous illumination of the flow tube. At the outlet of the flow tube an ozone analyzer (Thermo Environmental Instruments 49C), a dew point sensor (General Eastern HygroM4), and an UCPC (TSI 3025) for integral particle measurements were attached. Particle size distributions ( $d_p > 3$  nm) were determined using a Differential Mobility Particle Sizer (DMPS) consisting of a Vienna-type Differential Mobility Analyzer (DMA) and an Ultrafine Particle Counter (UCPC) (TSI 3025). From the measured mobility distributions, particle size distributions were determined using an inversion algorithm accounting for the counting efficiency of the UCPC, particle losses inside the DMA and the sampling lines connecting the outlet of the IFT-LFT to the DMPS system.  $NH_3$  concentrations of the carrier gas were determined before entering the flow tube using a wet annular denuder system described by Wyers et al. (1993).  $O_3$  produced from a low pressure Hg lamp was introduced through an inlet into the IFT-LFT after dilution with the carrier gas. The alkenes and  $SO_2$  premixed with the carrier gas were added through three symmetrically distributed ports around the inlet. Before adding the reactants, the carrier gas passed a humidifier. The total gas flow was  $3.6 \text{ l min}^{-1}$  resulting in a bulk residence time in the tube of 420 sec. Initial concentrations were (unit: molecule  $\text{cm}^{-3}$ ); alkenes:  $(1.5 - 18) \times 10^{10}$ ,  $O_3$ :  $(6.2 - 7.6) \times 10^{11}$ , and  $SO_2$ :  $(2.2 - 740) \times 10^{10}$ . Alkenes used in the experiments were  $\alpha$ -pinene, tetramethylethylene (TME) and *trans*-butene.



## Results and discussion

### *OH radicals from alkene ozonolysis*

**Particle number measurements (UCPC).** Figure 1 shows integral UCPC particle number measurements from the ozonolysis of  $\alpha$ -pinene in the presence of  $\text{SO}_2$  depending on the presence of the three different reactants in the carrier gas. In the absence of  $\text{SO}_2$ , from the ozonolysis of  $\alpha$ -pinene no particle formation was visible under the conditions used ( $\alpha$ -pinene:  $5.0 \times 10^{10}$  molecule  $\text{cm}^{-3}$  and  $\text{O}_3$ :  $6.4 \times 10^{11}$  molecule  $\text{cm}^{-3}$ ). This finding is in line with earlier observations from the *IFT*-*LFT* where particle formation only occurred for an  $\alpha$ -pinene conversion above  $3 \times 10^{11}$  molecule  $\text{cm}^{-3}$  (Berndt et al., 2003). From a modeling study, for the conditions used here an  $\alpha$ -pinene conversion of  $1.9 \times 10^9$  molecule  $\text{cm}^{-3}$  was calculated, see below. After adding  $\text{SO}_2$  ( $\text{SO}_2$ :  $7.4 \times 10^{11}$  molecule  $\text{cm}^{-3}$ ), formation of new particles took place. These particles most likely consisted of  $\text{H}_2\text{SO}_4$  and  $\text{H}_2\text{O}$ . Possible pathways leading to  $\text{H}_2\text{SO}_4$  are  $\text{OH} + \text{SO}_2$  and Criegee Intermediate +  $\text{SO}_2$ .  $\text{OH}$  radicals and the Criegee Intermediates represent reactive products of the alkene ozonolysis. Switching off either the  $\text{SO}_2$  or the  $\text{O}_3$  flow (in order to terminate the formation of  $\text{OH}$  and the Criegee Intermediates) the particle number went down to the background level, cf. Figure 1. This finding supports that  $\text{H}_2\text{SO}_4$  (as the oxidation product of  $\text{SO}_2$ ) is accountable for the measured particle formation. Similar behavior was also observed using *trans*-butene or tetramethylethylene (TME) instead of  $\alpha$ -pinene.

For the three alkenes investigated ( $\alpha$ -pinene, *trans*-butene, and TME) and relative humidities of 28% and 74%, UCPC particle measurements have been performed depending on the  $\text{SO}_2$  concentration in the carrier gas. Alkene and  $\text{O}_3$  concentrations were kept constant at  $5.0 \times 10^{10}$  molecule  $\text{cm}^{-3}$  and approximately  $7 \times 10^{11}$  molecule  $\text{cm}^{-3}$ , respectively. The  $\text{SO}_2$  concentrations were in the range  $(3.0 - 7.4) \times 10^{11}$  molecule  $\text{cm}^{-3}$  for the runs with  $\alpha$ -pinene,  $(1.8 - 7.4) \times 10^{11}$  molecule  $\text{cm}^{-3}$  for *trans*-butene and  $(2.2 - 11.1) \times 10^{10}$  molecule  $\text{cm}^{-3}$  for TME. The experimental findings for r.h. = 28% are depicted in Figure 2. It was possible to describe the experimental data by means of a power law according to eq. (I).

$$N_{\text{particle}} = \text{const.}[\text{SO}_2]^n \quad (\text{I})$$

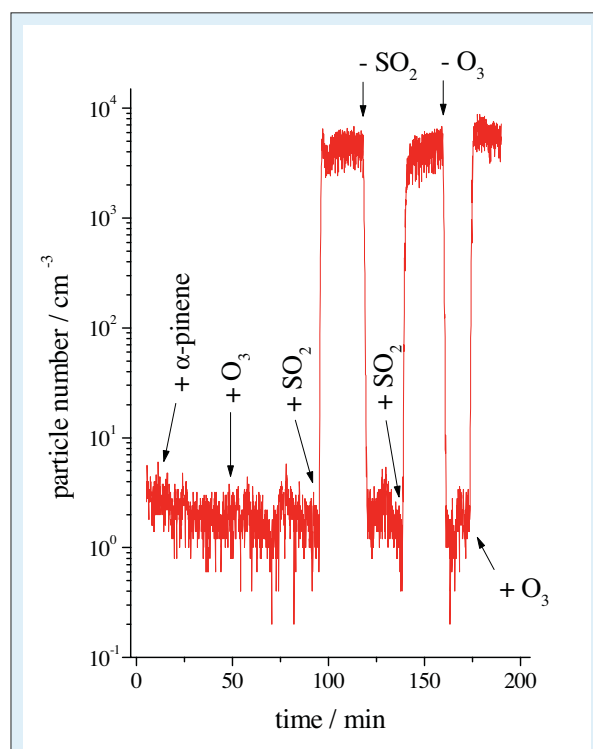


**Fig. 1:** Integral UCPC particle number measurements (> 3 nm) from the ozonolysis of  $\alpha$ -pinene in the presence of  $\text{SO}_2$  for different gas compositions (r.h. = 74%, if present  $\alpha$ -pinene:  $5.0 \times 10^{10}$ ,  $\text{O}_3$ :  $6.4 \times 10^{11}$ ,  $\text{SO}_2$ :  $7.4 \times 10^{11}$  molecule  $\text{cm}^{-3}$ ).

From the logarithmic expression, the exponent  $n$  was obtained for the measurements with a relative humidity of 28% to be  $5.6 \pm 0.2$  for  $\alpha$ -pinene,  $5.4 \pm 0.4$  for *trans*-butene, and  $5.5 \pm 0.4$  for TME. The corresponding exponents  $n$  for the experiments with a relative humidity of 74% were  $4.8 \pm 0.3$  for  $\alpha$ -pinene,  $4.8 \pm 0.4$  for *trans*-butene, and  $4.8 \pm 0.2$  for TME. Errors given represent  $1 \sigma$  limits. With a constant relative humidity,  $n$  was nearly independent of the alkene used in the reaction. This indicates that  $\text{H}_2\text{SO}_4$  (the oxidation product of  $\text{SO}_2$ ) is mainly responsible for the particle formation observed, whereas the influence of the different oxidation products of  $\alpha$ -pinene, *trans*-butene, and TME is of less importance. For each alkene and the higher humidity, however, there was a distinct decrease of the exponent  $n$  compared to the lower humidity. Assuming that with rising  $\text{SO}_2$  concentration the amount of  $\text{H}_2\text{SO}_4$  formed increased proportionally, the data observed here can be compared tentatively with results from an other study measuring particle formation as a function of the  $\text{H}_2\text{SO}_4$  concentration (Ball et al., 1999). Ball et al. reported decreasing values of  $n$  for increasing relative humidity,  $n = 13$  (r.h. = 2.3%) and  $n = 7.0$  (r.h. = 15%) (Ball et al., 1999). The exponents measured in the present study are in line with the expectation arising from the trend given by Ball et al. (1999).

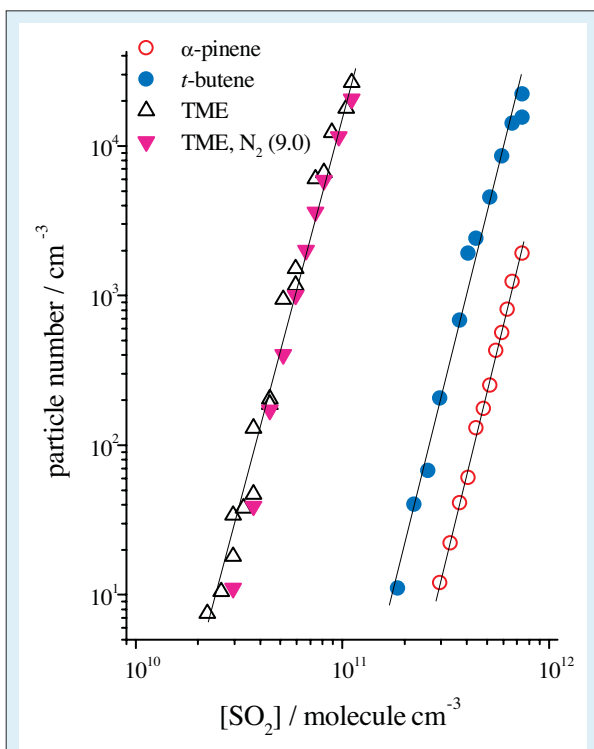
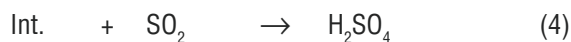
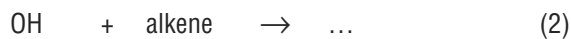
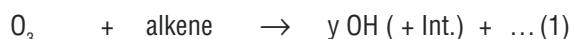


**Fig. 2:** Particle number measurements from the ozonolysis of  $\alpha$ -pinene, *trans*-butene and tetramethylethylene (TME) depending on the  $\text{SO}_2$  concentration in the carrier gas (UCPC measurements, r.h. = 28%). „ $\text{N}_2$  (9.0)“ stands for  $\text{N}_2$  with a purity of 99.999999%.

It is to be noted here that the size distribution measurements revealed a geometric mean size of the particles of around 3 nm. Therefore, the measurements were performed in a size range where the counting efficiency of the UCPC drops significantly with decreasing particle size. Assuming that with increasing  $\text{H}_2\text{SO}_4$  concentration the nucleated particles grow to larger sizes, they will be counted more efficiently with increasing  $\text{H}_2\text{SO}_4$  concentration. Consequently the exponents given above, which were determined directly from the measured particle numbers, are probably over-estimated.

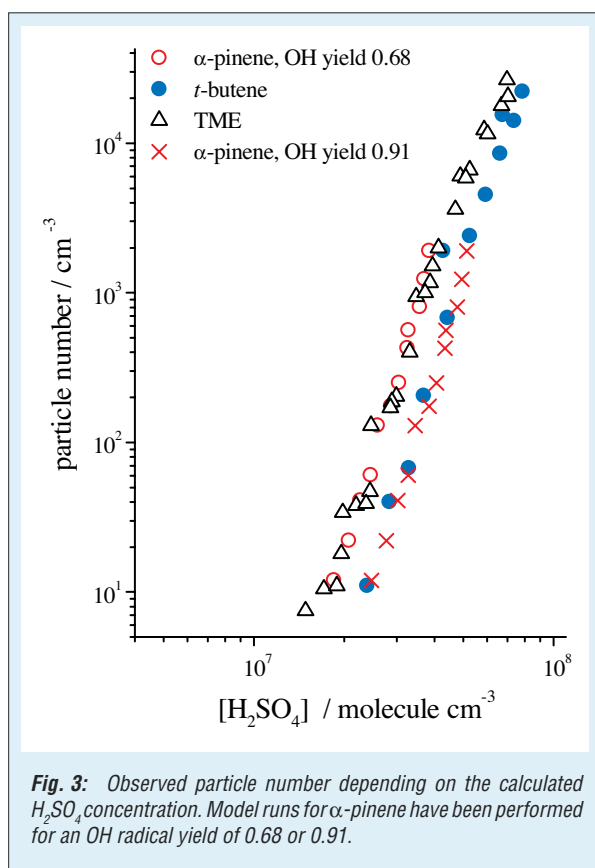
In order to investigate the possible role of unknown impurities of the carrier gas for the process of particle formation, for one case (TME) the synthetic air was substituted by high purity  $\text{N}_2$  (99.999999%). Using this  $\text{N}_2$  as the carrier gas, the experimental findings did not show a significant difference, cf. Figure 2. In Figure 2 “ $\text{N}_2$  (9.0)” stands for the high purity  $\text{N}_2$ . It is to be noted, that even with a purity of 99.999999% the total concentration of “non”  $\text{N}_2$ , i.e. of unknown species, was approximately  $10^{10}$  molecule  $\text{cm}^{-3}$ . As a result of this run it can be concluded, that there was no impurity with a concentration above  $10^{10}$  molecule  $\text{cm}^{-3}$  affecting the nucleation process in this system.

**Modeling of the  $\text{H}_2\text{SO}_4$  formation.** With the help of a modeling study it was tried to calculate the amount of  $\text{H}_2\text{SO}_4$  formed in the flow tube considering the following simplified reaction pathways:



“Int.” stands for the Criegee Intermediates formed in pathway (1) and probably for other intermediates (except for OH) oxidizing  $\text{SO}_2$ . The corresponding rate coefficients as well as the OH radical yields “y” were taken from the literature (if available) or estimated. Figure 3 shows the dependence of newly formed particles on the  $\text{H}_2\text{SO}_4$  concentration calculated. Almost all points lie on the same curve independent of the alkene used in the experiments. This suggests  $\text{H}_2\text{SO}_4$  as the dominating species in the nucleation process. In order to demonstrate the influence of uncertainties of the input parameters for the modeling results, for the  $\alpha$ -pinene system the calculations were performed using OH yields of 0.91 (Siese et al., 2001) and 0.68 (Berndt et al., 2003) in pathway (1). The value of 0.91 is the highest yield reported in the literature (Siese et al., 2001). The comparison of the calculated  $\text{H}_2\text{SO}_4$  concentrations for an OH yield of 0.68 and 0.91 shows that the differences emerging in Figure 3 can be explained by uncertainties of the OH yields or other input parameters such as the rate coefficients or by uncertainties arising from the model itself. As a result of these experiments, there was no clear indication for a participation of the different alkene oxidation products in the nucleation process.

For comparison, in field measurements performed at different continental sites with simultaneous particle and gaseous  $\text{H}_2\text{SO}_4$  detection, formation of new particles occurred for peak  $\text{H}_2\text{SO}_4$  concentrations of  $(1 - 5) \times 10^7$  molecule  $\text{cm}^{-3}$  with formation rates of about one particle  $\text{cm}^{-3} \text{ s}^{-1}$  (Birmili et al., 2000, Weber et al., 1999). The experiments from the present study indicated particle formation starting with approximately  $2 \times 10^7$  molecule  $\text{cm}^{-3}$  of  $\text{H}_2\text{SO}_4$ , cf. Figure 3. Here, the nucleation zone, and therefore, the time when nucleation effectively took place is not well characterized. Because in the *I/T*-LFT experiment the  $\text{H}_2\text{SO}_4$  concentration grew continuously in the course of the reaction, particle formation should mainly occur at the end of the flow tube with the highest  $\text{H}_2\text{SO}_4$  level. Therefore,



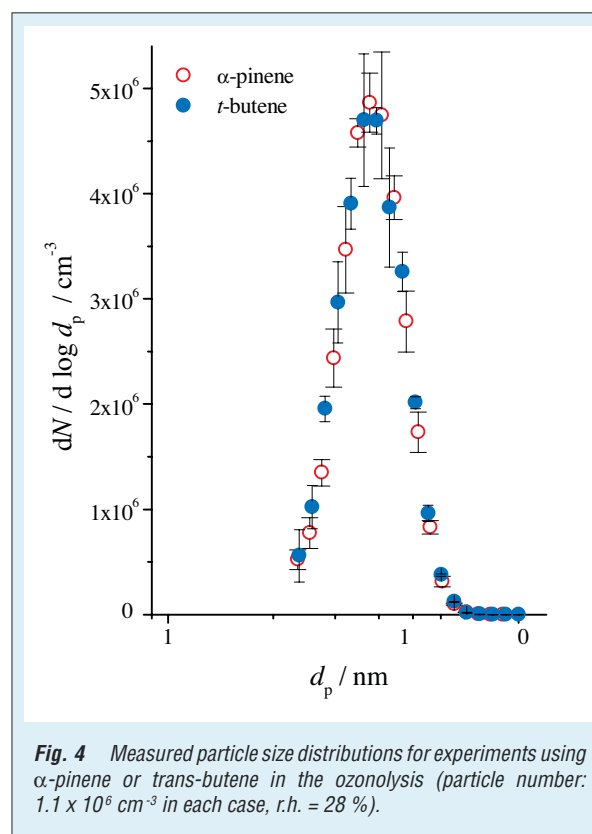
a nucleation time of only a few seconds can be assumed. This results in an estimate of the nucleation rate of a few particles  $cm^{-3} s^{-1}$  ( $N = 10$  particles  $cm^{-3}$  for  $[H_2SO_4]$  approximately  $2 \times 10^7$  molecule  $cm^{-3}$ , cf. Figure 3) to be in line with the values derived from the field measurements (Birmili et al., 2000, Weber et al., 1999). On the other hand, from laboratory studies nucleation rates of about one particle  $cm^{-3} s^{-1}$  were reported for  $H_2SO_4$  concentrations of  $10^{10}$  molecule  $cm^{-3}$  and more (Ball et al., 1999, Wyslouzil et al., 1991). Obviously, for a nearly identical nucleation rate there is a gap of approximately three orders of magnitude in the  $H_2SO_4$  concentration between the laboratory studies in the literature (Ball et al., 1999, Wyslouzil et al., 1991) and the field measurements including the laboratory study presented here. Two possible ideas to explain this discrepancy are:

i) The nucleation process in the present study as well as in the field measurements was controlled by the ternary nucleation  $H_2SO_4$ - $H_2O$ - $NH_3$  (Korhonen et al., 1999). Modeling studies predicted that a  $NH_3$  mixing ratio at low ppt-level strongly enhances the nucleation rate compared to the binary process,  $H_2SO_4$ - $H_2O$ . For the carrier gas used in the *I/T*-LFT experiments, by means of denuder measurements the  $NH_3$  concentration was found to be below the detection limit of  $6 \text{ ng m}^{-3}$  (concentration:  $2 \times 10^8$  molecule  $cm^{-3}$  or a mixing ratio: 9 pptv) for a integration time of

30 min. (Wyers et al., 1993). Because the detection limit of this denuder system was not sufficient enough, these measurements alone did not help to assess the possible contribution of  $NH_3$  for the particle formation.

ii) In the laboratory studies cited (Ball et al., 1997, Wyslouzil et al., 1991)  $H_2SO_4$  was taken from a liquid reservoir and the nucleation occurred in the reactor in the presence of  $H_2O$  without other additions. In contrast to that, in the present study and in the atmosphere in-situ formation of  $H_2SO_4$  took place in the presence of a series of other species (Criegee Intermediates, carbonylic substances, etc.).

**Size distribution measurements.** A series of experiments has been conducted with size distribution measurements at r.h. = 28% using  $\alpha$ -pinene or *trans*-butene as the alkenes. In order to obtain particle distributions with a geometric mean diameter larger than 3 nm, more nucleating matter had to be produced. Therefore, higher initial concentrations were chosen (alkenes:  $(5.0 - 18) \times 10^{10}$  molecule  $cm^{-3}$ ,  $SO_2$ :  $(1.5 - 7.4) \times 10^{12}$  molecule  $cm^{-3}$  and  $O_3$ : approximately  $7 \times 10^{11}$  molecule  $cm^{-3}$ ). To derive the total particle number as well as the particle volume, measured size distributions were integrated averaging at least three distributions. The reproducibility of the size distribution measurements was found to be excellent resulting in error limits for the particle number and the particle volume of lower than



$\pm 10\%$ . Figure 4 shows an example for experiments yielding a nearly identical particle number of  $1.1 \times 10^6 \text{ cm}^{-3}$  using  $\alpha$ -pinene or *trans*-butene in the ozonolysis (particle volume:  $3.8 \times 10^{-14} \text{ cm}^3 \text{ cm}^{-3}$  in each case). There is no significant difference between both particle distributions.

In Figure 5 the derived particle volume depending on the particle number for the two alkenes are summarized. In the data points there was no clear difference between the two systems investigated. This leads to the conclusion that the ozonolysis products of  $\alpha$ -pinene did not significantly contribute to the process of particle growth. Products of the ozonolysis of  $\alpha$ -pinene are  $C_{10}$  or  $C_9$  compounds, such as pinonaldehyde, pinonic acid or pinic acid with vapor pressures of  $10^{-2} - 10^{-7}$  Torr. Because of a very high vapor pressure of about 830 Torr for acetaldehyde, the main product from the ozonolysis of *trans*-butene, a contribution to the particle growth was not expected. Obviously, the newly formed particles mainly consisted of  $H_2SO_4$  and  $H_2O$ .

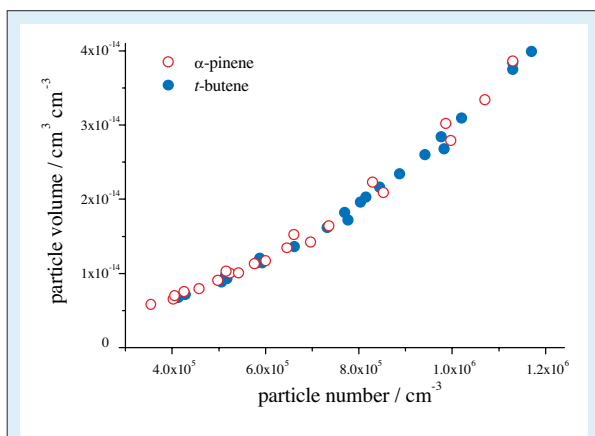


**Fig. 5** Particle volume as a function of the particle number from the ozonolysis of  $\alpha$ -pinene or *trans*-butene in the presence of  $SO_2$  (DMPS measurements, r.h. = 28%).

### OH radicals from $O_3$ photolysis

In further experiments OH radicals were produced by photolysis of  $O_3$  and subsequent reaction of  $O(^1D)$  atoms with water vapor. The OH radicals reacted with  $SO_2$  via pathway (3) yielding  $H_2SO_4$  finally. Furan was added to the reaction mixture as a scavenger for the determination of the amount of produced OH radicals. The disappearance of furan was measured by means of a GC technique (gas chromatography) equipped with a cryo-enrichment. These experiments have been performed at a relative humidity of 28%,  $SO_2$ :  $(2.6 - 14.3) \times 10^{10} \text{ molecule cm}^{-3}$  and  $O_3$ :  $(6.1 - 8.1) \times 10^{11} \text{ molecule cm}^{-3}$ . From the furan decay the resulting  $H_2SO_4$  concentration in the tube was calculated taking into account the wall loss according to pathway (6). The results are given in Figure 6 together with the data

from the ozonolysis experiments. Particle formation was observed starting with a  $H_2SO_4$  concentration of approximately  $10^7 \text{ molecule cm}^{-3}$ , roughly in accordance with the results from the ozonolysis experiments, cf. Figure 6. The difference between both sets of experiments can be explained probably by too simple model assumptions for the calculation of the  $H_2SO_4$  concentration.

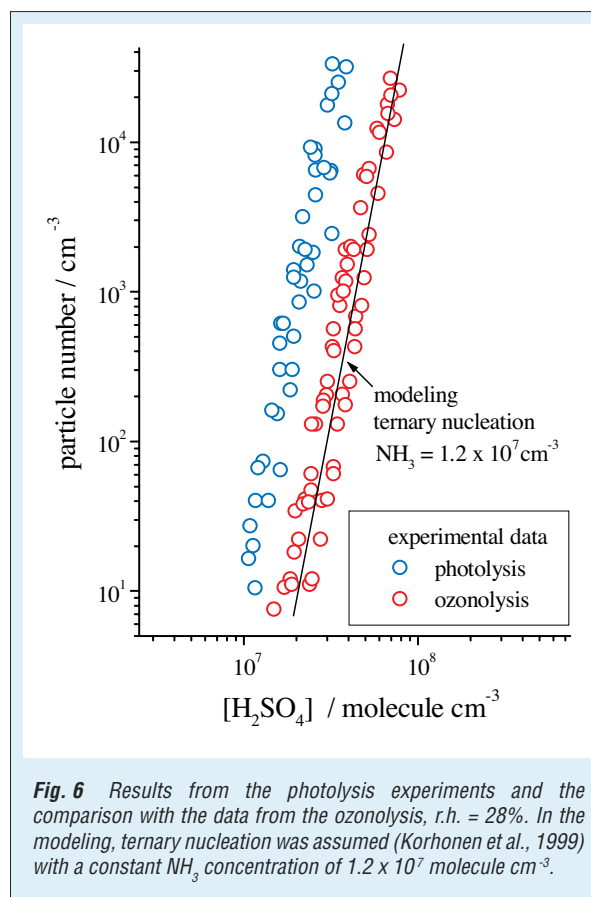


**Fig. 6** Results from the photolysis experiments and the comparison with the data from the ozonolysis, r.h. = 28%. In the modeling, ternary nucleation was assumed (Korhonen et al., 1999) with a constant  $NH_3$  concentration of  $1.2 \times 10^7 \text{ molecule cm}^{-3}$ .

Nevertheless, the results of the experiments with photolytic OH radical formation confirm the conclusions deduced from the ozonolysis experiments.  $H_2SO_4$  was the dominating species in the nucleation process under all experimental conditions used in this study. A contribution of organic oxidation products was of less or negligible importance. That suggests that in the real atmosphere particle formation can occur for  $H_2SO_4$  concentrations of a few  $10^7 \text{ molecule cm}^{-3}$ . This is in line with results from field measurements (Birmili et al., 2000, Weber et al., 1999).

### Modeling of the nucleation process

The calculations were based on box modeling of the reaction system described by pathways (1) – (6) inclusive ternary nucleation of a  $H_2SO_4$ ,  $NH_3$ , and  $H_2O$  vapor system. For the nucleation rate, a parameterization proposed by Napari (2000) was used, which is based on the nucleation theory

of Korhonen et al. (1999). The influence of intra-mode coagulation on the time evolution of newly formed particles was neglected. The box model was initialized with concentrations of SO<sub>2</sub>, alkene, and O<sub>3</sub> according to their tube injection values in the experiments. The integration time of 420 seconds was taken to be equal to the transport time inside the tube. To elucidate the dependency of newly formed particles on the H<sub>2</sub>SO<sub>4</sub> concentration, successive model runs have been performed with altered initial concentrations of SO<sub>2</sub>, alkene, and O<sub>3</sub> for a temperature of 295 K and a relative humidity of 28%. The NH<sub>3</sub> concentration was considered as a free parameter. Best agreement was found for an assumed NH<sub>3</sub> concentration of 1.2 x 10<sup>7</sup> molecule cm<sup>-3</sup> (mixing ratio: 0.5 pptv), cf. Figure 6. Note that the nucleation rate used here and, consequently, the final particle number are very sensitive to NH<sub>3</sub>, especially for a NH<sub>3</sub> mixing ratio below 15 pptv (Korhonen et al., 1999).

## References

- Ball, S. M., Hanson, D. R., Eisele, F. L. and McMurry, P. H. 1999.** Laboratory studies of particle nucleation: Initial results for H<sub>2</sub>SO<sub>4</sub>, H<sub>2</sub>O, and NH<sub>3</sub> vapors. *J. Geophys. Res.*, **104**, 23709-23718.
- Berndt, T., Böge, O. and Stratmann, F. 2003.** Gas-phase ozonolysis of  $\alpha$ -pinene: gaseous products and particle formation. *Atmos. Environ.*, **37**, 3933-3945.
- Birmili, W. and Wiedensohler, A. 2000.** New particle formation in the continental boundary layer: Meteorological and gas phase parameter influence. *Geophys. Res. Lett.*, **27**, 3325-3328.
- Hoffmann, T., Bandur, R., Marggraf, U. and Linscheid, M. 1998.** Molecular composition of organic aerosols formed in the  $\alpha$ -pinene/O<sub>3</sub> reactions: Implication for new particle formation Processes. *J. Geophys. Res.*, **103**, 25569-25578.
- Hoffmann, T., O'Dowd, C. D. and Seinfeld, J. H. 2001.** Iodine oxide homogenous nucleation: an explanation for coastal new particle production. *Geophys. Res. Lett.*, **28**, 1949-1952.
- Hoppel, W., Fitzgerald, J., Frick, G., Caffrey, P., Pasternack, L., Hegg, D., Gao, S., Leaitch, R., Shantz, N., Cantrell, C., Albrechtinski, T., Ambrusko, J. and Sullivan, W. 2001.** Particle formation and growth from ozonolysis of  $\alpha$ -pinene. *J. Geophys. Res.*, **106**, 27603-27618.
- Korhonen, P., Kulmala, M., Laksonen, A., Viisanen, Y., McGraw, R. and Seinfeld, J. H. 1999.** Ternary nucleation of H<sub>2</sub>SO<sub>4</sub>, NH<sub>3</sub>, and H<sub>2</sub>O in the atmosphere. *J. Geophys. Res.*, **D104**, 26349-26353.
- Kulmala, M., Laaksonen, A. and Pirjola, L. 1998.** Parametrization for sulfuric acid/water nucleation rates. *J. Geophys. Res.*, **103**, 8301-8307.
- Napari, I. 2002.** *Fortran Code of parameterization of ternary nucleation*. Report FIN-00024, University of Helsinki, department of Physical Sciences, division of atmospheric Science.
- Siese, M., Becker, K. H., Brockmann, K. J., Geiger, H., Hofzumahaus, A., Holland, F., Mihelcic, D. and Wirtz, K. 2001.** Direct measurements of OH radicals from ozonolysis of selected alkenes: A EURHORE simulation chamber study. *Environ. Sci. Technol.*, **35**, 4660-4667.
- Weber, R. J., McMurry, P. H., Malaudin III, R. L., Tanner, D. J., Eisele, F. L., Clarke, A. D. and Kapustin, V. N. 1999.** New particle formation in the remote troposphere: A comparison of observations at various sites. *Geophys. Res. Lett.*, **26**, 307-310.
- Wyslouzil, B. E., Seinfeld, J. H., Flagan, R. C. and Okuyama, K. 1991.** Binary nucleation in acid-water systems. II. Sulfuric acid-water and a comparison with methanesulfonic acid-water. *J. Chem. Phys.*, **94**, 6842-6850.
- Wyers, G. P., Otjes, R. P. and Slanina, J. 1993.** A continuous-flow denuder for the measurement of ambient concentrations and surface-exchange fluxes of ammonia. *Atmos. Environ.*, **27**, 2085-2090.

The agreement between experimental data and modeling run is excellent. If the ternary nucleation (H<sub>2</sub>SO<sub>4</sub>, NH<sub>3</sub>, and H<sub>2</sub>O) is responsible for the particles observed in this study, a more pronounced scatter of the experimental data is expected. The reproducibility from one day to the next, however, was reasonable. It is hard to believe that there was a constant NH<sub>3</sub> concentration of 1.2 x 10<sup>7</sup> molecule cm<sup>-3</sup> in the carrier gas during the whole course of the experiments. The modeling runs predicted a distinct change of the resulting particle number for small changes of the NH<sub>3</sub> concentration.

## Acknowledgement

We are grateful to Achim Grüner and Gerald Spindler for technical support during the NH<sub>3</sub> denuder measurements and Ismo Napari, University of Helsinki, for the kind release of the nucleation parameterization.

## Cooperation

- University of Helsinki, Department of Physical Sciences, Division of Atmospheric Science.





*Short contributions*



## First observations of high ultrafine particle numbers near the inversion of a continental planetary boundary layer

Holger Siebert, Frank Stratmann, Birgit Wehner

*Im Rahmen des im Frühjahr 2002 in Melpitz durchgeführten Feldexperiments SATURN wurde das Auftreten von neugebildeten, ultrafeinen Aerosolpartikeln unter verschiedenen meteorologischen Bedingungen untersucht. Als eine mögliche Ursache für Partikelneubildung werden in der aktuellen Literatur Mischungsprozesse, wie sie z.B. an der Grenzschichtinversion auftreten diskutiert.*

*Während SATURN konnten an einem Tag zum ersten Mal erhöhte Konzentrationen von ultrafeinen Partikeln an der Grenzschichtinversion mit Hilfe des fesselballongetragenen Systems ACTOS beobachtet werden. Zum Zeitpunkt der Messungen war die Inversion bereits in Auflösung begriffen, so dass intensive Durchmischung zweier vorher getrennter Luftmassen stattfinden konnte. Parallel zu den Ballonmessungen wurden zeitgleich am Boden größen aufgelöste Partikelmessungen durchgeführt. Diese Bodenmessungen zeigen erhöhte Konzentrationen von ultrafeinen Partikeln erst deutlich nach der ersten ballongestützten Beobachtung an der Inversion. Dies ist ein Indiz dafür, dass Partikel an der Inversion neu gebildet wurden und die am Boden beobachteten ultrafeinen Partikel durch Heruntermischen zu erklären sind.*

Events with high number concentrations of small particles have been observed in the atmosphere at various locations and under different meteorological conditions worldwide. Although these ultrafine particles appear to be caused by nucleation, the causes of these nucleation events are still unclear. Micrometeorological conditions that might facilitate new particle formation and growth to measurable ultrafine particles have been actively discussed in recent literature. A comprehensive discussion of different new particle formation scenarios is given by Bigg (1997) and Nilsson et al. (2001), who suggested that turbulent mixing processes are responsible for enhanced nucleation rates in the planetary boundary layer. The most effective mixing of two different air masses can be obtained around the inversion layer.

During the SATURN experiment (Stratmann et al., 2003) such a new particle formation event around the inversion layer was observed at one day with help of tethered balloon-borne and ground-based measurements.

### Experimental

In SATURN, the payload ACTOS (Airship-borne Cloud Turbulence Observation System) and the tethered balloon MAPS-Y were used for measurements in the planetary boundary layer (PBL). The temperature,  $T$ , was measured with an UFT (UltraFast Thermometer, fine-wire sensor) and the water vapor density,  $a$ , was measured with a Lyman- $\alpha$  absorption- and capacitive hygrometer with a time resolution of 10 Hz. A complete description of the measurement system is provided in Siebert et al. (2003).

Two condensation particle counters (CPCs) with different size ranges were added to ACTOS to measure particle number concentrations at a

sampling rate of 1 Hz. The lower cut-off of CPC-I was set to 10 nm ( $N_{10}$ ) and for CPC-II to 5 nm ( $N_5$ ). A pre-impactor inlet was used to set the upper limit to 1  $\mu\text{m}$ . The concentration of particles between 5 and 10 nm,  $N_{5-10} = N_5 - N_{10}$ , was calculated from the difference in measured number concentrations between the two CPCs and used as an indication of recently formed particles. A similar setup for balloon-borne aerosol measurements was presented by Kütz and Dubois (1997) and Heintzenberg et al. (1999).

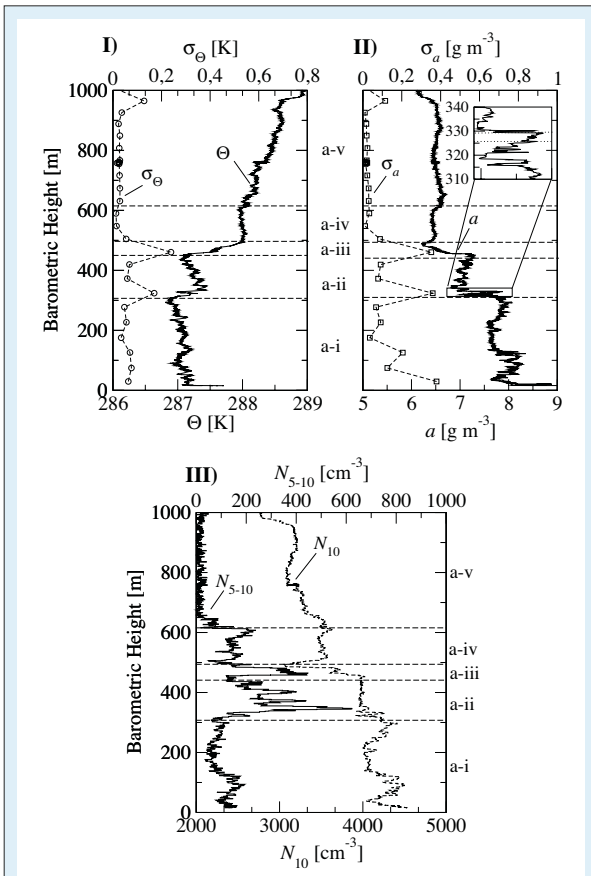
Ground-based particle number size distributions measured with a twin differential mobility particle sizer (TDMPS) complemented the airborne measurements. The TDMPS was operated at the same site where the balloon was launched.

### Results and Discussion

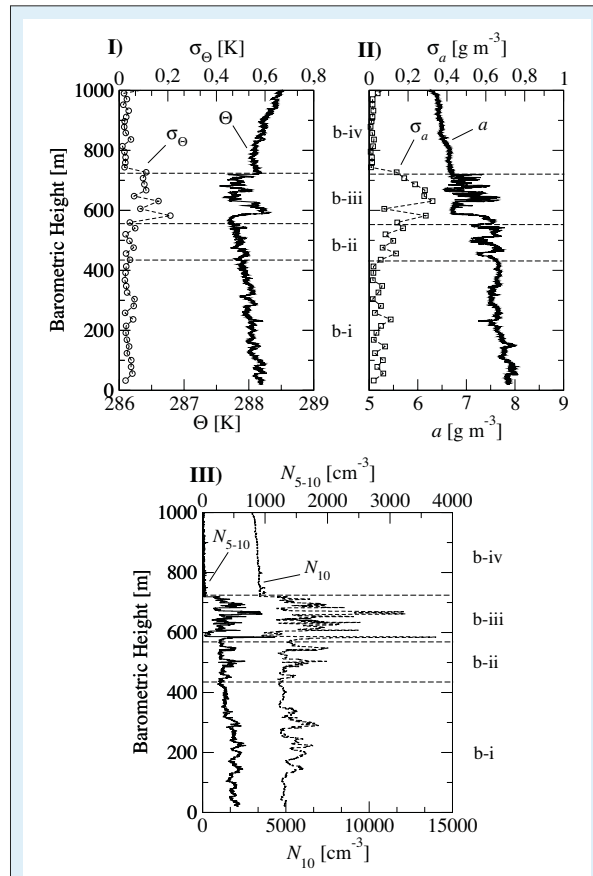
Here, two profile measurements are analyzed. The first profile represents an ascent from ground level up to about 1200 m, which lasted from 06:18 UTC to 06:38 UTC. The second profile covers the subsequent descent, which lasted from 06:42 UTC to 07:22 UTC. Because the inversion layer was in the state of dissolution, no further profile measurements with a significant inversion layer were possible for that day.

Figure 1 shows vertical profiles of the potential temperature  $\Theta$  with local standard deviation  $\sigma_\Theta$  (I), water vapor  $a$  with local standard deviation  $\sigma_a$  (II), and the particle number concentrations  $N_{10}$  and  $N_{5-10}$  (III) recorded during the ascent.

At this stage the PBL was mainly characterized by a well-mixed layer reaching from the ground up to 300 m, followed by a region with two inversion layers (above 300 m and between 450 and 500 m) and a residual layer starting at 600 m. The standard deviations of both thermodynamic variables have



**Fig. 1:** Tethered balloon-borne profile measurements of the potential temperature  $\Theta$  and its standard deviation  $\sigma_{\Theta}$  (I), water vapor density  $a$  and its standard deviation  $\sigma_a$  (II), and particle number concentrations  $N_{10}$  and  $N_{5-10}$  (III) measured during the ascent on May 30, 2002, between 06:18 - 06:38 UTC in Melpitz. Significant layers are labeled by a-i, a-ii, etc.



**Fig. 2:** Tethered balloon-borne profile measurements of the potential temperature  $\Theta$  and its standard deviation  $\sigma_{\Theta}$  (I), water vapor density  $a$  and its standard deviation  $\sigma_a$  (II), and particle number concentrations  $N_{10}$  and  $N_{5-10}$  (III) measured during the descent on May 30, 2002, between 06:42 - 07:22 UTC in Melpitz. Significant layers are labeled by b-i, b-ii, etc.

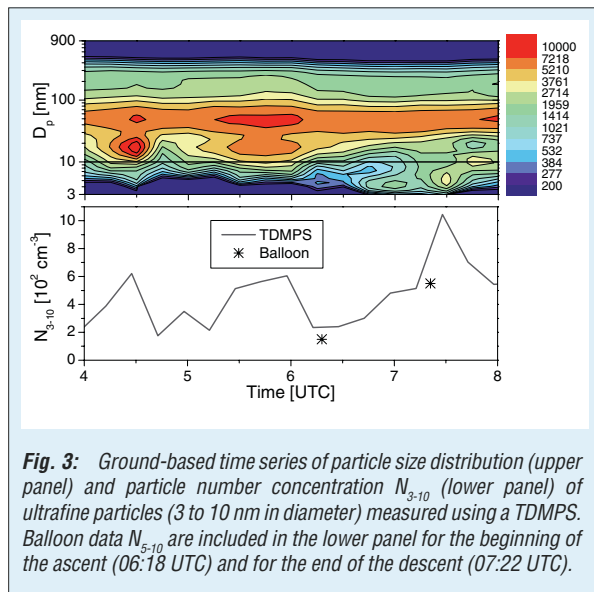
a significant maximum around the two inversions. Whereas  $N_{5-10}$  shows a near constant profile in the well mixed layer with number concentrations of about  $150 \text{ cm}^{-3}$ , concentrations in the region between the two inversion layers are up to about four times higher and fluctuating strongly. There were no ultrafine particles in the residual layer.

Figure 2 shows the structure during the subsequent descent. The well-mixed layer reached a height of about 430 m. Both thermodynamic parameters showed no significant structure in this layer and decreased slightly with increasing height. In the next lower 100 m (b-ii),  $\sigma_a$  increased to  $0.2 \text{ g m}^{-3}$ , whereas  $\sigma_{\Theta}$  remained unchanged from its values in the mixed layer. In region b-iii, a small temperature inversion correlated with a decrease in  $a$ . Above this inversion,  $a$  varied between the values for the mixed and residual layers due to extensive mixing between these two air masses.

In this state of the PBL evolution, plumes penetrate the inversion, causing high temperature fluctuations due to mixing of potentially warmer air parcels from above the inversion into the air of the mixed layer. Therefore, in the inversion layers,  $\sigma_{\Theta}$  and  $\sigma_a$  have significant maxima and the particle

number concentration  $N_{5-10}$  but also  $N_{10}$  show the highest fluctuations. The reason for the high values and fluctuations of  $N_{10}$ , which were not observed during the ascent, might be that ultrafine particles now have been grown up into the size range of  $N_{10}$ .

Figure 3 depicts the corresponding ground-based particle size distribution and number concentration measured using a TDMPs. The upper panel shows the size distribution between 4 UTC and 6 UTC, and the horizontal line marks the 10 nm limit. In the lower panel a time series of the particle number concentration  $N_{3-10}$  for particles from 3 to 10 nm in diameter is given. The balloon data are included for the two times when the balloon was close to the ground (at 06:18 UTC and 07:22 UTC). The balloon-borne concentrations  $N_{5-10}$  were at both times lower than  $N_{3-10}$ . The reason for this underestimation might be the smaller size range of  $N_{5-10}$ . During this period,  $N_{3-10}$  increased from 300 to  $750 \text{ cm}^{-3}$ . The size distribution indicates that the concentration peak of  $N_{3-10}$  near 7:30 UTC differed from the peaks at 4:30 UTC and 5:45 UTC, because particles less than 5 nm in diameter were present, indicating new particle formation. The first time the balloon



reached the inversion (around 06:25 UTC)  $N_{5-10}$  was up to  $600 \text{ cm}^{-3}$  but  $N_{3-10}$  was still at about  $250 \text{ cm}^{-3}$  and no particles with a diameter less than

5 nm in diameter were observed at ground. During the time of the second profile, an increase in ultrafine particle concentration ( $N_{3-10}$ ) was observed also at ground level including particles less than 5 nm in diameter.

In summary, regions with significantly enhanced concentrations of ultrafine particles were observed near the inversion layer. The PBL was in the state that allows convective plumes to penetrate the inversion layer, resulting in effective mixing of potentially warmer air masses from above the inversion into the lower regions. This results in high fluctuations in the potential temperature and water vapor density. Because the high values of  $N_{5-10}$  had a local maximum near the inversion layer, we conclude that these small particles were newly formed in those regions.

These observations agreed well with Easter and Peters (1994), who described a significantly enhanced nucleation rate under conditions of high temperature and humidity fluctuations, such as those found near an inversion.

## References

- Bigg, E. K. 1997.** A mechanism for the formation of new particles in the atmosphere. *Atmos. Res.*, **43**, 129-137.
- Easter, R. C. and Peters, L. K. 1994.** Binary homogeneous nucleation: Temperature and relative humidity fluctuations, nonlinearity, and aspects of new particle production in the atmosphere. *J. Appl. Meteor.*, **33**, 775-784.
- Heintzenberg, J., Wiedensohler, A. and Kütz, S. 1999.** Modification of a commercial condensation particle counter for boundary layer balloon-borne aerosol studies. *J. Atmos. Oceanic Technol.*, **16**, 597-601.
- Kütz, S. and Dubois, R. 1997.** Balloon-borne aerosol measurements in the planetary boundary layer: Particle production associated with a continental stratiform cloud. *Contr. Atmos. Phys.*, **70**, 109-116.
- Nilsson, E. D., Rannik, Ü., Kulmala, M., Buzorius, G. and O'Dowd, C. D. 2001.** Effects of continental boundary layer evolution, convection, turbulence and entrainment, on aerosol formation. *Tellus B*, **53 B**, 441-461.
- Siebert, H., Wendisch, M., Conrath, T., Teichmann, U. and Heintzenberg, J. 2003.** A new tethered balloon-borne turbulence platform for fine-scale observations within the cloudy boundary layer. *Bound.-Layer Meteor.*, **106**, 461-482.
- Stratmann, F., Siebert, H., Spindler, G., Wehner, B., Althausen, D., Heintzenberg, J., Hellmuth, O., Rinke, R., Schmieder, U., Seidel, C., Tuch, T., Uhrner, U., Wiedensohler, A., Wandinger, U., Wendisch, M., Schell, D. and Stohl, A. 2003.** New-particle formation events in a continental boundary layer: First results from the SATURN experiment. *Atmos. Chem. Phys.*, **3**, 1445-1459.

### Cooperation

- Wehrtechnische Dienststelle für Schiffe und Marinewaffen Eckernförde (WTD 71)
- enviscope GmbH (Frankfurt/Main)

### Airborne Measurements of Spectral Surface Albedo over Different Sea and Land Surfaces

Manfred Wendisch, Stephan Günnel, Evelyn Jäkel, Sebastian Schmidt and Holger Siebert

*Flugzeuggetragene Albedomessungen werden benutzt, um die spektrale Bodenalbedo für See- und Landoberflächen für den Wellenlängenbereich von 330-1670 nm abzuleiten. Die Daten wurden innerhalb von drei Feldkampagnen unter wolkenlosen Bedingungen gewonnen. Der maskierende Einfluss von Aerosolpartikeln und Gasmolekülen auf die Albedomessungen in Flugniveau wird mit einer neuen, nicht-linearen Methode korrigiert. Gemittelte Albedo-Daten für unterschiedliche See- und Landoberflächen werden präsentiert. Unterschiede zwischen den Messungen sowie Vergleiche zu Literaturdaten werden diskutiert. Die gemittelten Bodenalbedodaten können für Modellstudien oder die Auswertung von Feldmesskampagnen genutzt werden.*

#### Introduction

The surface albedo is an important boundary condition for atmospheric solar radiative transfer models. It determines the fraction of reflected and incident solar irradiances at the Earth's surface. The solar energy reflected by the surface is available for further radiative interactions (scattering/absorption on air molecules and aerosol/cloud particles) within the atmosphere. The complementary part, which is not reflected back to the atmosphere, is absorbed by the surface. It heats the ground, and is transformed into long-wave radiation and then re-emitted by the Earth's surface. In this way the surface albedo is crucial (i) for multiple scattering and absorption processes in the solar spectral range, and (ii) for the transformation of radiation energy from the solar to the terrestrial wavelength region. Thus the spectral surface albedo is a constraining factor for the surface and atmospheric energy budgets. It is important to characterize this boundary condition over different surfaces.

In general the albedo is defined as a ratio of up- and downward irradiances as a function of altitude. At the ground the albedo is identical with the surface albedo. At all other altitudes the albedo includes reflection from the surface and contributions due to reflection and multiple scattering within the atmosphere beneath the considered height. Usually this so-called atmospheric masking is corrected by linear extrapolation of airborne, height-dependent albedo measurements to the ground. However, this linear technique fails in the presence of significant amounts of aerosol particles below the flight altitude. Therefore Wendisch et al. (2004) introduce a non-linear approach to derive spectral surface albedo (areal-averaged) from airborne albedo measurements. In this contribution this non-linear method is applied to measurements in cloudless conditions over different sea and land surfaces.

#### Field Campaigns, Instrumentation and Method

Data from three field campaigns with different scientific objectives are included in this study. In 2000 the North-Sea experiment (NORTH-SEA-2000) was performed to investigate the influence of aerosol particles on the spectral radiative properties of a cloudless atmosphere. Spatial and temporal inhomogeneities of boundary layer clouds and their influence on atmospheric radiative transfer were studied during the Baltex Bridge Campaign in 2001 (BBC-2001). In 2002 the Cirrus Regional Study of Tropical Anvils and Cirrus Layers - Florida Area Cirrus Experiment (CRYSTAL-FACE-2002) investigated the microphysical and dynamical properties of cirrus anvil clouds.

The airborne spectral albedo measurements were accomplished using two unique instruments: the IFT-Albedometer (Wendisch et al., 2001; Wendisch, 2003; Wendisch and Mayer, 2003) and the Solar Spectral Flux Radiometer (SSFR) which was developed at the National Aeronautics and Space Administration (NASA) Ames Research Center (Pilewskie et al., 2003). Both instruments measure spectral up- and downward irradiances in the solar spectral range (Albedometer: 330-995 nm with a Full Width at Half Maximum, FWHM, of 2-3 nm; SSFR: 330-1670 nm with a FWHM between 9-12 nm). The spectral albedo at the flight level is calculated from the ratio of the up- and downward irradiances. To derive the surface albedo from the airborne albedo measurements at a certain flight altitude, a new method introduced by Wendisch et al. (2004) is applied. This technique consists of three steps: First, a non-linear extrapolation of the airborne downward irradiance measurements to the ground is performed using radiative transfer calculations. Second, assuming a hypothetical surface albedo, the upward irradiances at the ground are extrapolated to the flight level, again on the basis of radiative transfer simulations. Third, using the calculated and measured upward irradiances and introducing

simple analytic equations the extrapolated surface albedo is obtained which matches both the measured and calculated upward irradiances at the flight level. In this way time-consuming iterations, as usually applied in satellite retrievals of surface albedo, are avoided.

### Average Spectral Surface Albedo over Sea and Land

Not each radiation measurement campaign can afford a detailed characterization of the spectral surface albedo, because either the instrumentation or the appropriate data are not available. Also the spectral details of the surface albedo may not always be that important for the special purpose of the campaign. Therefore, averaged spectral surface albedos are derived from the three measurements campaigns. These data contain thousands of spectra which are categorized separately for each campaign into the two types *SEA* and *LAND*.

In Figure 1 the averaged spectral *SEA* albedos obtained in the NORTH-SEA-2000 (open triangles) and the CRYSTAL-FACE-2002 (open squares) campaigns are presented. Additionally the albedo for "water" by Bowker et al. (1985) is plotted as dashed line. The spectral sea albedo from the CRYSTAL-

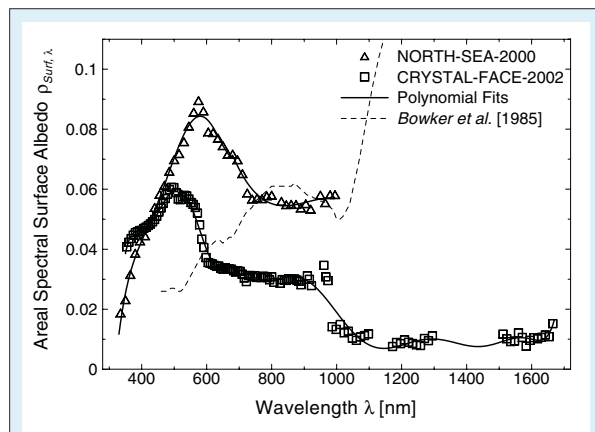


**Fig. 1:** Averaged areal spectral surface albedo over different *SEA* surfaces. The solid lines represent the respective parameterization using polynomial fits. Additionally spectral surface albedo data by Bowker et al. (1985) (type "water") are plotted as dashed line.

FACE-2002 experiment is lower compared to the results of both the NORTH-SEA-2000 campaign and the "water" albedo by Bowker et al. (1985) over most parts of the spectrum. The chlorophyll-a peak is obvious in both the NORTH-SEA-2000 and the CRYSTAL-FACE-2002 surface albedos, although the level is higher and the peak wavelength is shifted to larger wavelengths for the NORTH-SEA-2000 data set. The different levels can only partly be explained by the generally much larger solar zenith angles during the NORTH-SEA-2000 measurements. Different swell, sea water constituents, and ocean ground albedo in shallow

waters are further factors which can be responsible for the observed differences. The concentration of water constituents depend strongly on location and time. In September the North Sea may contain significant amounts of particulate material, yellow substance and chlorophyll, whereas the coastal waters of Florida are probably less contaminated. Yellow substance and particulate material can be characterized by a strong decrease in absorption with increasing wavelength while chlorophyll has an absorption maximum at around 430 nm. The scattering of particulate material depends only slightly on wavelength. A combined effect of these water constituents can explain the features of the albedo observed during NORTH-SEA-2000. Altogether these differences in the sea surface albedo illustrate how variable this quantity can be for different oceans.

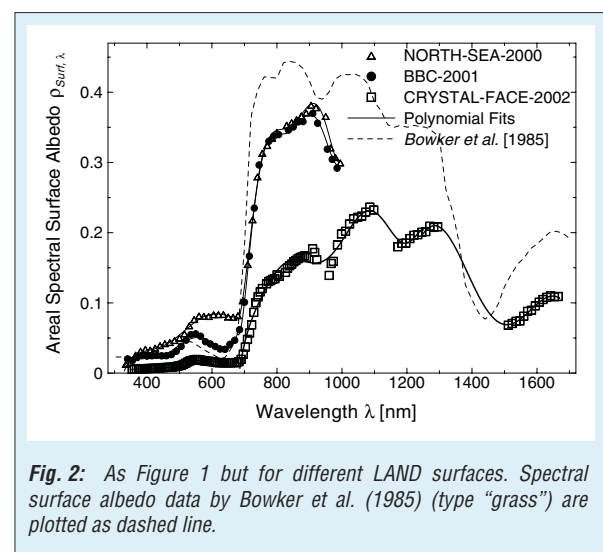


**Fig. 2:** As Figure 1 but for different *LAND* surfaces. Spectral surface albedo data by Bowker et al. (1985) (type "grass") are plotted as dashed line.

Figure 2 presents the averaged spectral surface albedos retrieved over *LAND* for the three measurement campaigns NORTH-SEA-2000 (open triangles), BBC-2001 (full dots), and CRYSTAL-FACE-2002 (open squares). Whereas the results for the two first campaigns are similar especially beyond 700 nm wavelength (the so-called vegetation step), the CRYSTAL-FACE-2002 spectral surface albedo over land is lower. Again, these different levels cannot be explained with the generally smaller solar zenith angle during the CRYSTAL-FACE-2002 measurements, and thus represent significant variations of natural land surface reflection. The first two campaigns were both performed in September with much living vegetation at the surface. The CRYSTAL-FACE-2002 took place in July over a terrain which strongly dries out in summer. However, all three data sets show a much less pronounced vegetation step compared to the literature data by Bowker et al. (1985) (type "grass").

Respective parameterization formulas for the spectral albedo functions in Figures 1 and 2 are given by Wendisch et al. (2004).

### Summary and Conclusions

Spectral albedo data from three field campaigns are used to derive typical spectral surface albedos within the wavelength range from 330-1670 nm over different types of sea and land surfaces. Such measurements are a crucial input for spectral radiative transfer calculations. The differences among the surface albedo measurements on the one hand, and the differences to the literature data reported by Bowker et al. (1985) on the other hand are significant. As a consequence

it is concluded that such literature data, which are strictly applicable for distinct surface types only, may not always be appropriate to analyze radiation data from airborne field campaigns. Instead, for a detailed analysis of radiation field experiments, a detailed characterization of the specific spectral reflection properties of the underlying surface is unavoidable. However, if such data or the appropriate instrumentation is not available, averaged spectral surface albedo data as those presented in this contribution can be used.

### References

- Bowker, D. E., Davis, R. E., Myrik, D. L., Stacy, K. and Jones, W. T. 1985.** Spectral reflectance of natural targets for use in remote sensing studies. NASA Reference Publication, **No. 1139**.
- Pilewskie, P., Pommier, J., Bergstrom, R., Gore, W., Howard, S., Rabbette, M., Schmid, B., Hobbs, P. V. and Tsay, S. C. 2003.** Solar spectral radiative forcing during the Southern African Regional Science Initiative. *J. Geophys. Res.*, **108**, 8486, doi: 10.1029/2002JD002411.
- Wendisch, M., Müller, D., Schell, D. and Heintzenberg, J. 2001.** An airborne spectral albedometer with active horizontal stabilization. *J. Atmos. Oceanic Technol.*, **18**, 1856-1866.
- Wendisch, M. 2003.** *Absorption of Solar Radiation in the Cloudless and Cloudy Atmosphere*. Habilitation, Universität Leipzig, 174 pp.
- Wendisch, M. and Mayer, B. 2003.** Vertical distribution of spectral solar irradiance in the cloudless sky - A case study. *Geophys. Res. Lett.*, **30**, 1183-1186, doi: 10.1029/2002GL016529.
- Wendisch, M., Pilewskie, P., Jäkel, E., Schmidt, S., Pommier, J., Howard, S., Jonsson, H. H., Guan, H., Schröder, M. and Mayer, B. 2004.** Airborne measurements of areal spectral surface albedo over different sea and land surfaces. *J. Geophys. Res.*, **accepted**.

#### Funding

- Deutsche Forschungsgemeinschaft
- Bundesministerium für Bildung, Wissenschaft, Forschung und Technologie
- National Research Council, The National Academies, USA

#### Cooperation

- enviscope GmbH, Frankfurt am Main
- Institut für Weltraumwissenschaften, Freie Universität Berlin
- Deutsches Zentrum für Luft- und Raumfahrt, Oberpfaffenhofen
- NASA Ames Research Center, Moffett Field, California, USA
- Bay Area Environmental Research Institute, Sonoma, California, USA
- Center for Interdisciplinary Remotely-Piloted Aircraft Studies, Marina, California, USA

## Siberian forest fire smoke travels around the world

Ulla Wandinger, Dietrich Althausen, Albert Ansmann, Ina Mattis, Detlef Müller

*Im Sommer 2003 wurden über mehrere Monate um einen Faktor 3-4 erhöhte Aerosolbelastungen über Leipzig in der freien Troposphäre beobachtet. Die Messungen erfolgten mit dem EARLINET-Lidar. Anhand von Satellitenbildern liess sich als Herkunftsgebiet das südöstliche Sibirien (östlich des Baikalsees) ausmachen. Dabei drifteten die Waldbrandwolken über Japan, den Pazifik, Nordamerika und den Nordatlantik nach Europa. Die Partikel beeinflussen den Strahlungshaushalt und die Wolkenbildung in der üblicherweise sehr sauberen freien Troposphäre.*

Unexpectedly high particle backscattering and extinction were measured with Raman lidar at Leipzig, Germany, in the free troposphere in May - July, 2003 (Mattis et al., 2003). We never observed such unusual aerosol conditions during the operational period of the lidar. The Leipzig lidar is part of the European Aerosol Research Lidar Network (EARLINET) and monitors the troposphere and stratosphere on a routine basis since 1997. From time to time lofted aerosol plumes from North America (Wandinger et al., 2002) and dust from Africa (Mattis et al., 2002) can be observed in the free troposphere over central Europe. All these events recorded during the past six years did not last longer than a few days to one week. In contrast, in the summer half year of 2003 significantly enhanced backscattering and extinction by particles were measured over longer time periods. The increased free tropospheric aerosol occurred at the time of Siberian forest fires that were exceptionally strong in May 2003. Fires were detected east of the Ural mountains all the way to the eastern border of Russia mainly between 50° - 55° N. The last extreme Siberian fires date back to the mid 1980ies. According to satellite observations rather dense smoke plumes were present over eastern Russia and northern China on May 15 - 20, 2003. Model calculations indicated high smoke particle optical depth of 2 - 10 at 500 nm. The Siberian smoke was transported eastward, crossed Japan and the Pacific Ocean, and was observed over central and eastern Canada on May 23 and 24, respectively. Satellite images showed smoke between Iceland and southern Scandinavia on May 27, 2003. In agreement with these satellite observations we registered a significant increase of the aerosol in the free troposphere in the end of May, 2003. The spectrally resolved optical properties observed in May - July, 2003 in the free troposphere clearly indicated aged smoke as discussed below. Modelling studies suggest that Russian forest fires are a significant source of pollution in the northern hemisphere (Wotawa et al., 2001), which can be distributed over the northern hemisphere by the prevailing westerlies

within 20 days after emission (Stohl et al., 2002). Forster et al. (2001) demonstrated that if washout is inefficient, very pronounced haze layers in the free troposphere can be created by aerosols from forest fire emissions and can be transported over very long distances.

Large-scale smoke events affect climate because of the relatively high optical depth, air chemistry because of the significantly enhanced particle optical depth in the UV, and satellite remote sensing in which aerosol effects have to be removed. These events may have also influenced cirrus formation because of the unusually high particle concentration in the upper troposphere.

Figure 1 shows the lidar observations of free tropospheric smoke layers on June 26, 2003. At that time, the particles were distributed over the entire free troposphere from 2.5 km up to about 11-km height. Well stratified aerosol layering was found with the highest aerosol concentrations around 6-km height as predicted by the above mentioned modelling studies.

The example from June 26, 2003, is presented in detail in Figure 2. Backscatter coefficients show a pronounced spectral behavior throughout the free

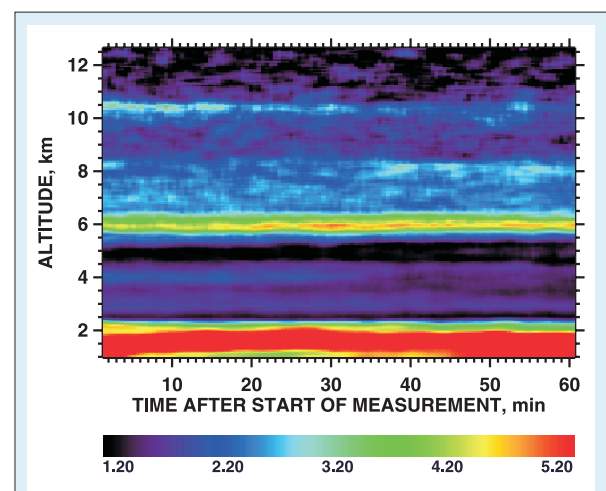


**Fig. 1:** Backscatter ratio (backscattering by particles and molecules relative to respective backscattering by molecules alone) at 1064 nm. The observation was taken on June 26, 2003, 2200-2300 UTC.

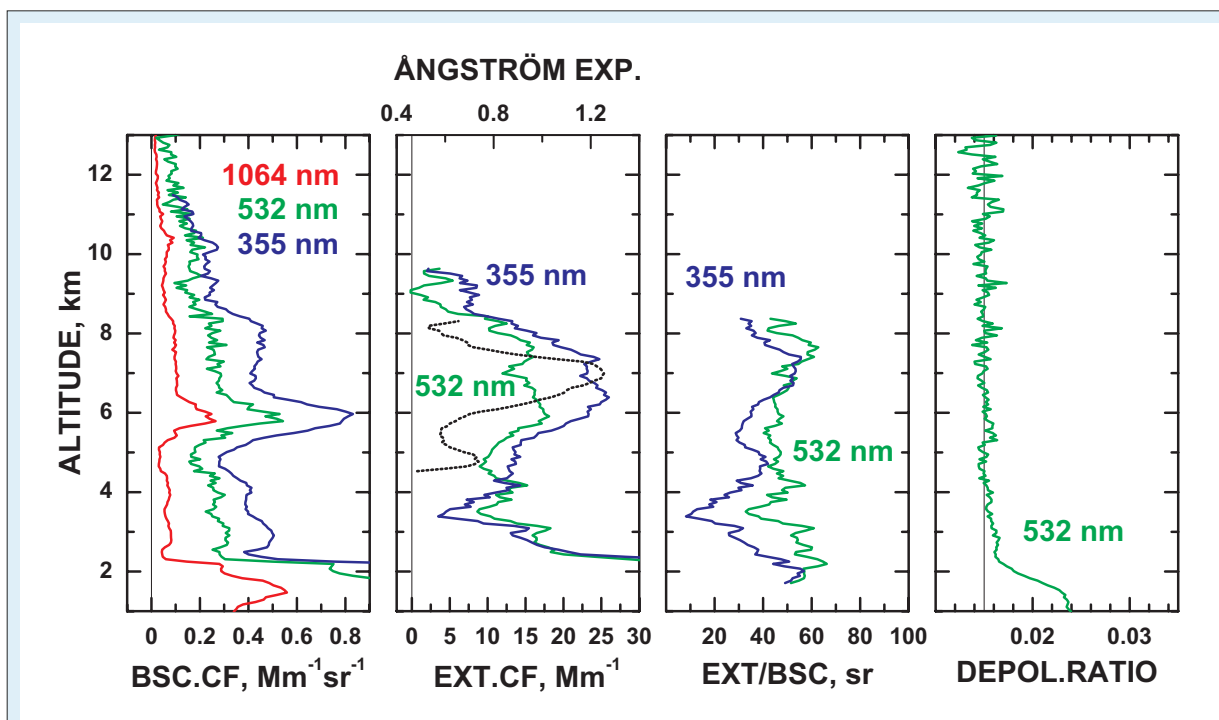


Fig. 2: Raman lidar observations (one-hour average on June 26, 2003) of the particle backscatter coefficients (BSC. CF), volume extinction coefficients of particles (EXT. CF) and respective 355 nm / 532 nm Ångström exponent (dotted black), extinction-to-backscatter ratio (EXT/BSC), and depolarization ratio. The depolarization ratio for pure molecular backscattering (vertical line) is shown for comparison.

troposphere (boundary layer top at 2200-m height). Volume extinction coefficients at 355 and 532 nm were as high as 15 and 25  $Mm^{-1}$  respectively, in the 4-8-km height range. The corresponding free tropospheric particle optical depths were with 0.05 (532 nm) and 0.1 (355 nm) of comparable magnitude as in thin visible cirrus clouds. The Ångström exponent took values mostly below one in the smoke layers. An interesting feature is presented in the plot of the extinction-to-backscatter ratio (lidar ratio). The 355-nm lidar ratio was lower than the 532-nm lidar ratio. This behavior clearly indicates aged smoke. Desert dust and lofted urban haze in the free troposphere would show the opposite behavior. Low depolarization ratios corroborate that desert dust (and ice clouds) were absent. Nonspherical particles would cause depolarization ratios larger than 0.1.

Similar optical properties were found over central Europe within an aged smoke plume that originated from forest fires in western Canada in August, 1998 (Wandinger et al., 2002). The optical properties of aged smoke are quite different from those of young smoke, mainly due to a significant shift of the size distribution towards larger particles (Westphal and Toon, 1991). Ångström exponents for young smoke of Canadian and eastern European forest fires calculated from Sun photometer observations were found to be  $>1.5$  (O'Neill et al., 2002, Balis et al., 2003).

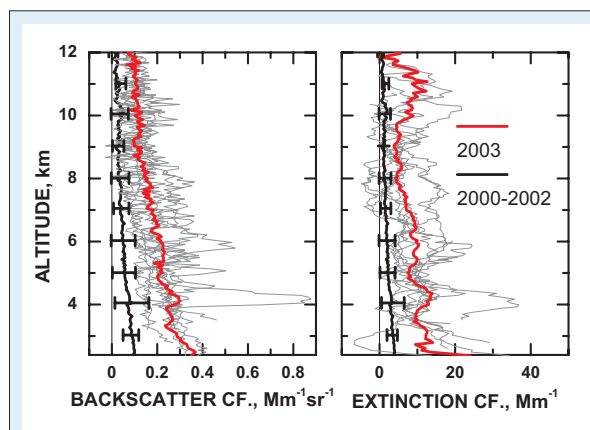


Fig. 3: Individual lidar observations (thin grey lines) and mean profiles (red lines) of the particle backscatter and extinction coefficients at 532 nm for the period from May 29 to July 14, 2003. Reference profiles representing the aerosol conditions measured with the same lidar in May-July of 2000-2002 are shown for comparison (thick black). Error bars (local standard deviations) indicate the atmospheric variability.

Figure 3 finally shows that aerosol backscattering and extinction at 532 nm were enhanced by a factor of 3-4 in May-July of 2003 compared to free-tropospheric conditions during the respective months of 2000, 2001, and 2002. The background mean particle optical depth is 0.017 for the 3-12-km height range. The respective mean optical depth for May-July 2003 was close to 0.075 at 532 nm.

## References

- Balis, D. S., Amiridis, V., Zerefos, C., Gerasopoulos, E., Andreae, M., Zanis, P., Kazantzidis, A., Kazadzis, S. and Papayannis, A. 2003.** Raman lidar and sunphotometric measurements of aerosol optical properties over Thessaloniki, Greece during a biomass burning episode. *Atmos. Environ.*, **47**, 4529-4538.
- Forster, C., James, P., Wotawa, G., Wandinger, U., Mattis, I., Althausen, D., Simmonds, P., O'Doherty, S., Jennings, S. G., Kleefeld, C., Schneider, J., Trickl, T., Kreipl, S., Jäger, H. and Stohl, A. 2001.** Transport of boreal forest fire emissions from Canada to Europe. *J. Geophys. Res.*, **106**, 22887-22906.
- Mattis, I., Ansmann, A., Müller, D., Wandinger, U. and Althausen, D. 2002.** Dual-wavelength Raman lidar observations of the extinction-to-backscatter ratio of Saharan dust. *Geophys. Res. Lett.*, **29**, doi: 10.1029/2002GL014721.
- Mattis, I., Ansmann, A., Wandinger, U. and Müller, D. 2003.** Unexpectedly high aerosol load in the free troposphere over central Europe in spring/summer 2003. *Geophys. Res. Lett.*, **30**, doi: 10.1029/2002GL018442.
- O'Neill, N.T., Eck, T. F., Holben, B. N., Smirnov, A., Royer, A. and Li, Z. 2002.** Optical properties of boreal forest fire smoke derived from Sun photometry. *J. Geophys. Res.*, **107**, doi: 10.1029/2001JD000877.
- Stohl, A., Eckhardt, S., Forster, C., James, P. and Spichtinger, N. 2002.** On the pathways and timescales of intercontinental air pollution transport. *J. Geophys. Res.*, **107**, 4684, doi:10.1029/2001JD001396.
- Wandinger, U., et al. 2002.** Optical and microphysical characterization of biomass-burning and industrial-pollution aerosols from multiwavelength lidar and aircraft measurements. *J. Geophys. Res.*, **107**, doi: 10.1029/2000JD000202.
- Westphal, D. L. and Toon, O. B. 1991.** Simulations of Microphysical, Radiative, and Dynamical Processes in a Continental-Scale Forest Fire Smoke Plume. *J. Geophys. Res.*, **96**, 22379-22400.
- Wotawa, G., Novelli, P. C., Trainer, M. and Granier, C. 2001.** Inter-annual variability of summertime CO concentrations in the Northern Hemisphere explained by boreal forest fires in North America and Russia. *Geophys. Res. Lett.*, **28**, 4575-4578.

**Funding**

- EU (EARLINET)

**Cooperation**

- EARLINET-Consortium

## LACIS: Instrumental development and measurements

Heike Wex, Alexei Kiselev, Martin Simmel, Frank Stratmann, Judith Zoboki

LACIS (Leipziger Aerosol Cloud Interaction Simulator) wurde im Jahr 2003 weiterentwickelt, so dass Messungen bei Drücken unabhängig vom Umgebungsdruck durchgeführt werden konnten. Damit wurde das Aufwachsen von Natriumchlorid- und Ammoniumsulfatpartikeln bei 1000 mbar bzw. 700 mbar und bei relativen Feuchten größer als 100% gemessen. Im Weiteren wurde ein optisches Messsystem entwickelt, mit dem Partikelgrößen ab 300 nm detektiert werden können. Die neue Optik wurde verwendet, um Gleichgewichtsdurchmesser für Partikel (Natriumchlorid und Ammoniumsulfat) bei relativen Feuchten von 85%-98.5% zu bestimmen. Die dabei gemessenen feuchten Partikelgrößen wurden mit Literaturwerten verglichen. Für alle Messungen wurden Vergleichsrechnungen mit dem FPM in FLUENT durchgeführt. Messungen und Rechnungen stimmten sowohl für übersättigte als auch für untersättigte Bedingungen gut überein.

In 2003 the development of the Leipzig Aerosol Cloud Interaction Simulator (LACIS, Stratmann et al., 2004) was continued and measurements regarding the particle/droplet growth at different system pressures and concerning equilibrium droplet sizes for pure salts were conducted.

In this context, LACIS was modified to enable measurements at pressures different from the ambient pressure. Growth of sodium chloride and ammonium sulfate particles was measured at system pressures of 1000 mbar and 700 mbar for different super-saturations in the LACIS flow tube. The sizes of the grown droplets were determined with a Fast-FSSP (Forward Scattering Spectrometer Probe, Brenguier et al., 1998). The results from these measurements were compared with values from model calculations performed with the FPM (Fine Particle Model, Wilck et al. 2002) in FLUENT 6 (Fluent, 2001). In these calculations, an accommodation coefficient of one for water on water is used (Kreidenweis et al. 2003). A comparison of the results gained can be seen in Figure 1. An overlap between the measured and the modeled values within the measurement uncertainty was found for both investigated salts (sodium chloride, ammonium sulfate) at both system pressures. The deviations between measurement and model are smaller than 5%.

Furthermore, to enable in-situ non-disturbing measurement of smaller droplets a new optical particle sizing system was built. The principle of the system is based on the measurement of light scattered by single droplets into a wide solid angle in the forward direction. The schematic arrangement of the optical components is shown in Figure 2. A He-Xe arc lamp is used as a source of white light. Scattered light is collected by elliptical mirrors and directed onto photomultiplier tubes, which are connected to the high-speed signal acquisition and procession system. Due to the combination of wide scattering angle with white

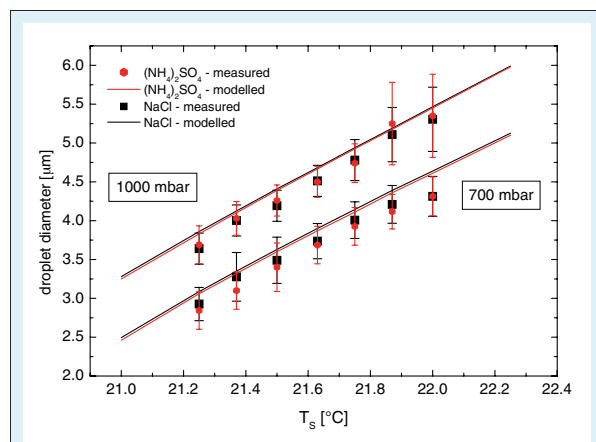


Fig. 1: Comparison of measured and calculated droplet sizes for two different salts and two different pressures at different super-saturations.

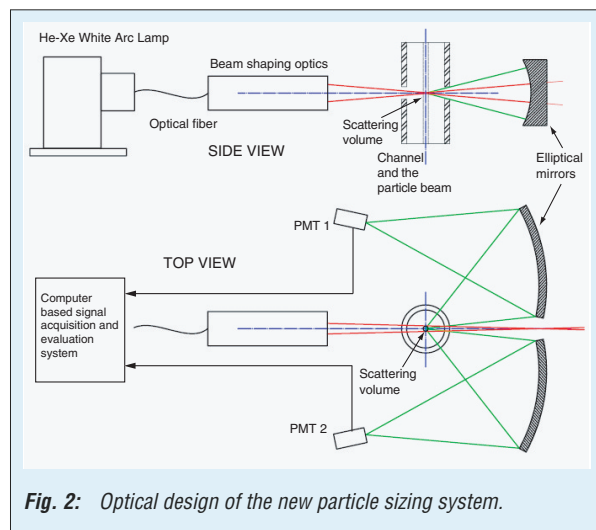
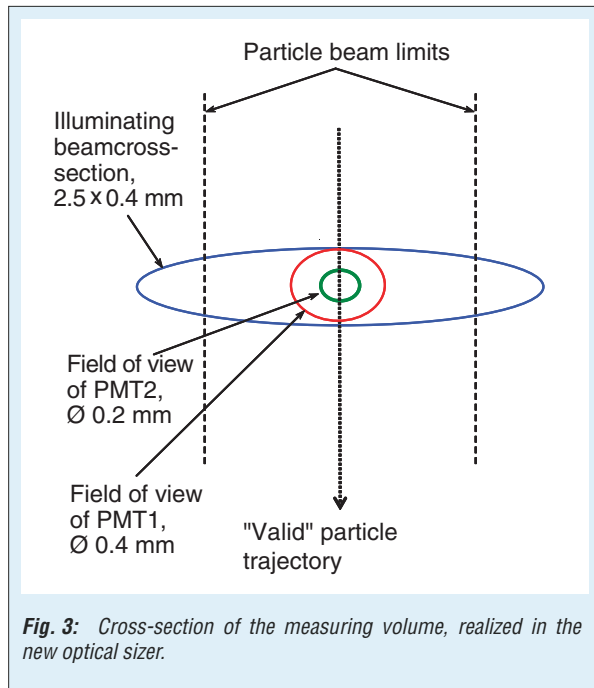


Fig. 2: Optical design of the new particle sizing system.

light (300 - 850 nm), the optical system possesses an unambiguous signal response function. Comparison of digitized signals in two optically divided channels allows evaluation of only those droplets, that are passing through the center

of measuring volume, where the illuminating light is most homogeneous (see Figure 3), thus reducing edge effects and coincidence, and therefore improving the accuracy of measurements. Implementation of a high resolution (16 bit) acquisition card allows to measure droplet sizes in the range 0.3 – 10  $\mu\text{m}$ .



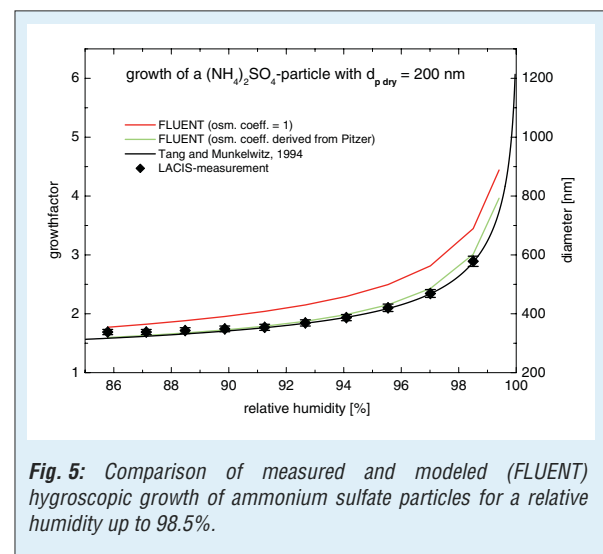
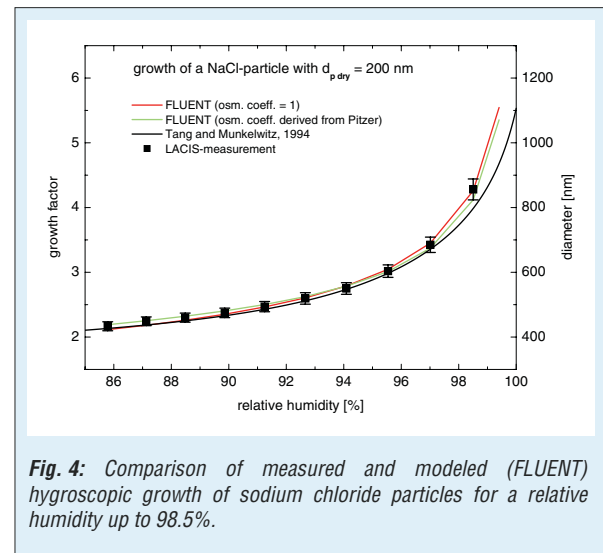
Utilizing the new optical system, measurements concerning the equilibrium sizes of pure sodium chloride and ammonium sulfate particles were carried out for relative humidities between 86% and 98.5%. The measured growth factors were compared to values derived from measurements of Tang and Munkelwitz, 1994. Additionally, droplet sizes theoretically determined utilizing the FPM in FLUENT were used in the comparison. The results of measurements and calculations are shown in Figure 4 and Figure 5. For the FLUENT calculations, different values for the osmotic coefficient in the Raoult part of the droplet growth law were used. First, the osmotic coefficient was set to be one, i.e. ideal behavior of the solution droplet was assumed. In a second run, the osmotic coefficient was used as derived from Pitzer and Maygora, 1973.

Both approaches agree well for sodium chloride and the calculated values are also in agreement with the measured data and with those derived from Tang and Munkelwitz, 1994 (Figure 4).

For ammonium sulfate the growth factors derived from the LACIS measurements, from Tang and Munkelwitz, 1994, and from the FLUENT calculation using the osmotic coefficient according to Pitzer and Maygora, 1973, are in good agreement. However, using the constant value of one for the osmotic coefficient, i.e. assuming ideal behavior for the solution droplet, yields

significant deviations from the other “non-ideal” data (Figure 5).

These findings maybe explained by comparing the osmotic coefficients of sodium chloride and ammonium sulfate. For sodium chloride the osmotic coefficient is around one, whereas for ammonium sulfate values around 0.7 can be found. Consequently, for ammonium sulfate deviations from the ideal solution behavior are more pronounced.



Summarizing the results it can be stated that for the investigated thermodynamic conditions:

- existing growth laws seem to be applicable to describe the growth of pure sodium chloride and ammonium sulfate particle assuming an **accommodation coefficient of one** for water on water.
- the osmotic coefficient according to Pitzer and Maygora, 1973, seems suitable to determine equilibrium droplet sizes of pure sodium chloride and ammonium sulfate even at relative humidities as high as **98.5%**.

### References

**Brenguier, J. L., Bourrienne, T., Coelho, A. A., Isbert, J., Peytavi, R., D.Trevarin and Wechsler, P. 1998.** Improvements of droplet size distribution measurements with the Fast-FSSP. *J. Atmos. Oceanic Technol.*, **15**, 1077-1090.

**Fluent 2001.** *FLUENT 6 Users Guide*. Fluent Inc., Lebanon, NY.

**Kreidenweis, S. M., Walcek, C. J., Feingold, G., Gong, W., Jacobson, M. Z., Kim, C.-H., Liu, X., Penner, J. E., Nenes, A. and Seinfeld, J. H. 2003.** Modification of aerosol mass and size distribution due to aqueous-phase SO<sub>2</sub> oxidation in clouds: Comparisons of several models. *J. Geophys. Res.*, **108**, 4213, doi: 10.1029/2002JD002697.

**Pitzer, K. S. and Mayorga, G. 1973.** Thermodynamics of electrolytes, II. Activity and osmotic coefficients for strong electrolytes with one or both ions univalent. *J. Phys. Chem.*, **77**, 2300-2308.

**Stratmann, F., Kiselev, A., Wurzler, S., Wendisch, M., Heintzenberg, J., Charlson, R. J., Diehl, K., Wex, H. and Schmidt, S. 2004.** Laboratory studies and numerical simulations of cloud droplet formation under realistic super-saturation conditions. *J. Atmos. Oceanic Technol.*, **accepted**.

**Tang, I. N. and Munkelwitz, H. R. 1994.** Water activities, densities and refractive indices of aqueous sulfates and sodium nitrate droplets of atmospheric importance. *J. Geophys. Res.*, **99**, 18801-18808.

**Wilck, M., Stratmann, F. and Whitby, E. R. 2002.** *A fine particle model for FLUENT: description and application*. 6th International Aerosol Conference, Taipei, Taiwan, **submitted**.

## Modeling the synoptic situation during SATURN: First results of mesoscale and large-eddy simulations

Jürgen Helmert

*Als Beitrag zum verbesserten Verständnis von aerosol-dynamischen Prozessen in der unteren Troposphäre fand vom 27. Mai bis 14. Juni 2002 das Feldexperiment SATURN an der Forschungsstation des IfT in Melpitz statt. Zur Untersuchung der meteorologischen Situation während der Intensivmessphase von SATURN wurden multiskalige Simulationen der meteorologischen Situation durchgeführt. Die Simulationsergebnisse zeigten eine gute Übereinstimmung mit gemessenen meteorologischen Parametern.*

### Motivation

To study nucleation events in the lower troposphere the field campaign “SATURN” was carried out from May, 27 to June, 14, 2002 at the Melpitz field research station of IfT (Stratmann et al., 2003). Ground based measurements and vertical soundings of meteorological and aerosol parameters were obtained. As a contribution to the SATURN experiment multiscale simulations of the meteorological conditions have been performed.

### Simulations

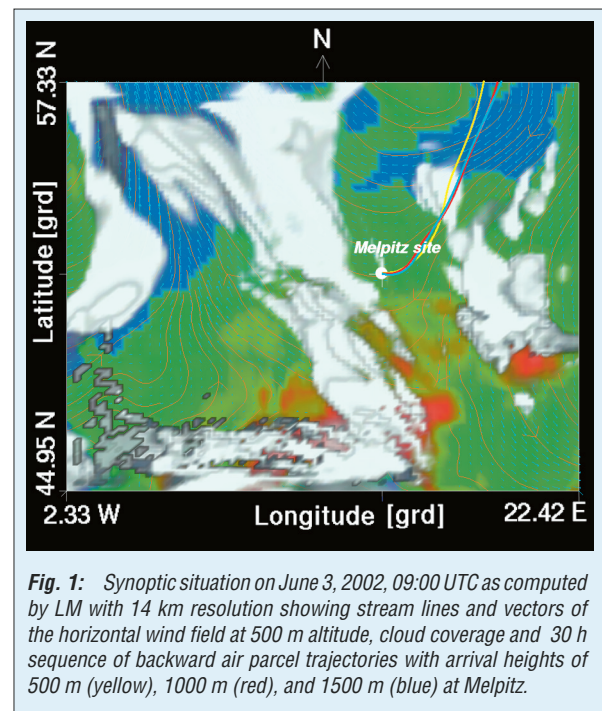
The mesoscale simulations are based on the Lokal-Modell (LM) of the Deutscher Wetterdienst (DWD) (Doms and Schättler, 1999). For initialization and large-scale forcing 6-hour analysis data of the global model (GME) were used. The simulations were performed with different grid resolutions (14 km, 7 km, 2.8 km, 1.1 km). The output from the coarser grid forced the subsequent runs with the finer grid. This method allows to resolve large-scale synoptic patterns in a domain of 1400 km x 1400 km as well as regional scale structures in a domain of 120 km x 120 km around Melpitz. The integration time was June 1, 00:00 UTC to June 4, 18:00 UTC. To examine the LM prediction of the planetary boundary layer (PBL), accompanying large-eddy simulation (LES) for June 3, 05:30 UTC to 10:30 UTC was performed. Here, the LES model of the Max-Planck-Institut für Meteorologie Hamburg (Chlond, 1992) was used. The domain size was 3.2 km x 3.2 km x 2.2 km (64 x 64 x 110 grid cells).

Vertical profiles of potential temperature and total water content for model setup were derived from SATURN soundings at 05:30 UTC. The LES was driven by a varying surface heat flux derived from ground-based sonic measurements. The model output was averaged over 30 minute-intervals to determine statistical moments (means, (co)variances).

### Results

The large-scale synoptical situation during the intensive measurement phase on June, 3 can be seen from the LM simulation with 14 km resolution (Figure 1). Predicted horizontal wind fields at 500 m altitude agree well with the observations at Melpitz, where weak winds from south-east were observed. A cloud system passed Germany eastwards crossing Melpitz at about noon.

Backward air parcel trajectories for interpretation of the measurements at Melpitz were determined from predicted 3D wind fields for arrival heights of 500 m, 1000 m, and 1500 m (Figure 1).



A comparison of the boundary layer development in the morning hours of June, 3 between LM 1.1 km simulation, LES, and SODAR measurements at the Melpitz site is given in Figure 2. Similar to the observations, LM and LES results show an increase of the boundary layer due to strong forcing of the surface heat flux. The evolution of temperature and water vapor at Melpitz derived from LM 1.1 km and

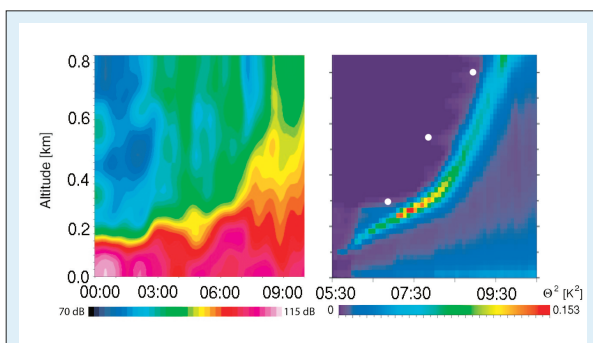


**Fig. 2:** Time evolution of the boundary layer height on June, 3, 2002 derived from SODAR measurements of the back-scattered signal intensity (left) from large-eddy simulation of the potential temperature variance (right) and from LM 1.1 km (white points) using eddy diffusivity coefficient.

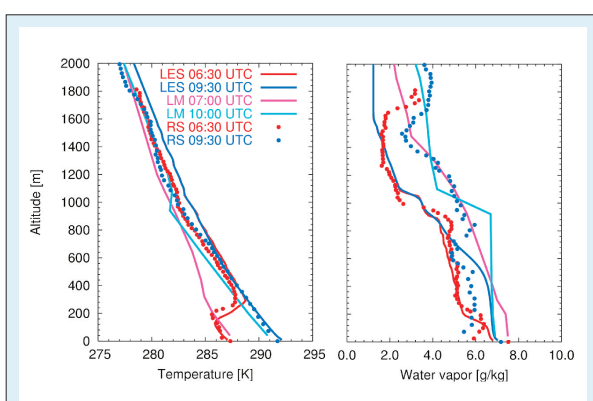


**Fig. 3:** Vertical profiles of temperature (left) and water vapor (right) as simulated by LM 1.1 km and large-eddy simulation (lines) and derived from rawinsondes measurements (points).

LES are compared in Figure 3 with rawinsondes soundings. Within the boundary layer, observations and simulations of the temperature agree well. However, LM predicts the breakup of nocturnal temperature inversion between 200 m and 300 m earlier than observed. At 06:30 UTC, after 1 hour integration time LES agrees well with measured water vapor. Although LES and LM predicted similar water vapor concentrations below 500 m at 09:30 UTC to 10:00 UTC the deviations to the measured water vapor are approximately of 15%.

The good agreement of LM with rawinsondes soundings of water vapor above the boundary layer at 10:00 UTC are due to large-scale forcing, which is not considered in LES.

### Summary and Outlook

The first simulation results of the synoptic situation during the SATURN campaign agree well with measurements. LM results were compared with large-eddy simulation showing a good agreement after breakup of the nocturnal temperature inversion. Thus, using the LM advantages of taking into account large-scale forcing it will be used in further simulations of chemistry transport and aerosol dynamical processes contributing to the understanding of nucleation events in the lower troposphere.

### Acknowledgements

Special thanks are due to O. Hellmuth, R. Wolke, O. Knoth, W. Schröder, B. Heinrich, F. Stratmann, H. Siebert and B. Wehner.

### References

- Chlond, A. 1992.** Three-dimensional simulation of cloud street development during a cold air outbreak. *Bound.-Layer Meteor.*, **58**, 161-200.
- Doms, G. and Schättler, U. 1999.** *The nonhydrostatic limited-area model LM (Lokal-Modell) of DWD.* Tech. Rep. Report Deutscher Wetterdienst, Geschäftsbereich Forschung und Entwicklung.
- Stohl, A., Wotawa, G., Seibert, P. and Kromp-Kolb, H. 1995.** Interpolation errors in wind fields as a function of spatial and temporal resolution and their impact on different types of kinematic trajectories. *J. Appl. Meteor.*, **34**, 2149-2165.
- Stratmann, F., Siebert, H., Spindler, G., Wehner, B., Althausen, D., Heintzenberg, J., Hellmuth, O., Rinke, R., Schmieder, U., Seidel, C., Tuch, T., Uhrner, U., Wiedensohler, A., Wandinger, U., Wendisch, M., Schell, D. and Stohl, A. 2003.** New-particle formation events in a continental boundary layer: First results from the SATURN experiment. *Atmos. Chem. Phys.*, **3**, 1445-1459.

## Coupled treatment of microphysics and chemistry in a parcel model

Oswald Knoth

*Ein gekoppeltes Mikrophysik-Chemie Model wird vorgestellt. Wasser wird in der Gas- und Flüssigphase wie jedes andere Spurengas behandelt. Das Modell ist frei konfigurierbar. Für die Zeitintegration wird ein implizites Rosenbrock Verfahren genutzt. Die notwendigen Gleichungssysteme werden unter Nutzung von Sparse-Techniken gelöst. Das Modell wird zur Simulation der Aktivierung und des Aufwachsens eines Ammoniumsulfataerosols und der gleichzeitigen Aufnahme und chemischen Umwandlung von  $SO_2$  und anderer Spurengase genutzt.*

### Introduction

The accurate and efficient description of aerosol microphysical and chemical processes is required for the assessment of radiative and chemical effects of natural and anthropogenic atmospheric aerosols. The combined modeling of microphysical and chemical processes in the gas and aqueous phase such as meteorological changes, transformation of chemical species in the gas and liquid phase and the transfer of species from one phase to the other is required. Since the aforementioned processes proceed on similar time scales the usual time splitting schemes which perform process by process in a sequential order are not appropriate. Essential parts of the model are outlined and an implicit time integration method is proposed for the model simulation. In contrast to the SPACCIM model where a microphysical and a cloud chemistry model are coupled the new approach treats both processes in a unified way both from the modeling and numerical point of view. It is argued that this new model type is better suited for incorporation in multidimensional atmospheric and transport models.

### The microphysical-chemical model

The model assumes a size-resolved particle spectrum consisting of water, dissolved chemical species and insoluble aerosol nuclei. The dissolved chemical species originate either from the cloud condensation nuclei or are transferred from the surrounding gas phase to the aqueous phase. Water vapor is treated as other trace gases in the atmosphere and cloud water as other chemical species in the cloud droplets. The transfer of water vapor and other species is modeled as a nonequilibrium process where the water vapor pressure is computed from a Köhler-type equation and the gas transfer by the theory of Schwartz.

The Raoult term of the Köhler equation accounts for the total ion concentration in the droplet and is used in the form:

$$R = \frac{\sum_i \frac{m^i}{M_i}}{\frac{m^w}{M_w}},$$

where  $m^i$  and  $M_i$  are the mass and corresponding molecular mass for all soluble species and  $m^w$  and  $M_w$  the same for water inside a droplet. The model is freely configurable in the sense that the number of species in both phases and the chemical reaction system including the phase transfer are part of the input. The model can be used in a fixed bin (Eulerian frame) or a moving bin (Lagrangian frame) mode. In the fixed bin approach the number concentration and the partial mass of each species is prognosed for each bin whereas in the moving bin approach only the partial masses have to be computed and the number concentration is fixed. In the latter case the model can be initialized with an arbitrary number of dry particles which differ in mass and composition. In the Eulerian setting (Tzivion et al., 1989) the prognostic variables are defined from the number distribution  $n(m)$ , a mass grid  $[m_k, m_{k+1}]$  and the local mass distribution

$$m = \sum_i m^i(m) \text{ by}$$

$$N_k = \int_{m_k}^{m_{k+1}} n(m) dm$$

and

$$M_k^i = \int_{m_k}^{m_{k+1}} n(m) m^i(m) dm$$

where the index  $k$  enumerates the bins and the index  $i$  the species contained in a droplet. Considering only condensation the model equations have the form

$$\dot{N}_k = - \int_{m_k}^{m_{k+1}} \frac{\partial}{\partial m} \dot{m}(m^1, \dots, m^l, c_G) n(m) dm$$

and

$$\dot{M}_k^i = - \int_{m_k}^{m_{k+1}} \frac{\partial}{\partial m} \dot{m}(m^1, \dots, m^l) n(m) m^i(m) dm + N_k \dot{m}^i(M_k^i / N_k, \dots, M_k^l / N_k, c_G)$$

where  $c_G$  is the vector containing gas phase concentrations, water vapor and the meteorological variables,  $\dot{m}$  gives the mass change due to phase transfer and chemical transformations. The meteorological variables describe an adiabatically lifted air parcel which is driven by a prescribed time-dependent updraft velocity, a fixed pressure gradient and starting values for temperature and pressure.

The model equations are integrated in time by a second order Rosenbrock method which requires the computation of the Jacobian of the right hand side of the model equations and the solution of linear systems with this Jacobian. Rosenbrock methods are integration methods of implicit type (solution of linear systems) which are the only ones which can integrate the very stiff aqueous phase chemistry with sufficiently large time steps. To handle realistic applications special techniques have to be used for computing and storing the Jacobian matrices, (cf. Wolke and Knoth, 2002). The sparse storage scheme and the exploitation of the block diagonal structure of the Jacobian results in computational costs per time step which are proportional to the number of species and the number of bins.

### Sulfur chemistry

The model is applied to an example from the aerosol parcel model component of the 5<sup>th</sup> International Cloud Modeling Workshop, (Kreidenweis et al., 2003). Dissolved constituents in cloud water result from the scavenging of a specified lognormal dry aerosol size distribution and dissolution of gases, and concentrations are modified by the oxidation of SO<sub>2</sub> by H<sub>2</sub>O<sub>2</sub> and O<sub>3</sub>. The chemical composition of cloud water is simulated for an air parcel lifted adiabatically at 0.5 m s<sup>-1</sup> starting from a height slightly below cloud base. The simulation time is 2596 s with the cloud base being reached at 196 s. The initial ammonium and sulfate concentrations of the dry aerosol represent a slightly acidic ammonium bisulfate. The initial ammonia gas concentration is not in equilibrium with this aerosol composition. For more details cf. Kreidenweis et al., 2003.

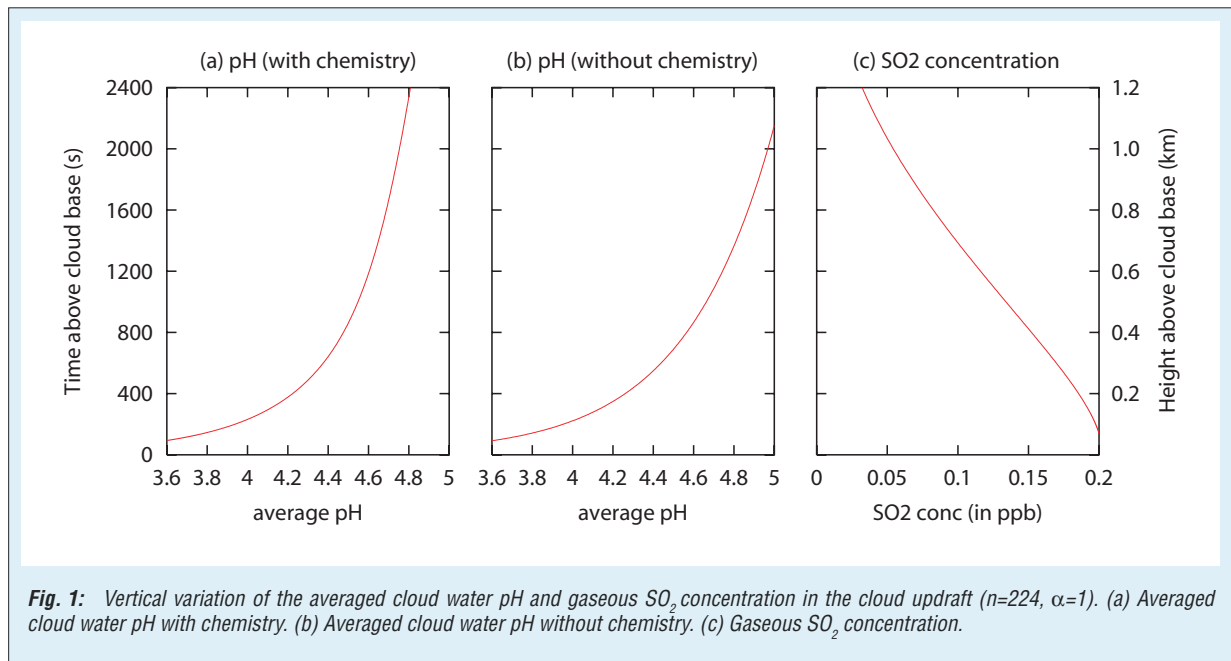
### Results

In Table 1 the number of activated particles is compared in dependency on the used grid resolution and two different values of the water condensation mass accommodation coefficient. The grid points for the different grids are logarithmically distributed with a factor ranging from 2<sup>2</sup> to 2<sup>8</sup>. The value of the accommodation coefficient represents a major uncertainty in modeling the condensational growth of cloud droplets. For a lower accommodation coefficient a higher number of particulate fractions are activated. Since the smaller fractions are better resolved also for the coarser grids and do not contribute much to the number concentration for the example the number of activated aerosols is similar for the different grids. On the other side for the larger accommodation coefficient the differences between the different grids are more pronounced. These discrepancies in the number concentration occur also between the different models contributing results to the model comparison and range for  $\alpha=1$  between 250 cm<sup>-3</sup> and 400 cm<sup>-3</sup>.

Number of bins $n$	Number of activated particles for $\alpha=.042$ in cm <sup>-3</sup>	Number of activated particles for $\alpha=1$ in cm <sup>-3</sup>
28	409	276
56	409	346
112	409	312
224	394	329
448	394	320

Tab. 1: Variation of drop number concentration with number of bins  $n$  and water condensation mass accommodation coefficient  $\alpha$ .

Figure 1a shows the calculated water-mass-weighted average cloud water pH as a function of time above cloud base. Due to the low water content near cloud base, and the acidic nature of the aerosols, cloud water pH starts with a value of 3.6. But as the acidic material is diluted the pH values increases rapidly. The observed increase in pH is mainly due to effects of dilution but is lower than without chemistry and phase transfer, c.f. Figure 1a and 1b. The model calculates an increase in sulfate mass by 180 ppt which is demonstrated by the loss of gaseous SO<sub>2</sub> in Figure 1c.



## References

- Kreidenweis, S. M., Walcek, C. J., Feingold, G., Gong, W., Jacobson, M. Z., Kim, C.-H., Liu, X., Penner, J. E., Nenes, A. and Seinfeld, J. H. 2003.** Modification of aerosol mass and size distribution due to aqueous-phase SO<sub>2</sub> oxidation in clouds: Comparisons of several models. *J. Geophys. Res.*, **108**, 4213, doi: 10.1029/2002JD002697.
- Tzivion, S., Feingold, G. and Levin, Z. 1989.** The evolution of raindrop spectra. Part II. Collisional collection/breakup and evaporation in a rainshaft. *J. Atmos. Sci.*, **46**, 3312-3327.
- Wolke, R. and Knuth, O. 2002.** Time-integration of multiphase chemistry in size-resolved cloud models. *Appl. Num. Math.*, **42**, 473-487.

### Determination of emission rates of diffuse sources by DOAS measurements and inverse dispersion modeling

Sandra Gerber, Eberhard Renner

*Grundlage für atmosphärische Ausbreitungsrechnungen ist die Kenntnis der Emissionsraten der betrachteten Quelle. Besonders bei diffusen Quellen ist deren Ermittlung oft mit großen Schwierigkeiten verbunden. In der hier vorliegenden Arbeit wird eine Methode vorgestellt, mit der es möglich ist, schwer zugängliche diffuse Quellen zu quantifizieren.*

*Dazu wurden ein DOAS (Differentielle Optische Absorptions- Spektroskopie)-Trassenmesssystem zur Messung von Ammoniakkonzentrationen und das Ausbreitungsmodell LASAT (Lagrange Simulation von Aerosol-Transport) zur Bestimmung der Quellstärke nach inverser Modellierung eingesetzt.*

#### Introduction

The knowledge of the emission rate of a source is one precondition for simulating accurate dispersion scenarios. Especially the estimation of the source strength of diffuse sources is a difficult task. In this contribution a method to quantify the emission rates of diffuse sources is introduced and first measurements are presented. The method couples the optical pathway averaging measuring system DOAS (differential optical absorption spectroscopy) and the Lagrangian particle model LASAT (Janicke, 2001) used for inverse modelling. First, the method was tested with the release of SO<sub>2</sub> as a tracer gas. After that, the ammonia emission of open land poultry farming and of manure storage of a dairy cattle house has been determined. The dependence between the ammonia emission of the manure and the temperature respectively the wind speed will be shown.

The choice of agricultural ammonia sources is of high use. Livestock farming causes a great number of diffuse ammonia sources which are difficult to characterize. Ammonia act as a climate gas and may damage vegetation and reduce biodiversity in natural ecosystems (Melhorn, 1993).

It will be shown that the method provides a flexible and high efficient opportunity to evaluate diffuse sources.

#### Experimental

Ammonia concentrations were measured by a commercial DOAS system from OPSIS (Furulund, Sweden). The meteorological parameters wind speed and wind directions were measured by an anemometer with vane. Turbulence was determined by an ultrasonic anemometer. Air temperature, air humidity and air pressure were measured with commercial sensors. The DOAS components emitter/receiver and analyser and the meteorological equipment were arranged on a mobile trailer. The DOAS reflector was fixed on a separate pylon.

#### Modeling concept

For the determination of emission rates of diffuse sources the following modeling concept was used. The emission rate used in the transport model is varied until the modeled concentration is comparable to the measured concentration; pathway-averaged both, within a defined error. To attain this goal, an iteration procedure is used.

The Lagrangian particle model LASAT is used for the simulations. The model releases a number of particles (10,000-20,000) from the source, which statistically reproduce the turbulent transport of the considered pollutant. Each particle is associated with a certain mass, in order to obtain a predicted concentration that is comparable to the measured concentration.

The Lagrangian model concept largely reflects the natural phenomena involved in turbulent diffusion and the method eliminates numerical diffusion. The method always yields non-negative mass densities and is mass conserving. Complex obstacle geometries can be considered.

#### Trace gas experiment

To check the proposed procedure a trace gas experiment was carried out. SO<sub>2</sub> was emitted with a defined constant emission rate as tracer gas. During the measurement period no significant change of wind direction took place, so the dispersion plume of the SO<sub>2</sub> was inside the DOAS measurement path. Figure 1 shows the measured concentrations and wind speed as well as the simulated concentrations, modeled with meteorological parameters from a common anemometer and modeled with data from an ultrasonic anemometer. If one used the parameters from the regular anemometer one must run a pre-processor of LASAT to compute the wind field for the dispersion simulation. The ultrasonic anemometer yields the necessary meteorological parameters directly.

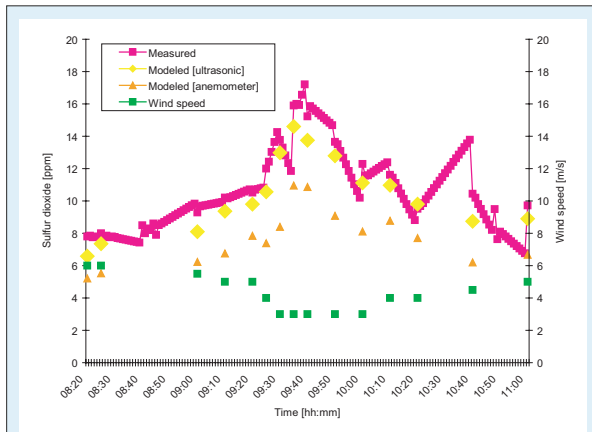


**Fig. 1:** Relation between measured concentration, modeled concentration (ultrasonic anemometer, anemometer with vane) and wind speed.

Best agreement between measured and modeled time series is achieved with the data from the ultrasonic anemometer. The differences between measured and modeled concentrations are in a range of 10 to 20%. Therefore, the data of an ultrasonic anemometer are used for the further investigations.

The relationship between the wind speeds and the concentrations is as expected: higher concentrations of  $\text{SO}_2$  at lower wind speeds and vice versa.

### Case study of manure storage

As one practical example the liquid manure box of a dairy cattle house was examined with the presented measuring system. The meteorological measurements and the pollutant measurements were made from March to June in 2002. The frequency of the wind direction and the measured ammonia concentrations show that during the measuring period at this location the main wind

direction East-South-East (about 30% of the time) was coupled with the highest ammonia concentrations. The measuring DOAS pathway was positioned perpendicular to the main wind direction East-South-East, in a distance of 60 m from the source. So, the ammonia plume was inside the DOAS pathway most of the time. For estimation of the emission rates only measured ammonia concentrations within a wind sector of  $30^\circ$  around East-South-East was used for the later inverse modeling.

The correlation of the ammonia emission rates and the air temperature subject to wind speed is shown in Figure 2.

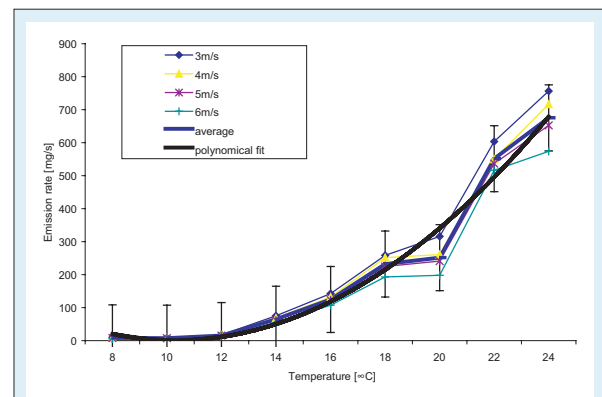


**Fig. 2:** Dependence of ammonia emission rates on temperature for different wind speeds.

One can recognize a clear dependency between the ammonia emission rates and the temperature for any wind speed. The ammonia emission rates rise with increasing temperature approximated by a polynomial of second order. The increasing emission rates at higher temperatures are described in the literature (Brose et al., 1998) and are caused by biochemical processes within the liquid manure.

### References

- Brose, G., Hartung, E. and Jungbluth, T. 1998.** Geruchs- und Spurengasemissionen eines Milchviehstalles. *Landtechnik*, **H 1**, 32-33.
- Janicke, L. 2001.** *Ausbreitungsmodell LASAT - Referenzbuch zu Version 2.10*. Gesellschaft für Umweltphysik, Dunum.
- Melhorn, G. 1993.** Entstehung, Ausbreitung und Wirkung von Schadgasen in der Tierproduktion. *Vet.-Med.*, **42**, 346-352.

#### Funding

- Landesamt für Umwelt und Geologie, Dresden

#### Cooperation

- Landesamt für Umwelt und Geologie, Dresden

## Flux measurements of main carbonyl compounds by the relaxed eddy accumulation (REA) technique

Cornelia Sedello, Hartmut Herrmann, Konrad Müller, Gerald Spindler

*Um die Oberflächen-Atmosphären-Wechselwirkungen von leichtflüchtigen Carbonylverbindungen (Formaldehyd, Acetaldehyd, Aceton u.a.) untersuchen zu können, wurde ein Relaxed Eddy Accumulation (REA) System entwickelt. Dieses wurde über zwei verschiedenen Oberflächen (Wiese und Fichtenwald) erfolgreich getestet. Die von Müller 1997 angewendete Methode zur Aufarbeitung der gesammelten Proben wurde an die mit der REA Technik gesammelten Proben angepasst.*

### Introduction

Since first investigations showed that volatile organic compounds (VOCs) from vegetation might be responsible for the formation of the “blue haze” above forested areas and that plants might contribute as much as 175 Tg of hydrocarbons to the atmosphere each year there has been interest in identifying the nature, sources and characteristics of biogenic emissions Kirstine (1998). Isoprene and monoterpenes are the dominant components of forest emissions, but at least 30% of the VOCs emitted by vegetation may be compounds other than isoprene and monoterpenes. To investigate the surface-atmosphere exchange of biogenic volatile organic compounds (BVOCs) other than isoprene and monoterpenes and to understand chemical processes affecting organic matter in the atmosphere a relaxed eddy accumulation system was developed to measure the vertical flow of carbonyl compounds like formaldehyde, acetaldehyde, acetone, and others over a coniferous forest and over grassland. The conditional sampling theory proposes that the vertical flux of a gas species can be measured by sampling air from updraught and downdraught motions into separate reservoirs over a suitable averaging period. This method is appropriate for atmospheric trace species which are relatively inert and can tolerate storage for an extended period without significant alteration.

### Experimental

The present REA system consists of three parts, the sonic anemometer (Gill R2, Lymington, Hampshire), the sampling device and a computer. The sonic anemometer gives a high resolution vertical wind signal which is used to control the switching of three valves. One valve is coupled to the upward (positive) vertical wind movements a second one to the downward (negative) vertical wind movements. The third valve is used for the so called dead band. This dead band is adjusted to the current turbulent conditions by the

standard deviation of the vertical wind:  $w_{\text{Threshold}} = 0.6 \sigma_w$  Guenther (1996). It is introduced to relax the system and thus to enable the conditional sampling of the carbonyl compounds of interest. The enrichment of the carbonyl compounds are performed on non-commercial cartridges which are filled with an inert adsorbent. The adsorbent is covered with an acidified 2,4-dinitrophenylhydrazine (2,4-DNPH) solution. To remove the ozone from the sampled air, ozone scrubbers ( $\text{MnO}_2$ ) are placed in front of the cartridges. The whole sampling device is controlled by the computer with the help of a Lab View® program. The sampling lasted 50 minutes with a sampling flow of  $2 \text{ L min}^{-1}$ . Investigations were made to transfer the elution method by Müller (1997) to the new requirements of the sampling with the REA. Due to the low solubility of the formed 2,4-DNPH derivatives of the carbonyl compounds in water, the excess 2,4-DNPH was partly removed by 2 times 1.5 ml water. The 2,4-DNPH derivatives were then eluted with 2 times 1.5 ml acetonitrile. Because of the very small amount of sampled air on each cartridge the received solution had to be evaporated down to 0.5 ml in a moderate nitrogen stream at

Compounds	Müller (1997) (1)	Villanueva-Fierro (2004) (2)	this study (3)
formaldehyde	0.08	0.8	0.02
acetaldehyde	0.05	0.9	0.01
acetone	0.04	1.5	0.01
propionaldehyde	0.04	1.1	0.01
methyl ethyl ketone	0.07	1.6	0.02
benzaldehyde	0.05	n.d.	0.01
trans-2-hexenal	0.05	n.d.	0.01
<b>Remarks:</b>	(1): detection limit in ppb for 150 l of sampled air and 3 ml sample solution (2): detection limit in ppb for 60-120 l of sampled air and 2 ml sample solution (3): detection limit in ppb for 100 l of sampled air and 0.5 ml solution		

**Tab. 1:** Detection limits in ppb of Müller (1997), Villanueva-Fierro (2004) and this study

45°C. Analysis of the samples was performed by HPLC-UV (High Pressure Liquid Chromatography) at 360 nm. Due to the preconcentration step we were able to improve the detection limit of Müller (1997). Table 1 shows the detection limits of Müller (1997), Villanueva-Fierro (2004) and this study.

With the determined concentrations we were able to detect fluxes of carbonyl compounds. The fluxes were calculated as follows:

$$F = b \sigma_w (c_{up} - c_{down}) \text{ Delany (1991)}$$

Where  $b$ =constant independent of stability ( $0.6 \pm 10\%$ )

$\sigma_w$  = standard deviation of vertical wind speed ( $\text{m s}^{-1}$ ).

### Results and discussion

REA measurements were made at two different sites. The first site is the IfT research station Melpitz over grassland in 6 m height in August 2003. The second site is the BITÖK (Bayreuth Institute for Terrestrial Ecosystem Research) research tower in the Fichtelgebirge. Measurements were made in 32 m height over a coniferous forest in September 2003 as part of the BEWA2000 project. Figure 1 shows the fluxes of the carbonyl compounds over a coniferous forest. The fluxes of the carbonyl compounds over grassland are shown in Figure 2. As can be seen clearly vertical fluxes are obtained with values up to  $0.3 \mu\text{g m}^{-1} \text{s}^{-1}$  for positive and up to  $0.4 \mu\text{g m}^{-1} \text{s}^{-1}$  for negative fluxes. Due to the fact that forests are stronger emitters than grassland the fluxes over a coniferous forest are higher. Emissions at noon and in the early afternoon are highest. One reason could be that emission corresponds to the warmer portion of the day as well as the time of highest light intensities Villanueva-Fierro (2004). As an example, the flux of formaldehyde reached a maximum of  $5 \mu\text{g m}^{-1} \text{s}^{-1}$  at noon whereas the values for the early morning and the late afternoon are far below this value. Further data interpretation needs to be done.

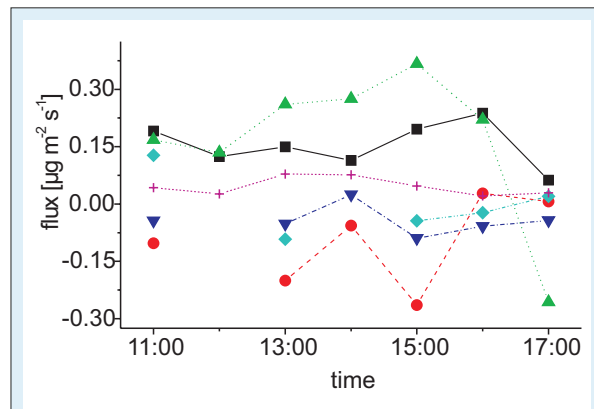


Fig. 1: Fluxes of carbonyl compounds at the Waldstein BITÖK tower (Fichtelgebirge, 21.09.2003) over a coniferous forest. (50 minutes sampling, starting time is time shown in the graph).

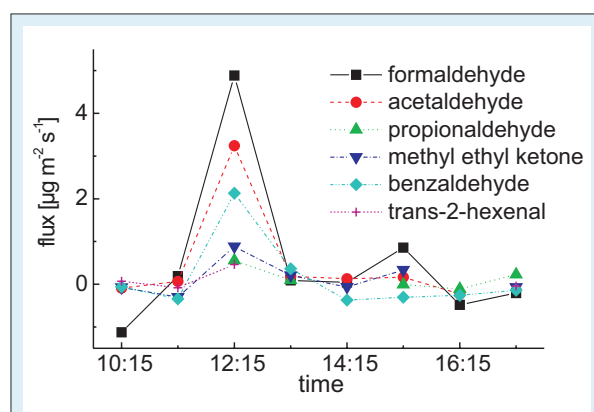


Fig. 2: Fluxes of carbonyl compounds in Melpitz (30.07.2003) over grassland. (Symbols are the same as in Fig 1; 50 minutes sampling, starting time is time shown in the graph).

### Summary

In this study fluxes of carbonyl compounds were determined with the help of the newly developed relaxed eddy accumulation (REA) system at two different sites. The results show different emission behavior of grassland and a coniferous forest. Due to the improvement of the analytical elution method we were able to detect even low concentrations caused by the small sampling volume.

### References

**Delany, A. C., Oncley, S. P., Businger, J. A. and Sievering, H. 1991.** *Adapting the conditional sampling concept for a range of different chemical species.* Proc. of the 7<sup>th</sup> AMS Symposium on Meteorological Observations and Instrumentation, New Orleans, Louisiana. 22-25.

**Guenther, A., Baugh, W., Davis, K., Hampton, G., Harley, P., Klinger, L., Vierling, L., Zimmerman, P., Allwine, E., Dilts, S., Lamb, B., Westberg, H., Baldocchi, D., Geron, C. and Pierce, T. 1996.** Isoprene fluxes measured by enclosure, relaxed eddy accumulation, surface layer gradient, mixed layer gradient, and mixed layer mass balance techniques. *J. Geophys. Res.*, **101**, 18555-18567.

**Kirstine, W., Galbally, I., Ye, Y. and Hopper, M. 1998.** Emissions of volatile organic compounds (primarily oxygenated species) from pasture. *J. Geophys. Res.*, **103**, 10605-10619.

**Müller, K. 1997.** Determination of aldehydes and ketones in the atmosphere - A comparative long time study at an urban and a rural site in Eastern Germany. *Chemosphere*, **35**, 2093-2106.

**Villeneuve-Fierro, I., Popp, C. J. and Martin, R. S. 2004.** Biogenic emissions and ambient concentrations of hydrocarbons, carbonyl compounds and organic acids from ponderosa pine and cottonwood trees at rural and forested sites in Central New Mexico. *Atmos. Environ.*, **38**, 249-260.

#### Funding

- Bundesministerium für Bildung und Forschung (BMBF) within the BEWA2000 project.

## Uptake of acetone, 2-butanone, 2,3-butanedione, and 2-oxo-propanal on a water surface

Matthias Schütze, Hartmut Herrmann

*An einem Einzeltropfen-Strömungsrohr wurde die Aufnahme von Aceton, 2-Butanon, 2,3-Butandion und 2-oxo-Propanal an einer wässrigen Oberfläche untersucht. Diese Methode erlaubt es, die Konzentration in der Flüssigphase in situ durch UV-VIS-Spektroskopie zu verfolgen.*

*Zur Quantifizierung der Geschwindigkeit des Phasentransfers wurden zunächst die Extinktionskoeffizienten dieser Ketone in wässriger Lösung bestimmt.*

*Wegen der Sättigung der Flüssigphase gemäß dem Henry'schen Gesetz verkleinerten sich die gemessenen Aufnahmekoeffizienten  $\gamma_{meas}$  mit der Zeit. Eine Anpassung einer Modellfunktion gemäß des sogenannten Widerstandsmodells an die experimentell bestimmten Zeitverläufe und eine darauffolgende Korrektur für den Effekt der Gasphasendiffusion lieferten Werte für die Massenakkommodationskoeffizienten:*

$$\alpha_{Aceton} = (5.4^{+4.5}_{-2.6}) \cdot 10^3, \alpha_{2-Butanon} = (2.1^{+0.9}_{-0.8}) \cdot 10^3, \alpha_{2,3-Butandion} = (1.0 \pm 0.3) \cdot 10^4 \text{ und } \alpha_{2-oxo-Propanal} = (1.5 \pm 0.5) \cdot 10^4.$$

The investigated ketones represent steps in the oxidation chain of atmospheric hydrocarbons. Because of their high solubility, these species can be taken up at the surfaces of liquid tropospheric particles, such as cloud droplets or deliquescent aerosol particles. It is necessary to know the parameters that govern this process in order to evaluate the rate of transfer and thereby the compounds' budgets in either phase.

The uptake of acetone, 2-butanone (methyl ethyl ketone), 2,3-butanedione (biacetyl), and 2-oxo-propanal (methylglyoxal) on water was investigated using a single drop flow tube experiment (Schütze and Herrmann, 2002). It allows to analyze single liquid drops that are placed on the center axis of a laminar flow tube by UV-VIS (spectral range including the ultra violet and visible regions) spectroscopy. Figure 1 shows the drop hanging on a pipette's tip inside the flow tube.

The reactor was operated at 10 kPa total pressure and at room temperature. The gas phase consisted of helium as the bath gas, water vapor in order to avoid evaporation of the drop, and a few volume percent of the respective ketone. Using a UV-VIS absorption cell upstream of the main flow tube, gas phase concentrations between 0.5 and 11 in units of  $10^{16}$  molecules  $\text{cm}^{-3}$  were determined for the ketones.

In order to quantify the amount of the hydrocarbon species taken up into the drop, the liquid face spectrum must be known. The spectra of acetone, 2-butanone, 2,3-butanedione, and 2-oxo-propanal were measured using a commercial spectrometer. Whereas the solution of the first three compounds were prepared by solving the pure liquid compound in water, this was not possible for the last one because of the formation of white precipitation indicating

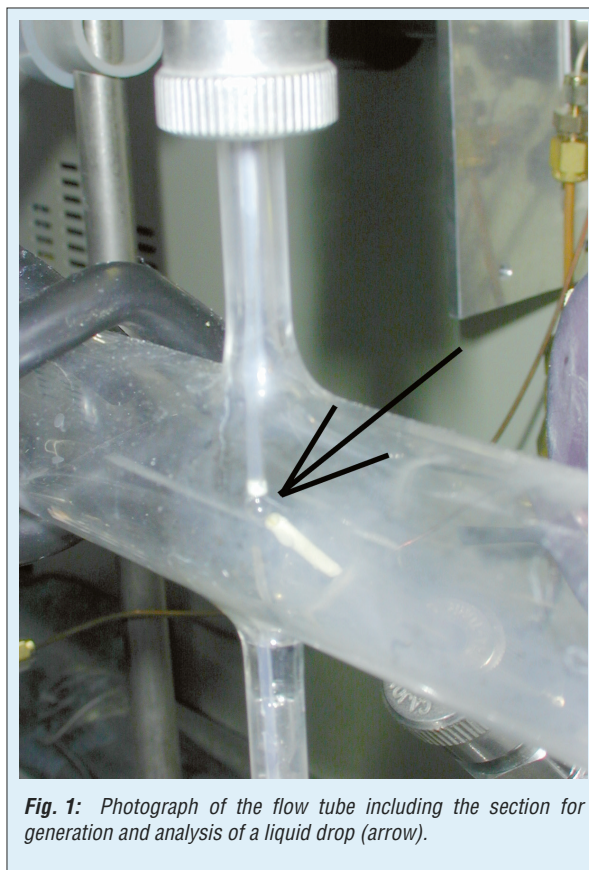


**Fig. 1:** Photograph of the flow tube including the section for generation and analysis of a liquid drop (arrow).

incomplete dissolution. Therefore the vapor of the pure substance was bubbled through a water bottle where the gas phase 2-oxo-propanal dissolved completely without formation of precipitation.

While the results for acetone and 2-butanone compare very well with literature data (Xu et al., 1993), no previous determinations of the absorption coefficients of 2,3-butanedione and 2-oxo-propanal were found. The maximum absorption coefficients are  $\epsilon_{265\text{nm}} = 17.5 \text{ l mol}^{-1} \text{ cm}^{-1}$ ,  $\epsilon_{267\text{nm}} = 20.5 \text{ l mol}^{-1} \text{ cm}^{-1}$ ,  $\epsilon_{284\text{nm}} = 26.5 \text{ l mol}^{-1} \text{ cm}^{-1}$ ,

and  $\epsilon_{284nm} = 16.0 \text{ l mol}^{-1} \text{ cm}^{-1}$  for acetone, 2-butanone, 2,3-butanedione, and 2-oxo-propanal, respectively.

Using these values, the time dependent liquid phase concentration of the ketones in a drop that is exposed to the gas phase containing the corresponding gas phase species was measured. The time profile for the acetone concentration during an experimental run is shown in Figure 2 as an example.

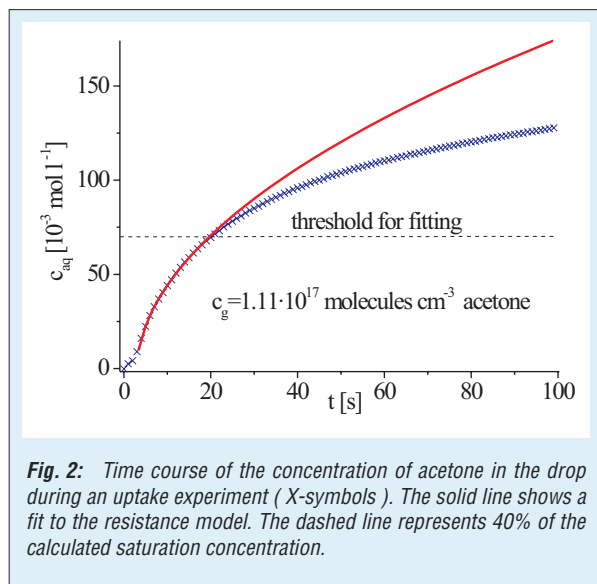


**Fig. 2:** Time course of the concentration of acetone in the drop during an uptake experiment (X-symbols). The solid line shows a fit to the resistance model. The dashed line represents 40% of the calculated saturation concentration.

The measured uptake coefficient  $\gamma_{\text{meas}}$  (= the net probability for the uptake of a gas phase molecule that hits the interface into the liquid phase) can be calculated from the slope of such a plot if the geometry of the system is known. It is independent of the gas phase concentration but decreases with increasing exposure time. This is due to the approach of Henry's law equilibrium which results in an increasing flux from the liquid phase back to the gas phase. Therefore the net uptake is decreasing and approaches zero when the equilibrium is fully established. At the beginning, the rate of the uptake is limited by gas phase diffusion (I) which recovers the surface gas phase concentration and the mass accommodation coefficient  $\alpha$  (II) which is the probability for a gas phase molecule that hits the surface to be incorporated into the liquid. The solubility in the liquid (III) becomes rate limiting as saturation of the liquid is approached. This is described in the so-called resistance model for a species that shows no liquid phase reaction by (Finlayson-Pitts and Pitts, 2000)

$$\frac{1}{\gamma_{\text{meas}}} = \frac{1}{\alpha} + \frac{1}{\Gamma_g} + \frac{v\sqrt{\pi t}}{4HRT\sqrt{D_l}}$$

where  $1/\Gamma_g$  represents the "resistance" term for the gas phase diffusion,  $v$  is the average molecular speed,  $t$  the exposure time,  $H$  the Henry's law constant,  $R$  the gas constant,  $T$  the temperature, and  $D_l$  the liquid phase diffusion constant.

A fit of this equation to the experimental data for the liquid phase concentration  $c_{\text{aq}}$  (proportional to  $\int \gamma_{\text{meas}} dt$ ) is shown in Figure 2 as a solid line. Only data below a threshold of 40% of the saturation concentration calculated from Henry's law were used for fitting because the resistance model was calculated for a planar surface. The sphere like shape of the drop leads to deviations from the model prediction if the inner regions of the drop become saturated which happens at later times.

The result of the fitting procedure is the initial uptake coefficient  $\gamma_0$  which is not affected by the liquid phase saturation any more. It is only a convolution of  $\alpha$  and the effect of the gas phase diffusion.

In order to correct for the latter, a computer model is employed which numerically solves the diffusion equation for the passage of a slice of the gas phase around the drop. After this procedure a value for the mass accommodation coefficient for each of the species can be given. The final results are

$$\alpha_{\text{acetone}} = (5.4^{+4.5}_{-2.6}) \cdot 10^{-3},$$

$$\alpha_{\text{2-butanone}} = (2.1^{+0.9}_{-0.8}) \cdot 10^{-3},$$

$$\alpha_{\text{2,3-butanedione}} = (1.0 \pm 0.3) \cdot 10^{-4},$$

$$\text{and } \alpha_{\text{2-oxo-propanal}} = (1.5 \pm 0.5) \cdot 10^{-4}.$$

The value for acetone is in excellent agreement with the results of a previous study that yielded  $\alpha_{\text{acetone}} = 5.4 \cdot 10^{-3}$  at  $T = 293 \text{ K}$  (Duan et al., 1993). There are no other experimental studies concerning the uptake of 2-butanone, 2,3-butanedione, and 2-oxo-propanal reported in the literature.

The results of the present study are in press at PCCP (Physical Chemistry Chemical Physics) (Schütze and Herrmann, 2004).

## References

- Duan, S. X., Jayne, J. T., Davidovits, P., Worsnop, D. R., Zahniser, M. S. and Kolb, C. E. 1993.** Uptake of gas-phase acetone by water surface. *J. Phys. Chem.*, **97**, 2284-2288.
- Finlayson-Pitts, B. J. and Pitts, J. N. J. 2000.** *Chemistry of the Upper and Lower Atmosphere*. Academic Press, San Diego, 944 pp.
- Schütze, M. and Herrmann, H. 2002.** Determination of phase transfer parameters for the uptake of  $\text{HNO}_3$ ,  $\text{N}_2\text{O}_5$  and  $\text{O}_3$  on single aqueous drops. *Phys. Chem. Chem. Phys.*, **4**, 60-67.
- Schütze, M. and Herrmann, H. 2004.** Uptake of acetone, 2-butanone, 2,3-butanedione, and 2-oxo-propanal on a water surface. *Phys. Chem. Chem. Phys.*, **6**, 965-971.
- Xu, H., Wentworth, P. J., Howell, N. W. and Joens, J. A. 1993.** Temperature dependent near-UV molar absorptivities of aliphatic aldehyds and ketones in aqueous solution. *Spectrochim. Acta A*, **26**, 1171-1178.

## NH<sub>3</sub>-concentrations in Melpitz and the Eastern Erzgebirge Mountains – test of a new measuring device

Gerald Spindler, Achim Grüner

*Ammoniak (NH<sub>3</sub>) ist das einzige basische Spurengas der Troposphäre, dass in nennenswerten Konzentrationen vorkommt und zusammen mit sauren Gasen an der Bildung von Partikelmasse beteiligt ist. Hauptquelle für NH<sub>3</sub> ist die Landwirtschaft. Um die Konzentration gasförmigen NH<sub>3</sub> zu bestimmen ist es wichtig, troposphärische Partikel abzutrennen. Das getestete Gerät arbeitet nach einem miniaturisierten nasschemischen Verfahren, bei dem NH<sub>3</sub> in einer Absorptionslösung zur konduktometrischen Detektion transferiert wird. Tests an drei Standorten (87 m ü. NN, Melpitz, 370 m ü. NN, Tharandt und 735 m ü. NN, Oberbärenburg) ergaben über Zeiträume mehrerer Tage Messreihen, deren mittlere Konzentration und Variabilität zwischen Tag und Nacht mit der Höhenlage abnimmt. Ursachen werden in zunehmender Quellferne und einer geringeren mittleren Temperatur mit höherer Lage gesehen.*

Atmospheric ammonia (NH<sub>3</sub>) is a major trace gas emitted from agricultural (Misselbrook et al. 2000) and other sources (Sutton et al. 2000). Ammonia can be deposited to and emitted from the earth's surface (Bytnerowicz and Fenn, 1996, Spindler et al. 2001). Ammonia is the dominant gaseous base present in the troposphere and influence the regional-scale tropospheric chemistry. NH<sub>3</sub> neutralizes mainly sulphur dioxide (SO<sub>2</sub>) and the oxidation product of nitrogen oxides (NO<sub>x</sub>), nitric acid (HNO<sub>3</sub>) to form ammonium sulphates and nitrates in particulates (Seinfeld, 1986). Ammonia is suspected to have a high impact on homogeneous particle nucleation (Korhonen, et al. 1999).

There are different possibilities to quantify the NH<sub>3</sub> concentration in the atmosphere, e.g., passive samplers that adsorb the basic NH<sub>3</sub>-gas at acid surfaces. NH<sub>3</sub> can also be measured by chemiluminescence after oxidation to NO, optical detection by laser and/or DOAS (differential optical absorption spectroscopy) is also possible. Often the detection limit and time resolution of these methods are too high for ambient NH<sub>3</sub> concentrations. Moreover, the separation of gaseous ammonia from ammonium in tropospheric particles is not complete. Therefore continuously working measuring systems based on a wet-chemical method were developed over the past years. In these rotating wet annular denuders gaseous NH<sub>3</sub> is separated from tropospheric particles by absorption in an acid absorption solution. The rotation forms an aqueous layer on the surface of the annular space. Downstream of the denuder NaOH is merged with the absorption solution, which results in the formation of gaseous ammonia, passes a semi-permeable membrane to a water stream in which the NH<sub>4</sub><sup>+</sup>-concentration is determined conductometrically (Wyers, 1993).

The new Ammonia Monitor – “AiRRmonia” by Mechatronics (Hoorn, The Netherlands) tested in the present study – is in principle a smaller version of a denuder system (Erisman et al. 2001). The rotating

wet annular denuder is replaced by a channel system positioned on a Teflon membrane, which is permeable to gases. The absorption solution flows in counter flow direction on the opposite side of the membrane. The sampling channel is dimensioned in such a way that ammonia passes the membrane completely and forms ammonium in the absorption solution. The sample solution flow rate towards the detector block is constant.

Test measurements with the “AiRRmonia” were carried out during the VERTIKO-Project (Vertical Transport of Energy and Trace Gases at Anchor Stations and Their Spatial/Temporal Extrapolation under Complex Natural Conditions) within the research programme AFO 2000 (German atmospheric research 2000) in summer and autumn 2003 at the IFT research station (Melpitz, grassland in North Saxony, near Torgau) and two stations in the Eastern Erzgebirge Mountains (Tharandt, climate station Wildacker as open area in the forest) and Oberbärenburg (forest station). The three stations reflect a gradient in altitude of 87, 370 and 735 m above NN for Melpitz, Tharandt and Oberbärenburg, respectively. Figure 2 presents the results of the ammonia concentration measurements for the three sites. The half hourly means were calculated from 10-minute means.

The test measurements show different mean concentrations for the three sites (Table 1). For Melpitz and Tharandt the NH<sub>3</sub> concentrations are higher than in Oberbärenburg. Mostly for Melpitz and Tharandt a typical pattern of the NH<sub>3</sub>-concentration between day and night is recognizable. A reason can be that during higher temperatures at daytime more NH<sub>3</sub> is in the gas phase, it emanates from evaporation of NH<sub>4</sub>NO<sub>3</sub> from particles and from agriculture in the surroundings. For Oberbärenburg the mean NH<sub>3</sub>-concentration is more than two times lower than in Melpitz or Tharandt and shows only little variation. Here no appreciable NH<sub>3</sub> sources are in the vicinity and temperatures are lower. Mean concentrations for the three sites decrease

Site	Melpitz	Tharandt	Oberbärenburg
Mean concentration [ $\mu\text{g m}^{-3}$ ]	$2.5 \pm 1.7$	$2.0 \pm 1.1$	$0.9 \pm 0.6$
Time slice (days)	03-07-01 to 07-29 (29)	03-05-19 to 06-22 (32)	03-10-15 to 10-29 (15)

Tab. 1: Mean concentration and standard deviation for  $\text{NH}_3$  at different sites.

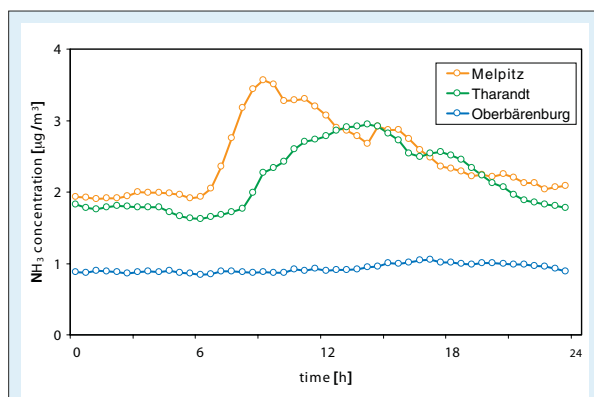


Fig. 1: Average daily course of  $\text{NH}_3$ -concentration at Melpitz, Tharandt and Oberbärenburg.

with increasing altitude. The measurements from Oberbärenburg demonstrate that the “AiRRmonia” system was able to detect also very low  $\text{NH}_3$ -concentrations.

The “AiRRmonia” can be an alternative to passive samplers and rotating wet annular denuders and works for 10 days without maintenance. In comparison to the former used denuder system the consumption of chemicals is less than 10%. The system has an independent internal data logger and an auto calibration system. Measuring is also possible during freezing conditions, because the compact system can be placed in-house. The test of this measuring device was successful and we will use this system in the future at the IFT-research-station Melpitz for routine measurements of the  $\text{NH}_3$ -concentration.

## References

- Bytnerowicz, A. and Fenn, M. A. 1996. Nitrogen deposition in California Forests: A review. *Environ. Pollut.*, **92**, 127-146.
- Erisman, J. W., Otjes, R., Hensen, A., Jongejan, P., van den Bulk, P., Khlystov, A., Mols, H. and Slanina, S. 2001. Instrument development and application in studies and monitoring of ambient ammonia. *Atmos. Environ.*, **35**, 1913-1922.
- Korhonen, P., Kulmala, M., Laksonen, A., Viisanen, Y., McGraw, R. and Seinfeld, J. H. 1999. Ternary nucleation of  $\text{H}_2\text{SO}_4$ ,  $\text{NH}_3$ , and  $\text{H}_2\text{O}$  in the atmosphere. *J. Geophys. Res.*, **D104**, 26349-26353.
- Misselbrook, T. H., van der Weerden, T. J., Pain, B. F., Jarvis, S. C., Chambers, B. J., Smith, K. A., Phillips, V. R. and Demmers, T. G. M. 2000. Ammonia emission factors for UK agriculture. *Atmos. Environ.*, **34**, 871-880.
- Seinfeld, J. H. and Pandis, S. N. 1998. *Atmospheric Chemistry and Physics*. John Wiley and Sons Inc., New York, 1326 pp.
- Spindler, G., Teichmann, U. and Sutton, M. A. 2001. Ammonia dry deposition over grassland - micrometeorological fluxgradient measurements and bidirectional flux calculations using an inferential model. *Q. J. Roy. Meteor. Soc.*, **127**, 795-814.
- Sutton, M. A., Dragosits, U., Tang, Y. S. and Fowler, D. 2000. Ammonia emissions from non-agricultural sources in the UK. *Atmos. Environ.*, **34**, 855-869.
- Wyers, G. P., Otjes, R. P. and Slanina, J. 1993. A continuous-flow denuder for the measurement of ambient concentrations and surface-exchange fluxes of ammonia. *Atmos. Environ.*, **27**, 2085-2090.

### Funding

- Bundesministerium für Bildung, Wissenschaft, Forschung und Technologie (BMBF)

### Cooperation

- Technische Universität Dresden
- Technische Universität Bergakademie Freiberg (Interdisziplinäres Ökologisches Zentrum (IÖZ))

## Aqueous phase reactions of free radicals with selected organic compounds

Saso Gligorovski, Hartmut Herrmann, Dirk Hoffmann, Kshama Parajuli

Die Reaktionen organischer Verbindungen mit OH-Radikalen sind wichtige Abbauwege für diese Stoffe in der Atmosphäre. Daneben können aber auch die Reaktionen des  $\text{NO}_3$ -Radikals und der Halogenradikale einen wichtigen Beitrag zum Abbau dieser Verbindungen liefern. Mittels verschiedener Laserphotolyse-Langwegabsorptionsanordnung (LP-LPLA) wurde die Kinetik dieser Reaktionen in der wässrigen Phase untersucht. Um verschiedene atmosphärische Bedingungen zu simulieren, wurden die Geschwindigkeitskonstanten nicht nur bei Raumtemperatur bestimmt, sondern auch als Funktion der Temperatur und der Ionenstärke. Die erhaltenen kinetischen Daten werden in das atmosphärische Multiphasenmodell CAPRAM eingebunden.

## Motivation

Oxygenated organic compounds are either directly emitted to the atmosphere as fuel additives or solvents or they are formed in the troposphere as intermediate products of chemical degradation of other volatile organic compounds. Their presence in the atmosphere also results in formation of other secondary pollutants and tropospheric ozone. Furthermore, more polar intermediates and products will be formed upon their gas phase oxidation which could be transferred to aqueous phase. The major degradation pathway of these organic compounds might be the reaction with OH,  $\text{NO}_3$  and halogens radicals in the tropospheric aqueous phase. The temperature dependence can be extremely important in determining the lifetimes and fates of certain species in the atmosphere, as well as their contribution to secondary pollutant formation (Finlayson-Pitts, 2000). For certain reactions in the troposphere the effect of ionic strength can be even more important than the effect of temperature (Herrmann, 2003). Thus, in the presented studies the temperature dependent and ionic strength dependent measurements of OH,  $\text{NO}_3$  and Br reactions with different organic carbonyl compounds in aqueous solution are performed.

## Kinetic studies

**OH-reactions.** Using a laser-photolysis-long-path-laser-absorption (LP-LPLA) set up and applying

a competition kinetic method the temperature-dependent rate constants for the reactions of OH radical with acetonylacetone, isobutyraldehyde and diacetyl have been measured. The activation parameters obtained from these investigations are summarized in Table 1.

Together with literature data of the available rate constants an Evans-Polanyi correlation is shown in the form  $\log k_{\text{H}}$  vs. BDE (bond dissociation energy) which indicates that reactions of the OH radical with oxygenated compounds proceed via an H-abstraction mechanism (Figure 1).

The correlation found here for  $380 \delta \text{ BDE} \delta 412 \text{ kJmol}^{-1}$  can be expressed as  $\log (k_{\text{H}}/\text{M}^{-1}\text{s}^{-1}) = (32 \pm 4) - (0.06 \pm 0.01) \cdot \text{BDE} / \text{kJmol}^{-1}$ ; with  $n = 9$ ;  $r = 0.99$ .

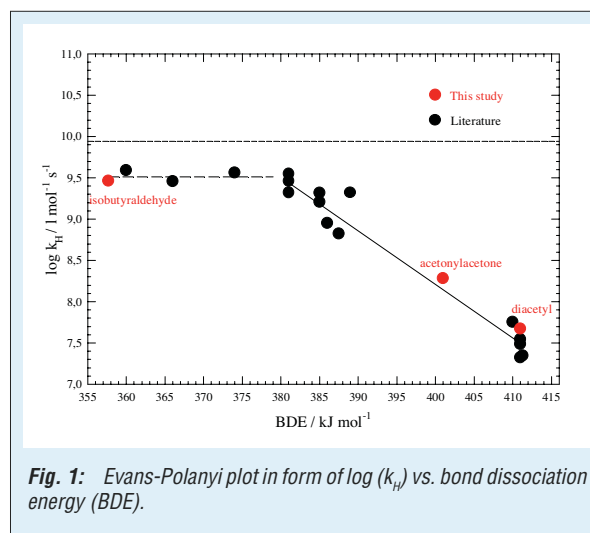


Fig. 1: Evans-Polanyi plot in form of  $\log (k_{\text{H}})$  vs. bond dissociation energy (BDE).

Compound	A /mol s	$E_{\text{A}}$ kJ/mol	$\Delta G^{\ddagger}$ kJ/mol	$\Delta H^{\ddagger}$ kJ/mol	$\Delta S^{\ddagger}$ J/K mol	BDE kJ/mol
Acetonylacetone	$(1.1 \pm 0.07) \cdot 10^{11}$	$(12 \pm 5)$	$(22 \pm 10)$	$(10 \pm 4)$	$-(42 \pm 3)$	401
Isobutyraldehyde	$(3.0 \pm 0.1) \cdot 10^{10}$	$(6 \pm 3)$	$(19 \pm 10)$	$(3.3 \pm 1.7)$	$-(53 \pm 3)$	411
Diacetyl	$(4.3 \pm 0.3) \cdot 10^{12}$	$(24 \pm 5)$	$(25 \pm 7)$	$(22 \pm 4)$	$-(11 \pm 1)$	358

Tab. 1: Activation parameters for the reaction of OH radical with oxygenated compounds and BDEs of the weakest C-H bond.

Radical	Reactant	$k_{(I \rightarrow 0)}$ ( $\text{l mol}^{-1}\text{s}^{-1}$ )	$k_{(I \rightarrow \infty)}$ ( $\text{l mol}^{-1}\text{s}^{-1}$ )	$k_{(I \rightarrow \infty)} / k_{(I \rightarrow 0)}$	$b$ ( $\text{l mol}^{-1}$ )	$I_{\text{eff}}$ ( $\text{l mol}^{-1}$ )
OH	Acetone	$(2.0 \pm 0.5) \cdot 10^8$	$(3.2 \pm 2.2) \cdot 10^8$	1.6	$(0.1 \pm 0.15)$	0 – 1.94
	2-Propanol	$(2.2 \pm 0.9) \cdot 10^9$	$(3.3 \pm 1.1) \cdot 10^9$	1.5	$(0.26 \pm 1.0)$	0 – 1.94
	2-Butanol	$(3.2 \pm 0.9) \cdot 10^9$	$(4.7 \pm 1.0) \cdot 10^9$	1.5	$(0.25 \pm 0.15)$	0 – 1.94

Tab. 2: Ionic strength effect for reactions of OH with different organic compounds.

The dashed line in the Figure 1 represents the diffusion limit which was calculated by the Smoluchowski equation. Assuming an H abstraction mechanism it can be concluded that molecules with a smaller C-H bond dissociation energy are more reactive but the measured rate constants of the aldehydes investigated here and elsewhere (Hesper, 2003; Schuchmann, 1988) seem to become independent of the bond dissociation energy for low BDE values (BDE  $\delta$  374  $\text{kJ mol}^{-1}$ ).

In the BDE range of 357.7 to 374  $\text{kJ mol}^{-1}$  the rate constant for the reactions with aldehydes is best represented by  $\bar{k}_{\text{H}} = 3.3 \cdot 10^9 \text{ l mol}^{-1} \text{ s}^{-1}$ .

Besides this the ionic strength dependency of OH reactions was investigated applying a competition kinetics method for the first time. The “reference” reaction of OH with thiocyanate anion for the competition kinetics study was investigated as a function of ionic strength. The motivation for this study was our desire to employ thiocyanate anion as the competitor in ionic strength dependent competition kinetics studies of OH reactivity in aqueous solution. Furthermore, the ionic-strength-dependent rate constants for the reaction of OH with acetone, 2-propanol and 2-butanol have been measured applying the obtained “reference” rate constants as a reference data set for the competition kinetic method. The rate constants obtained and kinetic salting coefficients ( $b$ ) are summarized in Table 2.

### NO<sub>3</sub>-reactions

NO<sub>3</sub> radicals were generated by flash photolysis of nitrate anions at  $\lambda = 248 \text{ nm}$  under acidic conditions ( $\text{pH} = 0.5$ ). The nitrate radical absorption was measured directly at 632.8 nm. Rate constants for reactions with substituted phenols were investigated at room temperature and the reaction of NO<sub>3</sub> with *p*-ethyl phenol was investigated as a function of temperature. Furthermore, for the first time the ionic strength dependence of NO<sub>3</sub> with *p*-cresol has been investigated at 298 K in the range of  $0,3 \leq I_{\text{eff}} [\text{mol/l}] \leq 2,41$  (Figure 2). Values of  $k(I \rightarrow 0) = (5.6 \pm 5.3) \cdot 10^8 \text{ M}^{-1} \text{ s}^{-1}$  and  $k(I \rightarrow \infty) = (2.3 \pm 0.2) \cdot 10^9 \text{ M}^{-1} \text{ s}^{-1}$  were obtained.

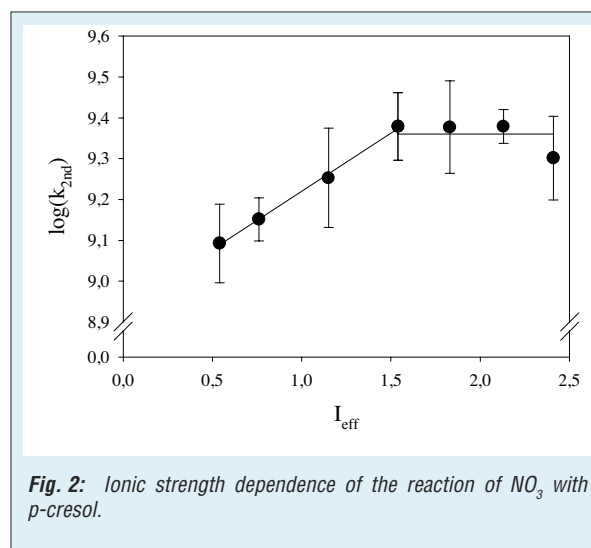


Fig. 2: Ionic strength dependence of the reaction of NO<sub>3</sub> with *p*-cresol.

### Halogen reactions

Model calculations suggest that halogens could play an important role in the aqueous tropospheric phase i.e. in cloud water and aerosol particles. Currently the reactivity of the halogens towards the atmospheric trace components has been studied to a small extent only and hence the knowledge of their fate in the atmosphere is quite sparse and needs more investigation. For this, we reproduced and stabilised a laser photolysis long path laser absorption method previously developed in our laboratory (Donati, 2002). At present Br kinetics

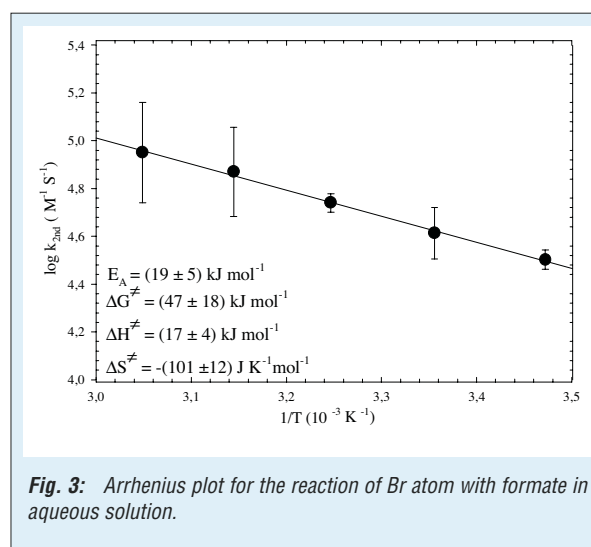


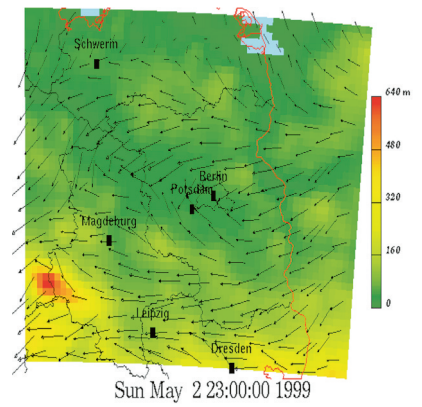
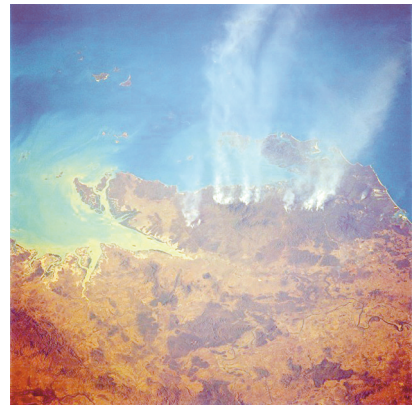
Fig. 3: Arrhenius plot for the reaction of Br atom with formate in aqueous solution.

with acid anions and aldehydes are studied. Figure 3 shows the results of the T-dependent measurements of rate constants for the reaction of Br with formate. In the future, this study will be continued by further measurements of halogens kinetics with atmospheric trace components to fill this gap of knowledge in atmospheric research.

The kinetic data obtained here will be used as input parameters in forthcoming versions of our multiphase reaction mechanisms CAPRAM within the SPACCIM model framework.

### References

- Atkins, P. W. 1986.** *Physical Chemistry*. Oxford University Press, Oxford, 240 pp.
- Benson, S. W. 1976.** *Thermochemical Kinetics* (2. Auflage ed.). John Wiley and Sons, New York, 72 pp.
- Donati, A. 2002.** *Zeitaufgelöste kinetische Untersuchungen halogenhaltiger Oxidantien in wässriger Phase*. Dissertation, 125 pp.
- Ervens, B., Buxton, G. V., Salmon, G. A., Williams, J., Bydder, M., Dentener, F., George, C., Mirabel, P., Wolke, R. and Herrmann, H. 2002.** CAPRAM2.4 (MODAC mechanism): An extended and condensed tropospheric aqueous phase mechanism and its application. *J. Geophys. Res.*, **108**, 4426.
- Evans, M. G. and Polanyi, M. 1938.** Inertia and driving force of chemical reactions. *T. Faraday. Soc.*, **43**, 11-29.
- Herrmann, H. 2003.** Kinetics of aqueous phase reactions relevant for atmospheric chemistry. *Chem. Rev.*, **103**, 4691-4716.
- Hesper, J. 2003.** *Spektroskopische und kinetische Untersuchungen von Reaktionen der Radikale O<sub>2</sub>- und OH in wässriger Phase*. Dissertation, 97 pp.
- Majdik, Z. and Herrmann, H. 2003.** *Multi-phase chemical mechanism development*. U. Schurath and K. H. Naumann (Ed.), In *EUROTRAC-2 Subproject CMD Final Report 2003*. p. 134-283.
- Schuchmann, M. N. and von Sonntag, C. 1988.** The rapid hydration of the acetyl radical. A pulse radiolysis study of acetaldehyde in aqueous solution. *J. Amer. Chem. Soc.*, **110**, 5698-5701.
- Wypych, G. 2001.** *Handbook of Solvents*. Toronto, 10 pp.



## *Appendices*



## Publications

### Book section

- Heintzenberg, J., Raes, F. and Schwartz, S. E. I. a. 2003. *Tropospheric aerosols*. G. Brasseur, R. G. Prinn, and A. A. P. Pszenny (Ed.), In *Atmospheric chemistry in a changing world - An integration and synthesis of a decade of tropospheric chemistry research*. Springer, Berlin, Germany: 125-156.
- Schurath, U., Peeters, J., Wayne, R. P., Moortgat, G. K., Grgic, I., George, C., Herrmann, H. and Poppe, D. 2003. *Chemical mechanism development : Overview of subproject CMD*. P. M. Midgley and M. Reuther (Ed.), In *Towards cleaner air for Europe - Science, tools and applications. Part 2: Overviews from the final reports of the EUROTRAC-2 subprojects*. Margraf Publishers, Weikersheim: **Part 2**, 73-98 (Chapter 5).
- Spindler, G., Grüner, A. and Plessow, K. 2003. *Immissionsmessungen und Abschätzung des Anteils des N-Eintrages durch trockene Deposition von NH<sub>3</sub> für die Forschungsstation Melpitz in Sachsen*. C. Bernhofer and V. Goldberg (Ed.), In *Tharandt Klimaprotokolle : Tagungsband 5. BIOMET-Tagung „Mensch-Pflanze-Atmosphäre“*. Eigenverlag der Technischen Universität Dresden, **9**, 126-128.

### Publications, peer-reviewed

- Anderson, T. L., Charlson, R. J., Schwartz, S. E., Knutti, R., Boucher, O., Rodhe, H. and Heintzenberg, J. 2003. Climate forcing by aerosols — a hazy picture. *Science*, **300**, 1103-1104.
- Ansmann, A., Bösenberg, J., Chaikovsky, A. P., Comerón, A., Eixmann, R., Freudenthaler, V., Ginoux, P., Konguem, L., Linné, H., Márquez, M. Á. L., Manoj, S., Matthias, V., Mattis, I., Mitev, V., Müller, D., Nickovic, S., Pelon, J., Sauvage, L., Sobolewsky, P., Stohl, A., Torres, O., Vaughan, G., Wandinger, U. and Wiegner, M. 2003. Long-range transport of Saharan dust to northern Europe: The 11-16 October 2001 outbreak with EARLINET. *J. Geophys. Res.*, **108**, 4783, doi: 10.1029/2003JD003757.
- Barker, H. W., Stephens, G. L., Partain, P. T., Bergman, J. W., Bonnel, B., Campana, K., Clothiaux, E. E., Clough, S., Cusack, S., Delamere, J., Edwards, J., Evans, K. F., Fouquart, Y., Freidenreich, S., Galin, V., Hou, Y., Kato, S., Li, J., Mlawer, E., Morcrette, J.-J., O'Hirok, W., Räisänen, P., Ramaswamy, V., Ritter, B., Rozanov, E., Schlesinger, M., Shibata, K., Sporyshev, P., Sun, Z., Wendisch, M., Wood, N. and Yang, F. 2003. Assessing 1D atmospheric solar radiative transfer models: Interpretation and handling of unresolved clouds. *J. Clim.*, **16**, 2676-2699.
- Berndt, T. and Böge, O. 2003. Gas-phase reaction of OH radicals with phenol. *Phys. Chem. Chem. Phys.*, **5**, 342-350.
- Berndt, T., Böge, O., Heintzenberg, J. and Claus, P. 2003. From atmospheric research to an industrial process: The formation of propylene oxide. *Ind. Eng. Chem. Res.*, **42**, 2870-2873.
- Berndt, T., Böge, O. and Stratmann, F. 2003. Gas-phase ozonolysis of  $\alpha$ -pinene: Gaseous products and particle formation. *Atmos. Environ.*, **37**, 3933-3945.
- Birmili, W., Berresheim, H., Plass-Dülmer, C., Elste, T., Gilge, S., Wiedensohler, A. and Uhrner, U. 2003. The Hohenpeissenberg aerosol formation experiment (HAFEX): A long-term study including size-resolved aerosol, H<sub>2</sub>SO<sub>4</sub>, OH, and monoterpenes measurements. *Atmos. Chem. Phys.*, **3**, 361-376.
- Dusek, U., Covert, D. S., Wiedensohler, A., Neusüß, C., Weise, D. and Cantrell, W. 2003. CNN spectra derived from size distributions and hygroscopic properties of the aerosol in coastal south-west Portugal during ACE-2. *Tellus*, **55B**, 35-53.
- Ervens, B., George, C., Williams, J. E., Buxton, G. V., Salmon, G. A., Bydder, M., Wilkinson, F., Dentener, F., Mirabel, P., Wolke, R. and Herrmann, H. 2003. CAPRAM 2.4 (MODAC mechanism): An extended and condensed tropospheric aqueous phase mechanism and its application. *J. Geophys. Res.*, **108**, 4426, doi: 10.1029/2002JD002202.
- Ervens, B., Gligorovski, S. and Herrmann, H. 2003. Temperature-dependent rate constants for hydroxyl radical reactions with organic compounds in aqueous solutions. *Phys. Chem. Chem. Phys.*, **5**, 1811-1824.
- Fiebig, M., Stohl, A., Wendisch, M., Eckhardt, S. and Petzold, A. 2003. Dependence of solar radiative forcing of forest fire aerosol on aging and state of mixture. *Atmos. Chem. Phys.*, **3**, 881-891.
- Franck, U., Herbarth, O., Wehner, B., Wiedensohler, A. and Manjarrez, M. 2003. How do the indoor distribution of airborne submicron and ultrafine particles in the absence of significant indoor sources depend on outdoor distributions? *Indoor Air*, **13**, 174-181.

- Franke, K., Ansmann, A., Müller, D., Althausen, D., Venkataraman, C., Reddy, M. S., Wagner, F. and Scheele, R. 2003. Optical properties of the Indo-Asian haze layer over the tropical Indian Ocean. *J. Geophys. Res.*, **108**, 4059, doi: 10.1029/2002JD002473.
- Früh, B., Eckstein, E., Trautmann, T., Wendisch, M., Fiebig, M. and Feister, U. 2003. Ground-based measured and calculated spectra of actinic flux density and downward UV irradiance in cloudless conditions and their sensitivity to aerosol microphysical properties. *J. Geophys. Res.*, **108**, 4509, doi: 10.1029/2002JD002933.
- Guazzotti, S. A., Suess, D. T., Coffee, K. R., Quinn, P. K., Bates, T. S., Wisthaler, A., Hansel, A., Ball, W. P., Dickerson, R. R., Neusüß, C., Crutzen, P. J. and Prather, K. A. 2003. Characterization of carbonaceous aerosols outflow from India and Arabia: Biomass/biofuel burning and fossil fuel combustion. *J. Geophys. Res.*, **108**, 4485, doi: 10.1029/2002JD003277.
- Heintzenberg, J., Hermann, M. and Theiss, D. 2003. Out of Africa: High aerosol concentrations in the upper troposphere over Africa. *Atmos. Chem. Phys.*, **3**, 1-8.
- Heintzenberg, J., Tuch, T., Wehner, B., Wiedensohler, A., Wex, H., Ansmann, A., Mattis, I., Müller, D., Wendisch, M., Eckhardt, S. and Stohl, A. 2003. Arctic haze over Central Europe. *Tellus B*, **55**, 796-807.
- Herrmann, H. 2003. Kinetics of aqueous phase reactions relevant for atmospheric chemistry. *Chem. Rev.*, **103**, 4691-4716.
- Hermann, M., Heintzenberg, J., Wiedensohler, A., Zahn, A., Heinrich, G. and Brenninkmeijer, C. A. M. 2003. Meridional distributions of aerosol particle number concentrations in the upper troposphere and lower stratosphere obtained by Civil Aircraft for Regular Investigation of the Atmosphere Based on an Instrument Container (CARIBIC) flights. *J. Geophys. Res.*, **108**, 4114, doi: 10.1029/2001JD001077.
- Herrmann, H., Majdik, Z.-T., Ervens, B. and Weise, D. 2003. Halogen production from aqueous tropospheric particles. *Chemosphere*, **52**, 485-502.
- Heusel-Waltrop, A., Diehl, K., Mitra, S. K. and Pruppacher, H. R. 2003. A laboratory and theoretical study on the uptake of SO<sub>2</sub> gas by large and small water drops containing heavy metal ions. *J. Atmos. Chem.*, **44**, 211-223.
- Iinuma, Y. and Herrmann, H. 2003. Method development for the analysis of particle phase substituted methoxy phenols and aromatic acids from biomass burning using capillary electrophoresis/electrospray ionization mass spectrometry (CE/ESI-MS). *J. Chromatogr. A*, **1018**, 105-115.
- Kerkweg, A., Wurzler, S., Reisin, T. G. and Bott, A. 2003. On the cloud processing of aerosol particles: An entraining air-parcel model with two-dimensional spectral cloud microphysics and a new formulation of the collection kernel. *Q. J. Roy. Meteor. Soc.*, **129**, 1-18.
- Lammel, G., Brüggemann, E., Gnauk, T., Müller, K., Neusüß, C. and Röhl, A. 2003. A new method to study aerosol source contributions along the tracks of air parcels and its application to the near-ground level aerosol chemical composition in Central Europe. *J. Aerosol Sci.*, **34**, 1-25.
- Lammel, G., Brüggemann, E., Müller, K. and Röhl, A. 2003. On the horizontal homogeneity of mass-related aerosol properties. *Environ. Monit. Assess.*, **84**, 265-273.
- Maßling, A., Wiedensohler, A., Busch, B., Neusüß, C., Quinn, P., Bates, T. and Covert, D. S. 2003. Hygroscopic properties of different aerosol types over the Atlantic and Indian Oceans. *Atmos. Chem. Phys.*, **3**, 1377-1397.
- Mattis, I., Ansmann, A., Wandinger, U. and Müller, D. 2003. Unexpectedly high aerosol load in the free troposphere over Central Europe in spring/summer 2003. *Geophys. Res. Lett.*, **30**, 2178, doi: 10.1029/2003GL018442.
- Müller, D., Franke, K., Ansmann, A., Althausen, D. and Wagner, F. 2003. Indo-Asian pollution during INDOEX: Microphysical particle properties and single-scattering albedo inferred from multiwavelength lidar observations. *J. Geophys. Res.*, **108**, 4600, doi: 10.1029/2003JD003538.
- Müller, D., Mattis, I., Wandinger, U., Ansmann, A., Althausen, D., Dubovik, O., Eckhardt, S. and Stohl, A. 2003. Saharan dust over a Central European EARLINET-AERONET site: Combined observations with Raman lidar and Sun photometer. *J. Geophys. Res.*, **108**, 4345, doi: 10.1029/2002JD002918.
- Naoe, H., Heintzenberg, J., Okada, K., Zaizen, Y., Hayashi, K., Tateishi, T., Igarashi, Y., Dokiya, Y. and Kinoshita, K. 2003. Composition and size distribution of submicrometer aerosol particles observed on Mt. Fuji in the volcanic plumes from Miyakejima. *Atmos. Environ.*, **37**, 3047-3055.
- Okada, K. and Heintzenberg, J. 2003. Size distribution, state of mixture and morphology of urban aerosol particles at given electrical mobilities. *J. Aerosol Sci.*, **34**, 1539-1554.
- Orsini, D. A., Ma, Y., Sullivan, A., Sierau, B., Baumann, K. and Weber, R. J. 2003. Refinements to the particle-into-liquid sampler (PILS) for ground and airborne measurements of water soluble aerosol composition. *Atmos. Environ.*, **37**, 1243-1259.

- Plewka, A., Hofmann, D., Müller, K. and Herrmann, H. 2003. Determination of biogenic organic compounds in airborne particles by solvent extraction, derivatisation and mass spectrometric detection. *Chromatographia*, **57**, S253-S259.
- Renner, E. and Münzberg, A. 2003. Impact of biogenic terpene emissions *Brassica napus* on tropospheric ozone over Saxony (Germany): Numerical investigation. *Environ. Sci. Pollut. Res.*, **10**, 147-153.
- Saathoff, H., Möhler, O., Schurath, U., Kamm, S., Dippel, B. and Mihelcic, D. 2003. The AIDA soot aerosol characterisation campaign 1999. *J. Aerosol Sci.*, **34**, 1277-1296.
- Schlünzen, K. H., Hinneburg, D., Knoth, O., Lambrecht, M., Leidl, B., Lopez, S., Lüpkes, C., Pankus, H., Renner, E., Schatzmann, M., Schoenemeyer, T., Trepte, S. and Wolke, R. 2003. Flow and transport in the obstacle layer: First results of the micro-scale model MITRAS. *J. Atmos. Chem.*, **44**, 113-130.
- Siebert, H., Wendisch, M., Conrath, T., Teichmann, U. and Heintzenberg, J. 2003. A new tethered balloon-borne payload for fine-scale observations in the cloudy boundary layer. *Bound.-Layer Meteor.*, **106**, 461-482.
- Sierau, B., Stratmann, F., Pelzing, M., Neusüß, C., Hofmann, D. and Wilck, M. 2003. A condensation-growth and impaction method for rapid off-line chemical-characterization of organic submicrometer atmospheric aerosol particles. *J. Aerosol Sci.*, **34**, 225-242.
- Spindler, G., Hesper, J., Brüggemann, E., Dubois, R., Müller, T. and Herrmann, H. 2003. Wet annular denuder measurements of nitrous acid: Laboratory study of the artefact reaction of NO<sub>2</sub> with S(IV) in aqueous solution and comparison with field measurements. *Atmos. Environ.*, **37**, 2643-2662.
- Stratmann, F., Siebert, H., Spindler, G., Wehner, B., Althausen, D., Heintzenberg, J., Hellmuth, O., Rinke, R., Schmieder, U., Seidel, C., Tuch, T., Uhrner, U., Wiedensohler, A., Wandinger, U., Wendisch, M., Schell, D. and Stohl, A. 2003. New-particle formation events in a continental boundary layer: First results from the SATURN experiment. *Atmos. Chem. Phys.*, **3**, 1445-1459.
- Tuch, T., Wehner, B., Pitz, M., Cyrus, J., Heinrich, J., Kreyling, W. G., Wichmann, H. E. and Wiedensohler, A. 2003. Long-term measurements of size-segregated ambient aerosol in two German cities located 100 km apart. *Atmos. Environ.*, **37**, 4687-4700.
- Twohy, C. H., Strapp, J. W. and Wendisch, M. 2003. Performance of a counterflow virtual impactor in the NASA icing research tunnel. *J. Atmos. Oceanic Technol.*, **20**, 781-790.
- Uhrner, U., Birmili, W., Stratmann, F., Wilck, M., Ackermann, I. J. and Berresheim, H. 2003. Particle formation at a continental background site: Comparison of model results with observations. *Atmos. Chem. Phys.*, **3**, 347-359.
- Wehner, B. and Wiedensohler, A. 2003. Long term measurements of submicrometer urban aerosols: Statistical analysis for correlations with meteorological conditions and trace gases. *Atmos. Chem. Phys.*, **3**, 867-879.
- Wendisch, M. and Meyer, B. 2003. Vertical distribution of spectral solar irradiance in the cloudless sky - A case study. *Geophys. Res. Lett.*, **30**, 1183-1186, doi: 10.1029/2002GL016529.
- Wex, H., Neusüß, C., Wendisch, M., Stratmann, F., Koziar, C., Keil, A., Wiedensohler, A. and Ebert, M. 2003. Particle scattering, backscattering, and absorption coefficients: An in situ closure and sensitivity study. *J. Geophys. Res.*, **107**, 8122, doi: 10.1029/2000JD000234.
- Wicktor, F., Donati, A., Herrmann, H. and Zellner, R. 2003. Laser based spectroscopic and kinetic investigations of reactions of the Cl atom with oxygenated hydrocarbons in aqueous solution. *Phys. Chem. Chem. Phys.*, **5**, 2562-2572.

### Conference proceedings

- Adler, S., Hermann, M. and Wiedensohler, A. 2003. *Pressure- and temperature-dependent counting efficiency of the CPC 7610 operated with FC43 as working fluid. European Aerosol Conference (EAC)*, Madrid, Spain, 31 August - 5 September. *J. Aerosol Sci.*, S1247-S1248.
- Althausen, D., Müller, D., Ansmann, A., Wandinger, U., Franke, K. and Wagner, F. 2003. *Vertical profiles of atmospheric particle parameters measured with a scanning 6-wavelength 11-channel aerosol lidar. Laser Radar Technology and Applications VIII conference at SPIE's 17th Annual AeroSense Symposium*, Orlando, Florida, USA, 21-25 April.

- Ansmann, A., Bösenberg, J., Chaikovsky, A. P., Eixmann, R., Freudenthaler, V., Garcia-Vizcaino, D., Komguem, L., Linné, H., Matthias, V., Mattis, I., Mitev, V., Müller, D., Munoz, C., Nickovic, S., Pelon, J., Sauvage, L., Sobolewsky, P., Srivastava, M. K., Vaughan, G., Wandinger, U. and Wiegner, M. 2003. *Co-ordinated vertical profiling of Saharan dust over western and central Europe with a continental lidar network: The 11-16 October 2001 outbreak*. 6th International Symposium on Tropospheric Profiling: Needs and Technologies, Leipzig, Germany, 14-20 September. 423-425.
- Ansmann, A., Müller, D., Mattis, I. and Wandinger, U. 2003. *Raman-lidar profiling of dust optical properties at UV and visible wavelengths*. 2nd International Workshop on Mineral Dust, Paris, France, 10-12 September.
- Arshinov, Y. F., Althausen, D., Ansmann, A., Bobrovnikov, S. M., Mattis, I., Müller, D., Serikov, I. B. and Wandinger, U. 2003. *Round-the-clock temperature profiling in the troposphere with Raman lidar*. 6th International Symposium on Tropospheric Profiling: Needs and Technologies, Leipzig, Germany, 14-20 September. 142-144.
- Barzagli, P. and Herrmann, H. 2003. *Study of the nitrate radical reactivity towards ortho-substituted phenols in aqueous solution*. Bunsentagung, Kiel, Germany, 29-31 May.
- Barzagli, P. and Herrmann, H. 2003. *Laser-based studies of reactions of free radicals with aromatic compounds in aqueous solution*. 28th International Conference on Solution Chemistry (ICSC), Debrecen, Hungary, 23-28 August.
- Berndt, T., Böge, O. and Stratmann, F. 2003. *Particle formation in the system O<sub>3</sub>/α-Pinene/SO<sub>2</sub>*. European Aerosol Conference (EAC), Madrid, Spain, 31 August - 5 September. J. Aerosol Sci., S1399-S1400.
- Diehl, K., Posselt, R., Simmel, M. and Wurzler, S. 2003. *Collision processes in mixed-phase clouds*. EGS-AGU-EUG Joint Assembly, Nice, France, 6-11 April.
- Diehl, K., Simmel, M. and Wurzler, S. 2003. *Model simulations of drop freezing in the immersion mode for a biomass burning situation*. European Aerosol Conference (EAC), Madrid, Spain, 31 August - 5 September. J. Aerosol Sci., S81-S83.
- Engelmann, R., Rhone, P. and Althausen, D. 2003. *The Mini Raman Lidar „Polly“ - Setup and experiments*. 6th International Symposium on Tropospheric Profiling: Needs and Technologies, Leipzig, Germany, 14-20 September. 240-242.
- Franck, U., Herbarth, O., Manjarrez, M., Wiedensohler, A., Tuch, T. and Holstein, P. 2003. *Indoor and outdoor fine particles: Exposure and possible health impact*. European Aerosol Conference (EAC), Madrid, Spain, 31 August - 5 September. J. Aerosol Sci., S1357-S1358.
- Garcia, S. G., Trautmann, T., Wendisch, M., Meywerk, J. and Venema, V. 2003. *3D effects on radiative transfer simulations for cloud fields measured in the BBC campaign*. EGS-AGU-EUG Joint Assembly, Nice, France, 6-11 April.
- Gligorovski, S. and Herrmann, H. 2003. *Laser-based studies for OH reactions with oxygenated species in the troposphere*. Bunsentagung, Kiel, Germany, 29-31 May.
- Heintzenberg, J., Hermann, M., Theiss, D. and van Velthoven, P. F. J. 2003. *Out of Africa: High aerosol concentrations in the upper troposphere over Tropical Africa*. 8th International Conference on Atmospheric Sciences and Applications to Air Quality, Tsukuba, Japan, 11-13 March.
- Heintzenberg, J. and Leck, C. 2003. *An analysis of eighteen years of soot sampling at the Australian Baseline Station at Cape Grim, Tasmania*. 8th International Conference on Atmospheric Sciences and Applications to Air Quality, Tsukuba, Japan, 11-13 March.
- Held, A., Brüggemann, E., Wiedensohler, A. and Klemm, O. 2003. *Turbulent exchange of particulate matter during BEWA2000*. AGU 2003 Fall Meeting, San Francisco, California, USA, 8-12 December.
- Held, A., Nowak, A., Wiedensohler, A. and Klemm, O. 2003. *Formation and turbulent vertical exchange of particulate matter over a coniferous forest*. European Aerosol Conference (EAC), Madrid, Spain, 31 August - 5 September. J. Aerosol Sci., S473-S474.
- Hellmuth, O., Wolke, R., Knoth, O., Renner, E., Schröder, W., Heinrich, B. and Benz, S. 2003. *Long-term simulation of ozone and PM using the model system LM-MUSCAT within the City Delta project*. 26th NATO/CCMS International Technical Meeting on Air Pollution Modelling and its Applications, Istanbul, Turkey, 26-30 May.
- Helmert, J. 2003. *Examination of the impact of mixing-length formulation on mesoscale simulation results: A Lokal-Modell case study*. Fifth International SRNWP-Workshop on Non-Hydrostatic Modelling, Bad Orb, Germany, 27-29 October.
- Henning, S., Bojinski, S., Diehl, K., Ghan, S., Nyeki, S., Weingartner, E., Wurzler, S. and Baltensberger, U. 2003. *Investigation of mixed-phase clouds at the Jungfrauoch*. European Aerosol Conference (EAC), Madrid, Spain, 31 August - 5 September. J. Aerosol Sci., S79-S80.
- Herrmann, H. 2003. *Cloud processing of organic material: Lab studies and model development*. Workshop on Secondary Aerosols, Wengen, Switzerland, 16-18 May. \*)

- Herrmann, H. 2003. *Modelling atmospheric aqueous phase chemistry*. IV. Informal Conference on Reaction Kinetics and Atmospheric Chemistry, Helsingør, Denmark, 13-15 June. \*)
- Igarashi, Y., Sawa, Y., Naoe, H., Okada, K., Takahashi, H., Tsutsumi, Y., Hayashi, K., Suzuki, I., Sakane, M., Kido, M., Akagi, T., Katayama, Y., Hatakeyama, S., Kaneyasu, N., Tsuno, H., Yoshioka, K., Watanabe, K., Heintzenberg, J. and Dokiya, Y. 2003. *Mt. Fuji Summer Campaigns on Atmospheric Chemistry, 1997-2002*. 8th International Conference on Atmospheric Sciences and Applications to Air Quality, Tsukuba, Japan, 11-13 March.
- Iinuma, Y., Böge, O., Gnauk, T. and Herrmann, H. 2003. *Characterisation of chemical and physical properties of  $\alpha$ -pinene oxidation particles from chamber experiments*. EGS-AGU-EUG Joint Assembly, Nice, France, 6-11 April.
- Knoth, O. and Hinneburg, D. 2003. *A cloud resolving model with a cut cell approach and implicit time stepping: Orographic flow applications*. GAMM 2003 Annual Conference of the „Gesellschaft für Angewandte Mathematik und Mechanik“, Abano T. - Padova, Italy, 24-28 March.
- Knoth, O. and Hinneburg, D. 2003. *A cloud resolving model with implicit time stepping: Orographic flow application*. Fifth International SRNWP-Workshop on Non-Hydrostatic Modelling, Bad Orb, Germany, 27-29 October.
- Knoth, O., Sehili, A.-M. and Wolke, R. 2003. *Discontinuous Galerkin methods for the condensation-coagulation equation*. 10th Seminar NUMDIFF on Numerical Solution of Differential and Differential-Algebraic Equations, Halle, Germany, 8-11 September.
- Lammel, G., Schneider, F., Röhl, A. and Gnauk, T. 2003. *Aerosols emitted from a livestock farm*. European Aerosol Conference (EAC), Madrid, Spain, 31 August - 5 September. J. Aerosol Sci., S475-S476.
- Lehmann, K., Maßling, A. and Wiedensohler, A. 2003. *Soluble particle volume fractions derived from hygroscopicity measurements and their dependence on different air mass imprinting*. European Aerosol Conference (EAC), Madrid, Spain, 31 August - 5 September. J. Aerosol Sci., S135-S136.
- Leinert, S. and Wiedensohler, A. 2003. *Hygroscopicity of 1 micrometer particles during ACE-Asia*. European Aerosol Conference (EAC), Madrid, Spain, 31 August - 5 September. J. Aerosol Sci., S137-S138.
- Majdik, Z.-T. and Herrmann, H. 2003. *Size resolved simulation of a tropospheric multiphase cloud model*. EGS-AGU-EUG Joint Assembly, Nice, France, 6-11 April.
- Majdik, Z.-T. and Herrmann, H. 2003. *Training on modeling atmospheric aqueous phase chemistry with CAPRAM*. IV. Informal Conference on Reaction Kinetics and Atmospheric Chemistry, Helsingør, Denmark, 13-15 June.
- Maßling, A., Wehner, B., Wiedensohler, A., Saathoff, H., Schnaiter, M. and Voutilainen, A. 2003. *Hygroscopic properties of organically coated diesel and palas soot particles*. EGS-AGU-EUG Joint Assembly, Nice, France, 6-11 April.
- Maßling, A., Wiedensohler, A. and Voutilainen, A. 2003. *Hygroscopic properties of submicrometer aerosol particles during ACE-Asia*. European Aerosol Conference (EAC), Madrid, Spain, 31 August - 5 September. J. Aerosol Sci., S9-S10.
- Matthias, V., Balis, D., Bösenberg, J., de Tomasi, F., Eixmann, R., Komguem, L., Mattis, I., Papayannis, A., Pappalardo, G., Rizi, V. and Wang, X. 2003. *Statistics of aerosol extinction profiles from EARLINET*. 6th International Symposium on Tropospheric Profiling: Needs and Technologies, Leipzig, Germany, 14-20 September. 426-428.
- Müller, D., Ansmann, A., Mattis, I., Wandinger, U. and Althausen, D. 2003. *Unexpectedly high aerosol load in the free troposphere observed with Raman lidar over Central Europe in spring/summer 2003*. AGU 2003 Fall Meeting, San Francisco, California, USA, 8-12 December.
- Müller, D., Ansmann, A., Mattis, I., Wandinger, U. and Althausen, D. 2003. *Characterization of Saharan dust from combined Raman lidar and sun photometer observations*. 2nd International Workshop on Mineral Dust, Paris, France, 10-12 September.
- Müller, D., Ansmann, A., Wandinger, U., Althausen, D., Mattis, I. and Franke, K. 2003. *Comprehensive characterization of tropospheric particles with Raman lidar*. Symposium on emerging environmental technologies in the 21st century, Kwangju Institute of Science and Technology (K-JIST), Gwangju, Republic of Korea, 4 November. \*)
- Müller, K. and Plewka, A. 2003. *Size segregated characterization of organic compounds in urban particulates*. European Aerosol Conference (EAC), Madrid, Spain, 31 August - 5 September. J. Aerosol Sci., S717-S718.

- Naoe, H., Heintzenberg, J., Okada, K., Zaizen, Y., Hayashi, K., Tateishi, T., Igarashi, Y., Dokiya, Y. and Kinoshita, K. 2003. *Composition and size distribution of submicrometer aerosol particles observed on Mt. Fuji in the volcanic plumes from Miyake-Jima*. 8th International Conference on Atmospheric Sciences and Applications to Air Quality, Tsukuba, Japan, 11-13 March.
- Okada, K. and Heintzenberg, J. 2003. *Electron microscopic examination of atmospheric aerosol particles sampled downstream of a DMA*. 20th Symposium on Aerosol Science and Technology, Tsukuba, Japan, 29-31 July. 13-14.
- Papayannis, A., Tsaknakis, G., Balis, D., Chaikovsky, A. P., de Tomasi, F., Mattis, I., Mitev, V., Pappalardo, G., Pelon, J., Perez, C., Puchalski, S., Rizi, V., Sauvage, L., Simeonov, V., Spinelli, N., Trickl, T., Vaughan, G., Wiegner, M., Matthias, V., Haagaard, A., Alpers, M. and Castanho, A. 2003. *Three years of observations of Saharan dust outbreaks over Europe monitored by a coordinated LIDAR Network in the frame of the EARLINET Project*. 6th International Symposium on Tropospheric Profiling: Needs and Technologies, Leipzig, Germany, 14-20 September. 225-227.
- Pappalardo, G., Bösenberg, J., Alpers, M., Balis, D., de Tomasi, F., Komguem, L., Matthias, V., Mattis, I., Mona, L., Papayannis, A., Rizi, V. and Spinelli, N. 2003. *Systematic lidar ratio measurements in the frame of EARLINET*. 6th International Symposium on Tropospheric Profiling: Needs and Technologies, Leipzig, Germany, 14-20 September. 429-431.
- Pilewskie, P., Guan, H., Platnick, S., Bergstrom, R., Wendisch, M. and Yang, F. 2003. *Retrieval of cirrus properties from solar spectral irradiance during CRYSTAL-FACE*. AGU 2003 Fall Meeting, San Francisco, California, USA, 8-12 December.
- Posselt, R., Diehl, K., Simmel, M. and Wurzler, S. 2003. *Surface tension effects on the condensational and collisional growth of cloud drops: Numerical sensitivity studies*. EGS-AGU-EUG Joint Assembly, Nice, France, 6-11 April.
- Schaap, M., Spindler, G., Schulz, M., Acker, K., Maenhaut, W., Berner, A., Wieprecht, W., Streit, N., Müller, K., Brüggemann, E., Putaud, J.-P., Puxbaum, H., Baltensberger, U. and ten Brink, H. 2003. *Artefacts in the sampling of nitrate studied in the „INTERCOMP“ campaigns of EUROTRAC-Aerosol*. European Aerosol Conference (EAC), Madrid, Spain, 31 August - 5 September. J. Aerosol Sci., S553-S554.
- Sedello, C., Müller, K., Spindler, G., Haferkorn, S. and Herrmann, H. 2003. *Determination of atmospheric fluxes of carbonyl compounds*. EGS-AGU-EUG Joint Assembly, Nice, France, 6-11 April.
- Siebert, H., Schell, D. and Stratmann, F. 2003. *Tethered-balloon borne measurements of particle number concentrations and turbulence in the planetary boundary layer with „ACTOS“*. European Aerosol Conference (EAC), Madrid, Spain, 31 August - 5 September. J. Aerosol Sci., S645-S646.
- Siebert, H., Stratmann, F. and Wehner, B. 2003. *New particle formation observed during the SATURN experiment at inversion layers - A case study -*. European Aerosol Conference (EAC), Madrid, Spain, 31 August - 5 September. J. Aerosol Sci., S1335-S1336.
- Sierau, B., Iinuma, Y. and Stratmann, F. 2003. *High time-resolved and size-segregated analysis of biomass burning aerosol particles using the new condensation-growth and impaction method C-GIS*. European Aerosol Conference (EAC), Madrid, Spain, 31 August - 5 September. J. Aerosol Sci., S951-S952.
- Simmel, M., Diehl, K., Wurzler, S., Brüggemann, E., Galgon, D., Gnauk, T., Herrmann, H., Lehmann, K., Maßling, A., Mertes, S., Nowak, A., Müller, K., Plewka, A., Wiedensohler, A., Zech, G., Acker, K., Möller, D., Wieprecht, W., Haunold, W., Ift, F., Jaeschke, W., Salkowski, T., Bächmann, K., Kramberger, H. and Srvcina, B. 2003. *Warm microphysics in an orographic cloud: Comparison of model results with field experimental data*. European Aerosol Conference (EAC), Madrid, Spain, 31 August - 5 September. J. Aerosol Sci., S157-S158.
- Simmel, M., Diehl, K., Wurzler, S. and FEBUKO-Team 2003. *Numerical simulation of the interactions between aerosols and cloud drops during the formation of an orographic cloud*. EGS-AGU-EUG Joint Assembly, Nice, France, 6-11 April.
- Spindler, G., Brüggemann, E., Gnauk, T., Müller, K. and Herrmann, H. 2003. *Size segregated characterization of  $PM_{10}$ ,  $PM_{2.5}$ ,  $PM_1$  and longterm measurements of  $PM_{10}$  downwind of a large conurbation in Germany*. 2003 AAAR PM Meeting, Particulate Matter: Atmospheric Sciences, Exposure and the Fourth Colloquium on PM and Human Health, Pittsburgh, Pennsylvania, USA, 31 March - 4 April.
- Spindler, G., Brüggemann, E., Gnauk, T., Müller, K. and Herrmann, H. 2003. *Size segregated characterization of  $PM_{10}$ ,  $PM_{2.5}$  and  $PM_1$  downwind of the Leipzig conurbation in Germany - An eight year study*. European Aerosol Conference (EAC), Madrid, Spain, 31 August - 5 September. J. Aerosol Sci., S455-S456.

- Stratmann, F., Kiselev, A., Wex, H., Wurzler, S., Wendisch, M., Heintzenberg, J., Diehl, K. and Schmidt, S. 2003. *Leipzig Aerosol Cloud Interaction Simulator (LACIS): First results*. EGS-AGU-EUG Joint Assembly, Nice, France, 6-11 April.
- Stratmann, F., Siebert, H., Spindler, G., Wehner, B., Schell, D., Althausen, D., Heintzenberg, J., Hellmuth, O., Stohl, A., Tuch, T., Uhrner, U., Wiedensohler, A., Wandinger, U. and Wendisch, M. 2003. *New-particle formation events in a continental boundary layer: First results from the SATURN experiment*. European Aerosol Conference (EAC), Madrid, Spain, 31 August - 5 September. *J. Aerosol Sci.*, S1333-S1334.
- ten Brink, H., Even, A., Müller, K., Spindler, G., Gnauk, T., Chi, X., Maenhaut, W., Hitznerberger, R., Berner, A., Bauer, H., Puxbaum, H., Turstic, J. and Putaud, J.-P. 2003. *Comparability of methods in use in Europe for measuring the carbon content in aerosol*. European Aerosol Conference (EAC), Madrid, Spain, 31 August - 5 September. *J. Aerosol Sci.*, S545-S546.
- Tuch, T., Wehner, B., Franck, U. and Wiedensohler, A. 2003. *Correlation between two measurement sites for ultrafine particles within one city*. European Aerosol Conference (EAC), Madrid, Spain, 31 August - 5 September. *J. Aerosol Sci.*, S485-S486.
- van Pinxteren, D., Brüggemann, E., Galgon, D., Gnauk, T., Lehmann, K., Maßling, A., Mertes, S., Müller, K., Nowak, A., Plewka, A., Wiedensohler, A. and Herrmann, H. 2003. *Physico-chemical characterisation of air, particles and cloud water in cloud experiments*. European Aerosol Conference (EAC), Madrid, Spain, 31 August - 5 September. *J. Aerosol Sci.*, S159-S160.
- van Pinxteren, D., Brüggemann, E. and Herrmann, H. 2003. *Determination of dicarboxylic acids in tropospheric particles and cloudwater*. EGS-AGU-EUG Joint Assembly, Nice, France, 6-11 April.
- Veselovskii, I., Kolgotin, A. and Müller, D. 2003. *Retrieval of bimodal aerosol size distribution with multiwavelength Mie-Raman lidar*. 6th International Symposium on Tropospheric Profiling: Needs and Technologies, Leipzig, Germany, 14-20 September. 363-365.
- Wehner, B., Rose, D., Maßling, A., Wiedensohler, A., Voutilainen, A., Schnaiter, M. and Saathoff, H. 2003. *Estimation of thickness of the coating using a volatility tandem DMA for coated soot particles during the AIDA SOOT2002 Campaign*. EGS-AGU-EUG Joint Assembly, Nice, France, 6-11 April.
- Wehner, B., Rose, D., Wiedensohler, A., Voutilainen, A., Schnaiter, M. and Saathoff, H. 2003. *Measurement of the coating by different volatility techniques during the AIDA soot coating campaign 2002*. European Aerosol Conference (EAC), Madrid, Spain, 31 August - 5 September. *J. Aerosol Sci.*, S463-S464.
- Wehner, B., Schmieder, U., Siebert, H., Stratmann, F., Spindler, G., Tuch, T. and Wiedensohler, A. 2003. *Horizontal variability of new particle formation during SATURN*. European Aerosol Conference (EAC), Madrid, Spain, 31 August - 5 September. *J. Aerosol Sci.*, S725-S726.
- Wehner, B., Schmieder, U., Tuch, T. and Wiedensohler, A. 2003. *Spatial variation of submicrometer aerosol number size distributions between urban measurement sites and with increasing distance to the city*. EGS-AGU-EUG Joint Assembly, Nice, France, 6-11 April.
- Wex, H., Kiselev, A., Stratmann, F., Diehl, K., Wurzler, S., Wendisch, M. and Heintzenberg, J. 2003. *Activation and growth of aerosol particles at atmospheric super-saturations: Results from the Leipzig Aerosol Cloud Interaction Simulator (LACIS)*. European Aerosol Conference (EAC), Madrid, Spain, 31 August - 5 September. *J. Aerosol Sci.*, S75-S76.
- Wiedensohler, A., Maßling, A., Wehner, B., Saathoff, H., Schnaiter, M. and Voutilainen, A. 2003. *Hygroscopic growth of soot particles coated with organic material*. European Aerosol Conference (EAC), Madrid, Spain, 31 August - 5 September. *J. Aerosol Sci.*, S13-S14.
- Wolke, R., Hellmuth, O., Knoth, O., Schröder, W., Heinrich, B. and Renner, E. 2003. *The chemistry-transport modeling system LM-MUSCAT: Description and Citydelta applications*. 26th NATO/CCMS International Technical Meeting on Air Pollution Modelling and its Applications, Istanbul, Turkey, 26-30 May.
- Wolke, R., Knoth, O., Hellmuth, O., Schröder, W. and Renner, E. 2003. *The parallel model system LM-MUSCAT for chemistry-transport simulations: Coupling scheme, parallelization and applications*. ParCo2003, Dresden, Germany, 2-5 September.
- Wolke, R., Knoth, O., Sehilli, A.-M. and Zoboki, J. 2003. *Time-integration schemes for atmospheric multiphase processes*. 10th Seminar NUMDIFF on Numerical Solution of Differential and Differential-Algebraic Equations, Halle, Germany, 8-11 September.
- Wurzler, S., Diehl, K., Simmel, M. and Posselt, R. 2003. *Possible effects of insoluble particles and turbulence on microphysics in mixed-phase clouds*. EGS-AGU-EUG Joint Assembly, Nice, France, 6-11 April.

- Wurzler, S., Herrmann, H., Wolke, R., Pöschl, U., Möhler, O., Schurath, U., EFEU-Team, FEBUKO-Team, MODMEP-Team, CARBAERO-Team and POSTA-Team 2003. *Multiphase processes*. EGS-AGU-EUG Joint Assembly, Nice, France, 6-11 April.
- Wurzler, S., Simmel, M., Diehl, K. and Langmann, B. 2003. *Numerical investigations of the effects of biomass burning on clouds using detailed sectional microphysics models*. EGS-AGU-EUG Joint Assembly, Nice, France, 6-11 April.
- Wurzler, S., Simmel, M., Posselt, R. and Diehl, K. 2003. *Surface tension effects on the condensational and collisional growth of cloud drops: Numerical sensitivity studies*. European Aerosol Conference (EAC), Madrid, Spain, 31 August - 5 September. J. Aerosol Sci., S169-S170.
- Yin, Y., Wurzler, S., Levin, Z. and Reisin, T. G. 2003. *Effects of cloud processed mineral dust particles on mixed phase clouds, precipitation formation and cloud optical properties*. EGS-AGU-EUG Joint Assembly, Nice, France, 6-11 April.
- Zdimal, V., Brus, D. and Stratmann, F. 2003. *Homogeneous nucleation rates of n-propanol carrier gas effect*. European Aerosol Conference (EAC), Madrid, Spain, 31 August - 5 September. J. Aerosol Sci., S1069-S1070.
- Zeromskis, E., Wandinger, U., Althausen, D., Engelmann, R., Rhone, P. and Foster, R. 2003. *Coherent Doppler lidar for wind profiling in the lower atmosphere*. 6th International Symposium on Tropospheric Profiling: Needs and Technologies, Leipzig, Germany, 14-20 September. 71-73.

\*) invited lectures

### Lectures

- Althausen, D. 2003. *Vertical profiling of atmospheric particle properties using lidar*. Pennsylvania State University, State College. Pennsylvania, USA. 29 April.
- Ansmann, A. 2003. *Major Saharan Dust Outbreak 11-16 October 2001*. First EARLINET symposium on the structure and use of the data base derived from systematic lidar observations. Hamburg, Germany. 11-12 February.
- Ansmann, A. 2003. *Active remote sensing of aerosol and clouds from space in the EARTH-CARE mission*. First EARLINET symposium on the structure and use of the data base derived from systematic lidar observations. Hamburg, Germany. 11-12 February.
- Bobrovnikov, S. M., Arshinov, Y. F., Serikov, I. B., Althausen, D., Ansmann, A., Mattis, I. and Wandinger, U. 2003. *Daytime temperature profiling in the troposphere with a pure rotational Raman lidar*. First EARLINET symposium on the structure and use of the data base derived from systematic lidar observations. Hamburg, Germany. 11-12 February.
- Böckmann, C., Wandinger, U. and al., e. 2003. *EARLINET - Backscatter lidar algorithm intercomparison*. First EARLINET symposium on the structure and use of the data base derived from systematic lidar observations. Hamburg, Germany. 11-12 February.
- Engelmann, R., Rhone, P., Althausen, D., Ansmann, A., Müller, T. and Wandinger, U. 2003. *Das Mini-Raman-LIDAR Polly: Optischer Aufbau und Erprobung des Systems*. DPG-Tagung. Hannover, Deutschland. 24.-28. März.
- Heintzenberg, J. 2003. *CARIBIC aerosol measurements over Africa*. Meteorological Research Institute. Tsukuba, Japan. 20 March. \*)
- Heintzenberg, J. 2003. *The Indian Ocean Experiment*. Meteorological Research Institute. Tsukuba, Japan. 27 March. \*)
- Heintzenberg, J. 2003. *Aerosolpartikel im globalen Wandel: Verbotene Klimaantriebe und Widersprüche*. DMG-Zweigverein. Frankfurt/Main. 30. April. \*)
- Hellmuth, O., Wolke, R., Knoth, O., Renner, E., Schröder, W., Heinrich, B. and Benz, S. 2003. *Status report: Validation study on LM-MUSCAT long-term simulation for the city area of Berlin*. 4th City-Delta Workshop. Valencia, Spain. 7-9 April.
- Mattis, I., Ansmann, A., Müller, D., Wandinger, U. and Althausen, D. 2003. *Dual-wavelength Raman lidar observations of the lidar ratio of Saharan dust*. First EARLINET symposium on the structure and use of the data base derived from systematic lidar observations. Hamburg, Germany. 11-12 February.
- Mattis, I., Fay, B. and Stohl, A. 2003. *Description of 2 trajectory models used within EARLINET*. First EARLINET symposium on the structure and use of the data base derived from systematic lidar observations. Hamburg, Germany. 11-12 February.

- Mattis, I., Müller, D., Wandinger, U. and Ansmann, A. 2003. *Statistical analysis of extinction and lidar ratio profiles observed with Raman lidar over Leipzig, Germany*. First EARLINET symposium on the structure and use of the data base derived from systematic lidar observations. Hamburg, Germany. 11-12 February.
- Mertes, S. 2003. *Feld-Untersuchungen zu Bildung und Wachstum von Eispartikeln in Mischphasenwolken mithilfe der Counterflow-Virtual-Impactor Technik*. 1. Workshop „Die troposphärische Eisphase“ TROPEIS. Frankfurt/Main, Deutschland. 5.-6. Mai.
- Müller, D., Ansmann, A., Althausen, D., Wandinger, U., Mattis, I. and Franke, K. 2003. *Optical and physical properties of south- and southeast Asian aerosol particles*. Laboratoire d'Optique Atmosphérique. Lille, France. 15 May.
- Müller, D., Ansmann, A., Althausen, D., Wandinger, U., Mattis, I. and Franke, K. 2003. *Aerosol profiling with Raman lidar*. University of Creteil. Paris, France. 4 June.
- Müller, D., Ansmann, A., Wandinger, U., Mattis, I., Franke, K. and Althausen, D. 2003. *Raman lidar retrievals*. AeroCom workshop. Paris, France. 2-3 June.
- Müller, D., Mattis, I., Ansmann, A., Althausen, D., Wandinger, U., Wehner, B. and Heintzenberg, J. 2003. *Arctic haze over Leipzig observed with Raman lidar in the framework of EARLINET*. CALIPSO/CloudSat Science Team Meeting. Broomfield, Colorado, USA. 3-7 March.
- Müller, D., Mattis, I., Böckmann, C., Ansmann, A., Wandinger, U., Althausen, D. and Heintzenberg, J. 2003. *Arctic haze event over Central Europe*. First EARLINET symposium on the structure and use of the data base derived from systematic lidar observations. Hamburg, Germany. 11-12 February.
- Müller, D., Mattis, I., Wandinger, U., Althausen, D., Ansmann, A., Dubovik, O., Eckhardt, S. and Stohl, A. 2003. *Saharan dust over a Central European EARLINET-AERONET site: Combined observations with Raman lidar and Sun photometer*. First EARLINET symposium on the structure and use of the data base derived from systematic lidar observations. Hamburg, Germany. 11-12 February.
- Pappalardo, G., Amodeo, A., Wandinger, U., Matthias, V., Bösenberg, J., Alpers, M., Amiridis, V., de Tomasi, F., Frioud, M., Iarlori, M., Komguem, L., Larcheveque, G., Papayannis, A., Schumacher, R. and Wang, X. 2003. *Aerosol extinction algorithm intercomparison for the Raman lidar in the frame of EARLINET*. First EARLINET symposium on the structure and use of the data base derived from systematic lidar observations. Hamburg, Germany. 11-12 February.
- Rhone, P., Engelmann, R., Althausen, D., Ansmann, A., Müller, T. and Wandinger, U. 2003. *Mini-Raman-LIDAR Polly: Development of the data acquisition software and automation*. DPG-Tagung. Hannover, Germany. 24-28 March.
- Spindler, G., Grüner, A. and Plessow, K. 2003. *Immissionsmessungen und Abschätzung des Anteils des N-Eintrages durch trockene Deposition von NH<sub>3</sub> für die Forschungsstation Melpitz in Sachsen*. 5. BIOMET-Tagung „Mensch-Pflanze-Atmosphäre“. Dresden, Deutschland. 3.-5. Dezember.
- Wandinger, U. 2003. *Aerosol modification over Europe*. First EARLINET symposium on the structure and use of the data base derived from systematic lidar observations. Hamburg, Germany. 11-12 February.
- Wehner, B. 2003. *Größenverteilungen und Volatilität von Aerosolpartikeln in der urbanen Atmosphäre*. Oberseminar „Aerosole und Klima“, Forschungszentrum Karlsruhe, IMK-AAF. Karlsruhe, Deutschland. 16. Januar.
- Wendisch, M. 2003. *Solar radiative budget of arctic aerosol layers and low-level stratus clouds*. ASTAR Projekt-Treffen, Alfred-Wegener-Institut. Bremerhaven, Germany. 30 January.
- Wendisch, M. 2003. *Absorbed solar irradiances in the atmosphere: Uncertainties in measurements and calculations*. NASA Ames Research Center. Moffet Field, California, USA. 3 June. \*)
- Wendisch, M. 2003. *Absorption of solar radiation: How well can we model and measure it?* NCAR. Boulder, CO, USA. 10 October. \*)
- Wendisch, M., Schmidt, S., Jäkel, E., Siebert, H. and Kiselev, A. 2003. *Flugzeugmessungen des IFT während BBC-2001*. 4D-WOLKEN Projekttreffen. Heidelberg, Deutschland. 25. März.
- Wiedensohler, A., Wehner, B., Tuch, T. and Franck, U. 2003. *What kinds of measurements are necessary to characterize the aerosol exposure to humans in Beijing?* Sino-German Center for Science Promotion. Beijing, China. 17 January. \*)

\*) invited lectures

### University Courses

Winter Semester	2002/2003	University Leipzig Faculty for Physics and Geosciences
<u>Heintzenberg, J.</u>	Frontlines of Atmospheric Research	1 HPW*)
<u>Heintzenberg, J.</u> Stratmann, F. Wiedensohler, A.	Atmospheric Aerosols I	2 HPW
<u>Herrmann, H.</u>	Atmospheric Chemistry I Atmospheric Chemistry Seminar Atmospheric Chemistry Lab	2 HPW 2 HPW block course
<u>Renner, E.</u>	Modeling of transport and chemical transformation of air pollutants	2 HPW
<u>Wendisch, M.</u>	Airborne Physical Measurement Methods	1 HPW
<u>Althausen, D.</u>	Optical Measurement Techniques	1 HPW
<u>Wandinger, U.</u>	Atmospheric Optics	1 HPW
<u>Trautmann, Th.</u> Wendisch, M. Heintzenberg, J.	Radiation on the Atmosphere	1 HPW
<u>Trautmann, Th.</u> Heintzenberg, J. Wurzler, S.	Cloud Physics	2 HPW

Summer Semester	2003	University Leipzig Faculty for Physics and Geosciences
<u>Heintzenberg, J.</u> Ansmann, A. Dubois, R. Klugmann, D. Siebert, H.	Modern Meteorological Instruments I	1 HPW*)
<u>Heintzenberg, J.</u> Stratmann, F. Wiedensohler A. Hellmuth, O.	Atmospheric Aerosols II	2 HPW
<u>Herrmann, H.</u>	Atmospheric Chemistry II Atmospheric Chemistry Seminar	2 HPW 2 HPW
<u>Renner, E.</u> Hellmuth, O. Knoth, O. Wolke, R.	Mesoscale Meteorological Modeling	2 HPW
<u>Wendisch, M.</u>	Airborne Physical Measurement Methods	1 HPW
<u>Trautmann, Th.</u> Wendisch, M. Heintzenberg, J.	Radiative Transfer in Clouds	2 HPW

Winter Semester	2003/2004	University Leipzig Faculty for Physics and Geosciences
<u>Heintzenberg, J.</u>	Frontlines of Earth System Research	1 HPW <sup>*)</sup>
<u>Heintzenberg, J.</u> <u>Stratmann, F.</u> <u>Wiedensohler, A.</u>	Atmospheric Aerosols I	2 HPW
<u>Herrmann, H.</u>	Atmospheric Chemistry I	2 HPW
	Atmospheric Chemistry Seminar	2 HPW
	Atmospheric Chemistry Lab	block course
<u>Renner, E.</u>	Modeling of transport and chemical transformation of air pollutants	2 HPW
<u>Althausen, D.</u>	Optical Measurement Techniques	1 HPW
<u>Wandinger, U.</u>	Atmospheric Optics	1 HPW

<sup>\*)</sup> Hours per Week

### Master theses

<b>University Leipzig Faculty for Physics and Geosciences</b>	
Lehmann, Katrin	Die Charakterisierung der hygroskopischen Eigenschaften von Aerosolpartikeln an einem kontinentalen Standort
Banse, Dorothea	A theoretical study of particle/droplet activation and growth in the Leipzig Aerosol Cloud Interaction Simulator (LACIS)
Schmieder, Uta	Horizontale Variabilität von Partikelneubildungsereignissen während SATURN
Engelmann, Ronny	Entwicklung eines Mini-Ramanlidar und Aufbau einer kombinierten Send- und Empfangseinheit für ein Doppler-Wind-Lidar
Rüd, Carsten	Bestimmung von Metallen in Aerosolpartikeln und Wolkenwasser mittels Atom-Absorptionsspektroskopie
Benz, Stephan	Langzeitsimulation von Ozon und Partikel mit dem Vorhersagesystem LM-MUSCAT
Heide, Barbara	Verifikation von Bewölkungsvorhersagen des Lokal-Modells des Deutschen Wetterdienstes unter Zuhilfenahme von Meteosat-7 Satellitenbildern
Posselt, Rebekka	Numerische Untersuchungen zur Kollision und Koaleszenz von Wolkenpartikeln

<b>University of West Saxony at Zwickau Faculty for Physical / Computer Sciences</b>	
Adler, Sascha	Untersuchung der Funktionsfähigkeit von Kondensationspartikelzählern mit FC-43 als Arbeitssubstanz

**Doctoral theses**

<b>University Leipzig Faculty for Physics and Geosciences</b>	
Leinert, Stephan	Hygroscopicity of Micrometer-Sized Aerosol Particles – a New Measurement Technique
Franke, Kathleen	Optische und physikalische Eigenschaften süd- und südostasiatischer Aerosolpartikel: Beobachtungen mit einem Sechswellenlängenlidar auf den Malediven während INDOEX
Helmert, Jürgen	Determination of characteristic turbulence length scales from large-eddy simulation of the convective planetary boundary layer
Jaenisch, Volker	Der Einfluss turbulenter Mischungsprozesse auf die Bildungsraten atmosphärischer Aerosolpartikel
Uhrner, Ulrich	New particle formation and growth in the lower troposphere: A comparison of model results with observations at a continental background site

<b>University Leipzig Faculty for Chemistry and Mineralogy</b>	
Barzaghi, Paolo	Kinetics and mechanisms of the reactions of OH and NO <sub>3</sub> with phenol and substituted phenols in aqueous solution
Hesper, Johannes	Spektroskopische und kinetische Untersuchungen von Reaktionen der Radikale O <sub>2</sub> <sup>-</sup> und OH in wässriger Phase

**Habilitation / Lecturer**

<b>University Leipzig Faculty for Physics and Geosciences</b>	
Dr. Wendisch, Manfred	Absorption of Solar Radiation in the Cloudless and Cloudy Atmosphere

### Guest scientists

Dr. Y. Arshinov I. Serikov Dr. S. Bobrovnikow	10. Febr./ 10. May	Russ. Academy of Sciences Inst.f. Atmosph. Optics, Tomsk, Russia
Dr. A. Nadeev Dmitri Karpushenko	3. March/ 30. April	Russ. Academy of Sciences
Prof. Dr. M. R. Hoffmann	22./ 25. May	California Institute of Technology, Engineering & Applied Science, USA
Alexei Kolgotin	8. Aug./ 20. Oct.	Moscow State Technical University, Russia
Dr. Fred Brechtel	10. Aug./ 31. Aug.	Brookhaven National Laboratory, Upton, USA
Dr. Jens Bösenberg Holger Linné	26. Aug./ 30. Sept.	Max-Planck-Institut für Meteorologie, Hamburg
Prof. Igor Morozov	28. Sept./ 30. Nov.	Institute for Chemical Physics, Russian Academy of Sciences, Center for Environmental Sciences
WU Zhijun	5. Oct./ 5. Dec.	Peking University, China
Pavla Rezacova	1. Oct 03/ 31. Jan. 04	Charles University Prag, Czech Republic

### Visits of IfT-scientists at other research institutions

	Period of stay	Institutions
Dr. Manfred Wendisch	1. July 03/ 31. Dec. 04	NASA Ames Research Center, Moffett Field, USA
Paolo Barzagli	1. Oct./ 31. Dec.	University of Technology Vienna
Prof. Jost Heintzenberg	22. Jan./ 2. Febr.	Stockholm University Department of Meteorologie
Prof. Jost Heintzenberg	8. March/ 1. April	Meteorological Research Institute Tsukuba, Japan

## Scientific events

Event	Place and date	Number of participants
Project Meeting EFEU and data workshop	Leipzig 11.-12. Febr.	15 national
Project Meeting MODMEP	Leipzig 24. May	15 national
Project Meeting FEBUKO	Frankfurt/M 4.-5. June	21 national
VDI-Meeting Particle counting in ambient air	Leipzig 11.-12. June	10 national
EFEU Laboratory Campaign (II)	Mainz 23. June - 4. July	10 national
5. Workshop BEWA	Waldstein 07.- 08. July	5 national
Project Meeting EFEU	Hamburg 31. July - 1. Aug.	18 national
EFEU Laboratory Campaign (III)	Mainz 15.-27. Sept.	12 national
Project Meeting MODMEP	Leipzig 11. Nov.	15 national
Joint Meeting FEBUKO/MODMEP	Leipzig 12. Nov.	12 national
EEF-Forum Sachsen	Leipzig 8. Dec.	10 national
Field Measuring Campaign BBC Cloud II (Baltex Bridge Campaign)	Cabauw/Rotterdam/NL 1.-23. May	100 international
Calibration workshop "Spectrometer"	Leipzig 11.-12. June	10 international
6th International Symposium on Tropospheric Profiling (ISTP)	Leipzig 14.-20. Sept.	200 international
Global Aerosol Watch (GAW) Nephelometer Intercomparison / Calibration Workshop	Leipzig 03.-14. November	10 international

### Membership

#### Althausen, Dietrich

- Lidar Expert Network “Laser Remote Sensing of Water Vapor and Wind”
- Member of the steering committee, Speaker of the Working Group “Reference system” (together with G. Ehret/DLR)

#### Ansmann, Albert

- NASDA-ESA EarthCARE Joint Mission Advisory Group

#### Heintzenberg, Jost

- Ordentliches Mitglied der Sächsischen Akademie der Wissenschaften
- Außerordentliches Mitglied Berlin-Brandenburgische Akademie der Wissenschaften
- Wissenschaftlicher Beirat des Deutschen Wetterdienstes
- Sprecher der Sektion E der Wissenschaftsgemeinschaft “Gottfried Wilhelm Leibniz”
- Editorial Board Tellus B, Atmospheric Research
- Scientific Advisory Board of the Research Institute for Humanity and Nature, Kyoto, Japan
- ESF Scientific User Committee for EUFAR (European Fleet for Atmospheric Research)
- Permanent Scientific Advisory Committee of the Centro de Geofísica de Evora, Portugal

#### Herrmann, Hartmut

- Sprecher der Gruppe “Mehrphasenprozesse” im BMBF-Programm AFO 2000
- Mitglied des Wissenschaftlichen Beirats der Kommission zur Reinhaltung der Luft (KRdL) im VDI
- IUPAC Committee “Aqueous Solution Kinetics Data for Atmospheric Chemistry”
- GdCh, Fachgruppe Umweltchemie und Ökotoxikologie Arbeitskreis “Atmosphärenchemie”

#### Renner, Eberhard

- DECHEMA/GVC-Arbeitsausschuss “Schadstoffausbreitung”
- Scientific Committee of the NATO/CCMS ITM conference series, German member

#### Stratmann, Frank

- “Scientific Programm Committee” der Europäischen Aerosolkonferenz

#### Wandinger, Ulla

- International Coordination-group on Laser Atmospheric Studies (ICLAS)
- Committee on Laser Atmospheric Studies of the American Meteorological Society (CLAS)
- COST-720, European Co-operation in the field of Scientific and Technical Research - 720: Integrated Ground-Based Remote-Sensing Stations for Atmospheric Profiling, Working group 1

#### Wendisch, Manfred

- Koordinator (Aerosol Mikrophysik) im EUFAR (European Fleet for Atmospheric Research) Projekt

#### Wiedensohler, Alfred

- “Scientific Advisory Group” für Aerosole innerhalb des “Global Watch”-Programmes der World Meteorological Organization
- Editorial Board Member “Atmosphere, Water, Air and Soil Pollution”
- VDI-Ausschuss “Partikelzählung in der Atmosphäre”
- Sprecher der Aerosol-Arbeitsgruppen innerhalb der EAA (European Aerosol Assembly)
- “Scientific Programm Committee” der Europäischen Aerosolkonferenz

## Cooperation

### National cooperation

Research Project	Cooperation Partners
4D-CLOUDS (Inhomogene Bewölkung - Ihr Einfluss auf die Austausch- und Transportprozesse in der Atmosphäre)	<ul style="list-style-type: none"> <li>• Technische Universität Dresden</li> <li>• Freie Universität Berlin</li> <li>• Institut für Küstenforschung, Geesthacht</li> <li>• Meteorologisches Institut der Universität Bonn</li> <li>• Universität Heidelberg, Institut für Umweltphysik, Heidelberg</li> <li>• Universität Leipzig, Institut für Meteorologie</li> <li>• Deutsches Zentrum für Luft- und Raumfahrt e.V</li> </ul>
TRANSVAER (Vertical transport of particles between planetary boundary layer and free troposphere)	<ul style="list-style-type: none"> <li>• Max-Planck-Institut für Meteorologie Hamburg</li> </ul>
ATLID (EarthCARE lidar performance Study)	<ul style="list-style-type: none"> <li>• Meteorologisches Institut der Universität München</li> </ul>
VIRTUAL (Access to scientific software through internet within the virtual laboratory)	<ul style="list-style-type: none"> <li>• Deutsches Zentrum für Luft- und Raumfahrt, Neustrelitz</li> </ul>
Urban Aerosol	<ul style="list-style-type: none"> <li>• Umweltforschungszentrum Leipzig-Halle, Leipzig</li> </ul>
STINHO (Structure of turbulent fluxes under Inhomogeneous surface conditions)	<ul style="list-style-type: none"> <li>• Universität Leipzig, Institut für Meteorologie</li> <li>• Deutscher Wetterdienst Lindenberg</li> <li>• TU Braunschweig</li> <li>• Universität Hannover, Institut für Meteorologie und Klimatologie</li> <li>• Universität Beyreuth, Lehrstuhl für Pflanzenökologie</li> <li>• Universität Beyreuth, Abteilung Mikrometeorologie</li> <li>• Universität Freiburg, Meteorologisches Institut</li> </ul>
FEBUKO (Field investigations of budgets and conversations of particle phase organics in tropospheric cloud processes)	<ul style="list-style-type: none"> <li>• Zentrum für Umweltforschung Frankfurt</li> <li>• Brandenburgische Technische Universität Cottbus</li> <li>• Technische Universität Darmstadt</li> </ul>
BEWA 2000 (Regional biogenic emissions of reactive volatile organic compounds)	<ul style="list-style-type: none"> <li>• Universität Innsbruck, Österreich</li> <li>• Institut für Meteorologie und Klimaforschung Karlsruhe</li> <li>• Technische Universität Darmstadt, Germany</li> <li>• Universität Freiburg</li> <li>• Universität Tübingen</li> <li>• Bergische Universität - Gesamthochschule Wuppertal</li> <li>• Max-Planck-Institut für Biogeochemie, Jena</li> <li>• Bayreuther Institut für Terrestrische Ökosystemforschung</li> <li>• Max-Planck-Institut für Chemie, Mainz</li> </ul>

Research Project	Cooperation Partners
<b>VERTICO</b> (Vertikaltransporte von Energie und Spurenstoffen an Ankerstationen und ihre räumlich/zeitliche Extrapolation unter komplexen natürlichen Bedingungen)	<ul style="list-style-type: none"> <li>• Technische Universität Dresden</li> <li>• Albert-Ludwigs-Universität Freiburg</li> <li>• Universität Bayreuth</li> <li>• Universität Göttingen</li> <li>• TU Bergakademie Freiberg</li> <li>• Deutscher Wetterdienst Lindenberg</li> <li>• Bundesforschungsanstalt für Landwirtschaft Braunschweig</li> <li>• Universität Basel</li> </ul>
The influence of turbulence on particle formation in the meso-scale	<ul style="list-style-type: none"> <li>• Deutscher Wetterdienst,</li> <li>• Abt. Forschung u. Entwicklung, Potsdam</li> </ul>
Particle transport and deposition	<ul style="list-style-type: none"> <li>• Gerhard-Mercator-Universität, Duisburg Inst. für Energie- und Umwelttechnik, Duisburg</li> </ul>
On the impact of LES derived turbulence length-scales on predicted mesoscale fields using the Local Model	<ul style="list-style-type: none"> <li>• Max-Planck-Institut für Meteorologie, Hamburg</li> <li>• Deutscher Wetterdienst,</li> <li>• Abt. Forschung u. Entwicklung, Potsdam</li> </ul>
<b>AFO 2000, EFEU</b> Development of a detailed and a moment based cloud microphysical modul for the investigation of the effects of the biomass burning on clouds	<ul style="list-style-type: none"> <li>• Universität Leipzig, Institut für Meteorologie</li> <li>• Max-Planck-Institut für Chemie, Biochemie, Mainz</li> <li>• Max-Planck-Institut für Meteorologie, Hamburg</li> </ul>
<b>AFO 2000, MODMEP</b> Modeling of tropospheric multiphase processes: Tools and chmical mechanisms	<ul style="list-style-type: none"> <li>• Max-Planck-Institut für Meteorologie, Hamburg</li> <li>• Brandenburgische Technische Universität Cottbus</li> </ul>

International cooperation

Research Project	Cooperation Partners
Characterization of mineral dust from lidar and sunphotometer observations	<ul style="list-style-type: none"> <li>AERONET, NASA - Goddard Space Flight Center, Greenbelt, USA</li> </ul>
CALIPSO (Cloud-Aerosol Lidar and Infrared Pathfinder Satellite Observations)	<ul style="list-style-type: none"> <li>NASA - Langley Research Center, Hampton, USA</li> </ul>
Measurements of vertical temperature	<ul style="list-style-type: none"> <li>Institute for Atmospheric Optics, Tomsk, Russia</li> </ul>
BBC (Baltex Bridge Campaign)	<ul style="list-style-type: none"> <li>21 partners from: Holland, Germany, UK, France, Poland, Sweden</li> </ul>
INSPECTRO (Influence of clouds on the spectral actinic flux in the lower troposphere)	<ul style="list-style-type: none"> <li>Forschungszentrum Karlsruhe, Institut für Meteorologie und Klimaforschung</li> <li>University of Manchester, Institute of Science and Technology</li> <li>University of Innsbruck</li> <li>Norwegian Institute for Air Research</li> <li>Deutsches Zentrum für Luft- und Raumfahrt</li> <li>Aristotle University of Thessaloniki</li> <li>National Research Council Institute of Atmospheric Physics</li> <li>University of East Anglia</li> <li>Norwegian University of Science and Technology</li> <li>Meteorologie Consult GmbH</li> <li>University of Leicester</li> </ul>
ICRCCM-III (Inter Comparison of Radiation Codes in Climate Models, Phase III)	<ul style="list-style-type: none"> <li>26 partners from: USA, Russia, Australia, Canada, Germany, UK, France, Japan, Finland</li> </ul>
UFAR (European Fleet for Airborne Research)	<ul style="list-style-type: none"> <li>Météo-France, Toulouse, France</li> <li>Enviscope, Frankfurt</li> <li>Max-Planck-Institut für Chemie, Mainz</li> <li>National University of Ireland, Galway, Ireland</li> <li>University of Manchester Institute of Science and Technology, Manchester, UK</li> </ul>
EARLINET (European Aerosol Research Lidar Network)	<ul style="list-style-type: none"> <li>18 partners from: Germany, Sweden, Greece, Spain, Italy, Switzerland, Byelorussia, Portugal, France</li> </ul>
Development of inversion methods for microphysical particle characterization on the basis of lidar observations	<ul style="list-style-type: none"> <li>Physics Instrumentation Center, Moscow, Russia</li> </ul>
Retrieval of microphysical particle properties from observations with eye-safe lidar and Sun photometer	<ul style="list-style-type: none"> <li>National Oceanographic and Atmospheric Administration, Boulder, USA</li> </ul>

Research Project	Cooperation Partners
Investigations on tropical cirrus observed with lidar and satellite during INDOEX (Characterization of aerosols over the Indian Ocean, Indian Ocean Experiment)	<ul style="list-style-type: none"> <li>National Center for Atmospheric Research, Boulder, USA</li> </ul>
Combined lidar-satellite observations for identification of sources of mineral dust observed during INDOEX	<ul style="list-style-type: none"> <li>Laboratoire d'Optique Atmospherique, Universite des Sciences et Technologies de Lille, France</li> </ul>
CVI development for sampling and characterization of atmospheric ice nuclei	<ul style="list-style-type: none"> <li>Paul Scherrer Institute, Villingen Switzerland</li> </ul>
LACIS (Leipzig Aerosol Cloud Interaction Simulator)	<ul style="list-style-type: none"> <li>Institute for Atmospheric Optics, Tomsk, Russia</li> </ul>
ACE-ASIA (Aerosol Characterization Experiment Asia)	<ul style="list-style-type: none"> <li>University of Washington, Seattle, USA</li> <li>Pacific Marine Environmental Laboratory, Seattle, USA</li> </ul>
World Calibration Center	<ul style="list-style-type: none"> <li>World Meteorological Organization, Geneva, Switzerland</li> <li>Umweltbundesamt, Berlin</li> </ul>
CARIBIC (Civil Aircraft for Regular Investigation of the atmosphere Based on an Instrument Container)	<ul style="list-style-type: none"> <li>11 partners from: Germany, France, Holland, Switzerland, Sweden, UK</li> </ul>
Hygroscopicity of supermicron particle	<ul style="list-style-type: none"> <li>University of Washington, Seattle, USA</li> <li>Pacific Marine Environmental Laboratory, Seattle, USA</li> </ul>
CREATE (Construction, Use and Delivery of an European Aerosol Database)	<ul style="list-style-type: none"> <li>11 partners from: Ireland, Norway, France, Switzerland, Holland, Finland, Greece, Germany</li> </ul>
Characterization of the number and chemical size distribution as well as hygroscopicity of fine and ultrafine particles in Beijing	<ul style="list-style-type: none"> <li>Peking University, China</li> </ul>
MOST (Multiphase chemistry of Oxygenated Species in the Troposphere)	<ul style="list-style-type: none"> <li>11 partners from: France, Ireland, Germany, UK, Switzerland, Spain, Greece</li> </ul>
CITY-DELTA (Inter-comparison of long-term model responses to urban-scale emission reduction scenarios)	<ul style="list-style-type: none"> <li>JRC-IES, Institute for Environment and Sustainability, Ispra, Italy</li> <li>EMEP, European Monitoring and Evaluation Program</li> <li>TNO Environment, Energy and Process Innovation, Apeldoorn, Holland</li> <li>IIASA, The International Institute for Applied Systems Analysis, Laxenburg, Austria</li> </ul>

## Boards

### Scientific advisory board

Name	Institution
Prof. Dr. E. Schaller (Chair)	Brandenburgische Technische Universität Cottbus Lehrstuhl für Umweltmeteorologie
Prof. Dr. J. Lelieveld	Max-Planck-Institut für Chemie, Mainz
Prof. Dr. P. Lemke	Stiftung Alfred-Wegener-Institut für Polar- und Meeresforschung, Bremerhaven
Prof. Dr. U. Schurath	Forschungszentrum Karlsruhe GmbH Institut für Meteorologie und Klimaforschung
Prof. Dr. F.-J. Lübken	Leibniz-Institut für Atmosphärenphysik an der Universität Rostock
Prof. Dr. Th. Peter	Institut für Atmosphäre und Klima ETH, Zürich, Schweiz
Privat-Dozent Dr. G. Adrian	Deutscher Wetterdienst Geschäftsbereich Forschung und Entwicklung, Offenbach
Dr. R. Delmas	Laboratoire de Glaciologie et Géophysique de l'Environnement (LGGE), St. Martin d'Here Cedex, Frankreich
Dr. I. Tegen	Max-Planck-Institut für Biochemie, Jena

### Boards of trustees

Name	Institution
MinR`in Dr. P. Karl Dresden	Sächsisches Staatsministerium für Wissenschaft und Kunst,
Dr. G. Hahn Prof. Dr. H. Graßl	Bundesministerium für Bildung und Forschung, Bonn Max-Planck-Institut für Meteorologie, Hamburg

### Member of the IfT-Association (e.V.)

Name	Institution
Prof. Dr. P. Warneck (Chair)	Max-Planck-Institut für Chemie, Mainz
MinR`in Dr. P. Karl Dresden	Sächsisches Staatsministerium für Wissenschaft und Kunst,
Dr. G. Hahn	Bundesministerium für Bildung und Forschung, Bonn
Prof. Dr. B. Brümmer	Universität Hamburg Meteorologisches Institut
Prof. Dr. W. Engewald	Universität Leipzig Fakultät für Chemie und Mineralogie
Dr. D. Koch	Bruker Saxonia Analytik GmbH, Leipzig



## Wolken für die Wissenschaft

Am Institut für Troposphärenforschung entsteht eine Anlage, die den Himmel auf die Erde holen soll

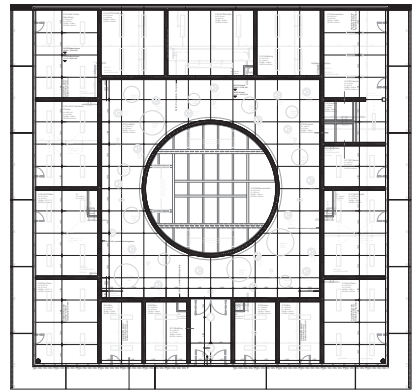
Lange schien das Projekt angesichts leerer Kassen am besten aufgehört zu haben. Aber letztendlich hat die am Leipziger Institut für Troposphärenforschung (IFT) seit drei Jahren geplante „Wolkenkammer“ doch noch kräftigen Aufwind bekommen.

Ende des Monats wird im Wissenschaftspark an der Fernosestraße der Grundstein für die Großforschungsanlage gelegt. 2,7 Millionen Euro investieren Bund und Land in das Vorhaben, und IFT-Direktor Professor Jan Holtenberg schweift furchig im sicheren Himmel. „Das wird ein international einflussreicher Komplex, in dem wir die Wolkenbildung realitätsnah nachbauen können.“

Bisher gebe es zwar schon so genannte „Vollkammern“, aber in diesen sei die Dynamik der physikalischen wie chemischen Prozesse nur partiell und nicht umfassend nachvollziehbar, erklärt Holtenberg. „Wir werden selbst die notwendigen Nachversäge, die hoch oben ablaufen, in dem Labor künstlich erzeugen und dann analysieren können.“

Die Wolken im Labor haben will das Institut für Troposphärenforschung in diesem Gebäude. Sein Wahrzeichen wird ein 14 Meter hoher Turm sein, der die eigentliche Simulationsanlage aufweist. Grundsteinlegung ist Ende des Monats. Zeichnung: Architekturbüro Schutz & Schutz

Im Regeneringebäude des IFT soll der Hochdruck-Betrieb sein, der Erde. Bisher greift die IFT 1992 war das von Leibniz-Institut für Troposphärenforschung



**Ift-Intern**



## Öffentlichkeitsarbeit

### IFT in den Medien

RUNDFUNK/ PRESSE	FERNSEHEN	JournalistIn RedakteurIn	IFT / Name /Thema	Datum Interview/ Aufnahmen	Sendung/Ver- öffentlichung
Deutschlandfunk		Dr. Uta Bilow	<u>Dr. T. Berndt</u> Propylene-Oxid-Verfahren	11. Juli	13. Aug. Deutschlandfunk Forschung aktuell
	MDR Aktuell	Claudia Berlin	<u>Prof. Dr. J. Heintzenberg</u> Intern. Symposium on Tropospheric Profiling 14.-20. September	14. Sept.	15. Sept.
	MDR Sachspiegel		<u>Prof. Dr. J. Heintzenberg</u> Intern. Symposium on Tropospheric Profiling 14.-20. September	15. Sept.	15. Sept.
Deutschlandfunk		Hartmut Schade	<u>Dr. Ulla Wandinger</u> Intern. Symposium on Tropospheric Profiling 14.-20. September	15. Sept.	
	MDR – aktuell		<u>Pressemitteilung</u> Leipziger Forscher machen Wolken nach, Wolken im Labor	28. Sept.	www.mdr.de/ nachrichten/ sachsen
MDR 1 - RADIO SACHSEN			<u>Pressemitteilung</u> Grundsteinlegung Wolkenlabor	14. Okt.	15. Okt. Nachrichten- Sendungen
Radio Leipzig 91.3		Viktoria Herrmann	<u>Prof. Dr. J. Heintzenberg</u> Grundsteinlegung Wolkenlabor	27. Okt.	28. Okt. Nachrichten- Sendungen
Hit Radio Antenne Sachsen			<u>Pressemitteilung</u> Grundsteinlegung		28. Okt. Nachrichten- sendungen

### IFT in der Presse

ZEITUNG	DATUM	Titel	IFT – Interview (JournalistIn)
Leipziger Volkszeitung	9. Mai	Phänomen über Leipzig <i>Sahara-Staub färbt Himmel milchig</i>	<u>Dr. A. Ansmann</u> (Mario Beck)
Wirtschaft und Wissenschaft 2/2003 Transferbrief Leipzig (Industrie- und Handelskammer)	26. Juni	<i>Wissenschaftler des IFT bereiten Ausgründung vor</i>	<u>Dr. D. Klugmann</u>
Frankfurter Allgemeine Zeitung	9. Juli	<i>Atmosphäre als Vorbild für die Chemiker</i>	<u>Dr. T. Berndt</u>

ZEITUNG	DATUM	Titel	Ift – Interview (JournalistIn)
Leipziger Volkszeitung	16. Sept.	Institut für Troposphärenforschung richtet Konferenz aus / Neue Messmethoden für meteorologische Prognosen vorgestellt <i>Wissenschaftler von der Pleiße helfen Wetterfröschen</i>	<u>Prof. Dr. J. Heintzenberg</u> (Mario Beck)
Sächsische Zeitung	22. Sept.	Artikel zum 6th Internat. Symposium on Tropospheric Profiling	<u>Dr. Ulla Wandinger</u> (Marlies Heinz)
Leipziger Volkszeitung	16. Okt.	Am Institut für Troposphärenforschung entsteht eine Anlage, die den Himmel auf die Erde holen soll <i>Wolken für die Wissenschaft</i>	<u>Pressemitteilung</u> (Mario Beck)
Leipziger Volkszeitung und im Internet www.lvz.de	29. Okt.	<i>Wolkiges Wissenschaftsprojekt bei strahlendem Sonnenschein gestartet</i>	<u>Grundsteinlegung Wolkenlabor</u> (Mario Beck)
Sächsische Zeitung und im Internet www-sz-online.de	28. Okt.	Am Leipziger Institut für Troposphärenforschung wird der Grundstein für ein neues Labor gelegt <i>Forscher auf Wolke sieben</i>	<u>Prof. Dr. J. Heintzenberg</u> (Manfred Schulze)
BILD Zeitung	28. Okt.	<i>Prof. Heintzenberg will Wolken und Regen selber machen</i>	<u>Prof. Dr. J. Heintzenberg</u> (Matthias W. Weidemann)

### Ift Allgemeine Aktivitäten

Anlass	Ort, Datum	Aktivität
Gustav-Hertz-Gymnasium Leipzig	Leipzig, 5. Februar	<u>Dr. U. Wandinger</u> Vorstellung Laser-Labor für Schüler/Innen der 12. Klasse
Berufsinformationstag Gymnasium Taucha	Taucha b. Leipzig 29. April	<u>Hartmut Haudek</u> Vorstellung Berufsbild: Wissenschaftlicher Gerätebau
<i>Universitäts-campus</i> Tag der Universität	Stadtzentrum Leipzig 17. Mai	<u>Dr. Thomas Tuch</u> Demonstrations-Experiment Atemlufttest Video „Dicke Luft“
Waldorfschule Leipzig Abiturienten	Leipzig 2. Juli	<u>Prof. Dr. J. Heintzenberg</u> Vorstellung der Forschungsarbeiten des Instituts, der Abt. Physik
<i>6th Intern. Symposium on Tropospheric Profiling</i> Laborbesichtigung Teilnehmer am Symposium	Leipzig 19. Sept.	<u>Wissenschaftler des Instituts</u> Vorstellung: ACTOS-Plattform Laminarreaktor Wolkenkammer DOAS/Raman-Lidar
Bildungs- und Wissenschaftsforum INDIEN	Berlin 24./25. Sept.	<u>Dr. Detlef Müller</u> Poster zur Zusammenarbeit IfT mit indischer Forschungseinrichtung
ROTARY CLUB Leipzig-Brühl 4. Schülerkongress	Leipzig 7. Nov.	<u>Prof. Dr. J. Heintzenberg</u> Referent zum Thema: „Studium der Naturwissenschaften“ vor Schülern der Thomasschule Leipzig und des Evangelischen Schulzentrums Leipzig



